NUCLEAR DATA AND MEASUREMENTS SERIES

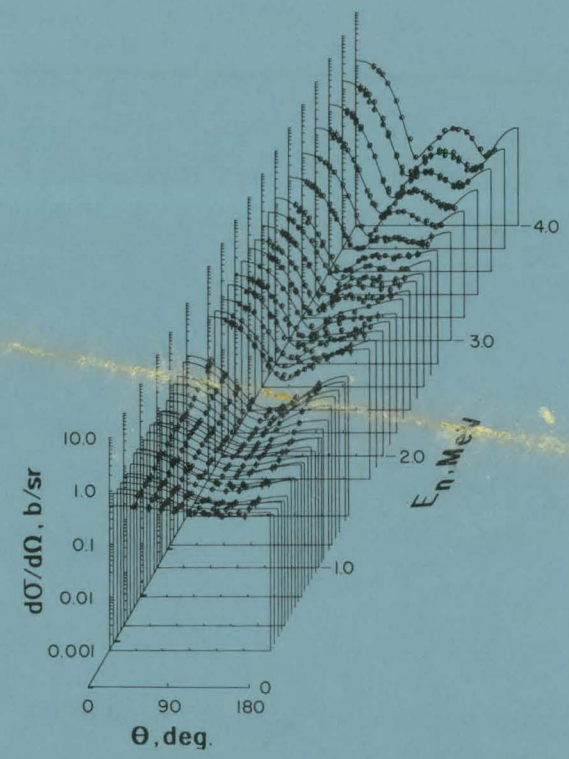

U of C-AUA-USDOE

ARGONNE NATIONAL LABORATORY,
ARGONNE, ILLINOIS 60439, U.S.A.

DISCLAIMER

ANL/NDM--58

DE82 013579

ANL/NDM-58

REVIEW OF MEASUREMENT TECHNIQUES FOR THE NEUTRON RADIATIVE-CAPTURE PROCESS

by

W. P. Poenitz

July 1981

Applied Physics Division
Argonne National Laboratory
9700 South Cass Avenue
Argonne, Illinois 60439
USA

NUCLEAR DATA AND MEASUREMENTS SERIES

The Nuclear Data and Measurements Series presents results of studies in the field of microscopic nuclear data. The primary objective is the dissemination of information in the comprehensive form required for nuclear technology applications. This Series is devoted to: a) measured microscopic nuclear parameters, b) experimental techniques and facilities employed in measurements, c) the analysis, correlation and interpretation of nuclear data, and d) the evaluation of nuclear data. Contributions to this Series are reviewed to assure technical competence and, unless otherwise stated, the contents can be formally referenced. This Series does not supplant formal journal publication but it does provide the more extensive information required for technological applications (e.g., tabulated numerical data) in a timely manner.

OTHER ISSUES IN THE ANL/NDM SERIES ARE:

ANL/NDM-1 Cobalt Fast Neutron Cross Sections-Measurement and Evaluation by P. T. Guenther, P. A. Moldauer, A. B. Smith, D. L. Smith and J. F. Whalen, July 1973.

ANL/NDM-2 Prompt Air-Scattering Corrections for a Fast-Neutron Fission Detector: $E_n \leq 5$ MeV by Donald L. Smith, September 1973.

ANL/NDM-3 Neutron Scattering from Titanium; Compound and Direct Effects by E. Barnard, J. deVilliers, P. Moldauer, D. Reitmann, A. Smith and J. Whalen, October 1973.

ANL/NDM-4 ^{90}Zr and ^{92}Zr; Neutron Total and Scattering Cross Sections by P. Guenther, A. Smith and J. Whalen, July 1974.

ANL/NDM-5 Delayed Neutron Data - Review and Evaluation by Samson A. Cox, April 1974.

ANL/NDM-6 Evaluated Neutronic Cross Section File for Niobium by R. Howerton, Lawrence Livermore Laboratory and A. Smith, P. Guenther and J. Whalen, Argonne National Laboratory, May 1974.

ANL/NDM-7 Neutron Total and Scattering Cross Sections of Some Even Isotopes of Molybdenum and the Optical Model by A. B. Smith, P. T. Guenther and J. F. Whalen, June 1974.

ANL/NDM-8 Fast Neutron Capture and Activation Cross Sections of Niobium Isotopes by W. P. Poenitz, May 1974.

ANL/NDM-9 Method of Neutron Activation Cross Section Measurement for E_n = 5.5-10 MeV Using the D(d,n)He-3 Reaction as a Neutron Source by D. L. Smith and J. W. Meadows, August 1974.

ANL/NDM-10 Cross Sections for (n,p) Reactions on ^{27}Al, $^{46,47,48}Ti$, $^{54,56}Fe$, ^{58}Ni, ^{59}Co and ^{64}Zn from Near Threshold to 10 MeV by Donald L. Smith and James W. Meadows, January 1975.

ANL/NDM-11 Measured and Evaluated Fast Neutron Cross Sections of Elemental Nickel by P. Guenther, A. Smith, D. Smith and J. Whalen, Argonne National Laboratory and R. Howerton, Lawrence Livermore Laboratory, July 1975.

ANL/NDM-12 A Spectrometer for the Investigation of Gamma Radiation Produced by Neutron-Induced Reactions by Donald L. Smith, April 1975.

ANL/NDM-13 Response of Several Threshold Reactions in Reference Fission Neutron Fields by Donald L. Smith and James W. Meadows, June 1975.

ANL/NDM-14 Cross Sections for the $^{66}Zn(n,p)^{66}Cu$, $^{113}In(n,n')^{113m}In$ and $^{115}In(n,n')^{115m}In$ Reactions from Near Threshold to 10 MeV by Donald L. Smith and James W. Meadows, July 1975.

ANL/NDM-15 Radiative Capture of Fast Neutrons in ^{165}Ho and ^{181}Ta by W. P. Poenitz, June 1975.

ANL/NDM-16 Fast Neutron Excitation of the Ground-State Rotational Band of ^{238}U by P. Guenther, D. Havel and A. Smith, September 1975.

ANL/NDM-17 Sample-Size Effects in Fast-Neutron Gamma-Ray Production Measurements: Solid-Cylinder Samples by Donald L. Smith, September 1975.

ANL/NDM-18 The Delayed Neutron Yield of ^{238}U and ^{241}Pu by J. W. Meadows January 1976.

ANL/NDM-19 A Remark on the Prompt-Fission-Neutron Spectrum of ^{252}Cf by P. Guenther, D. Havel, R. Sjoblom and A. Smith, March 1976.

ANL/NDM-20 Fast-Neutron-Gamma-Ray Production from Elemental Iron: $E_n \lesssim$ 2 MeV by Donald L. Smith, May 1976.

ANL/NDM-21 Note on the Experimental Determination of the Relative Fast-Neutron Sensitivity of a Hydrogenous Scintillator by A. Smith, P. Guenther and R. Sjoblom, June 1976.

ANL/NDM-22 Note on Neutron Scattering and the Optical Model Near A=208 by P. Guenther, D. Havel and A. Smith, September 1976.

ANL/NDM-23 Remarks Concerning the Accurate Measurement of Differential Cross Sections for Threshold Reactions Used in Fast-Neutron Dosimetry for Fission Reactors by Donald L. Smith, December 1976.

ANL/NDM-24 Fast Neutron Cross Sections of Vanadium and an Evaluated Neutronic File by P. Guenther, D. Havel, R. Howerton, F. Mann, D. Smith, A. Smith and J. Whalen, May 1977.

ANL/NDM-25 Determination of the Energy Scale for Neutron Cross Section Measurements Employing a Monoenergetic Accelerator by J. W. Meadows, January 1977.

ANL/NDM-26 Evaluation of the IN-115(N,N')IN-115M Reaction for the ENDF/B-V Dosimetry File by Donald L. Smith, December 1976.

ANL/NDM-27 Evaluated (n,p) Cross Sections of ^{46}Ti, ^{47}Ti and ^{48}Ti by C. Philis and O. Bersillon, Bruyeres-le-Chatel, France and D. Smith and A. Smith, Argonne National Laboratory, January 1977.

ANL/NDM-28 Titanium-II: An Evaluated Nuclear Data File by C. Philis, Centre d'Etudes de Bruyères-le-Châtel, R. Howerton, Lawrence Livermore Laboratory and A. B. Smith, Argonne National Laboratory, June 1977.

ANL/NDM-29 Note on the 250 keV Resonance in the Total Neutron Cross Section of ^{6}Li by A. B. Smith, P. Guenther, D. Havel and J. F. Whalen, June 1977.

ANL/NDM-30 Analysis of the Sensitivity of Spectrum-Average Cross Sections to Individual Characteristics of Differential Excitation Functions by Donald L. Smith, March 1977.

ANL/NDM-31 Titanium-I: Fast Neutron Cross Section Measurements by P. Guenther, D. Havel, A. Smith and J. Whalen, May 1977.

ANL/NDM-32 Evaluated Fast Neutron Cross Section of Uranium-238 by W. Poenitz, E. Pennington, and A. B. Smith, Argonne National Laboratory and R. Howerton, Lawrence Livermore Laboratory, October 1977.

ANL/NDM-33 Comments on the Energy-Averaged Total Neutron Cross Sections of Structural Materials by A. B. Smith and J. F. Whalen, June 1977.

ANL/NDM-34 Graphical Representation of Neutron Differential Cross Section Data for Reactor Dosimetry Applications by Donald L. Smith, June 1977.

ANL/NDM-35 Evaluated Nuclear Data File of Th-232 by J. Meadows, W. Poenitz, A. Smith, D. Smith and J. Whalen, Argonne National Laboratory and R. Howerton, Lawrence Livermore Laboratory, February 1978.

ANL/NDM-36 Absolute Measurements of the $^{233}U(n,f)$ Cross Section Between 0.13 and 8.0 MeV by W. P. Poenitz, April 1978.

ANL/NDM-37 Neutron Inelastic Scattering Studies for Lead-204 by D. L. Smith and J. W. Meadows, December 1977.

ANL/NDM-38 The Alpha and Spontaneous Fission Half-Lives of ^{242}Pu by J. W. Meadows, December 1977.

ANL/NDM-39 The Fission Cross Section of ^{239}Pu Relative to ^{235}U from 0.1 to 10 MeV by J. W. Meadows, March 1978.

ANL/NDM-40 Statistical Theory of Neutron Nuclear Reactions by P. A. Moldauer, February 1978.

ANL/NDM-41 Energy-Averaged Neutron Cross Sections of Fast-Reactor Structural Materials by A. Smith, R. McKnight and D. Smith, February 1978.

ANL/NDM-42 Fast Neutron Radiative Capture Cross Section of ^{232}Th by W. P. Poenitz and D. L. Smith, March 1978.

ANL/NDM-43 Neutron Scattering from ^{12}C in the Few-MeV Region by A. Smith, R. Holt and J. Whalen, September 1978.

ANL/NDM-44 The Interaction of Fast Neutrons with ^{60}Ni by A. Smith, P. Guenther, D. Smith and J. Whalen, January 1979.

ANL/NDM-45 Evaluation of $^{235}U(n,f)$ between 100 KeV and 20 MeV by W. P. Poenitz, July 1979.

ANL/NDM-46 Fast-Neutron Total and Scattering Cross Sections of ^{107}Ag in the MeV Region by A. Smith, P. Guenther, G. Winkler and J. Whalen, January 1979.

ANL/NDM-47 Scattering of MeV Neutrons from Elemental Iron by A. Smith and P. Guenther, March 1979.

ANL/NDM-48 ^{235}U Fission Mass and Counting Comparison and Standardization by W. P. Poenitz, J. W. Meadows and R. J. Armani, May 1979.

ANL/NDM-49 Some Comments on Resolution and the Analysis and Interpretation of Experimental Results from Differential Neutron Measurements by Donald L. Smith, November 1979.

ANL/NDM-50 Prompt-Fission-Neutron Spectra of ^{233}U, ^{235}U, ^{239}Pu and ^{240}Pu Relative to that of ^{252}Cf by A. Smith, P. Guenther, G. Winkler and R. McKnight, September 1979.

ANL/NDM-51 Measured and Evaluated Neutron Cross Sections of Elemental Bismuth by A. Smith, P. Guenther, D. Smith and J. Whalen, April 1980.

ANL/NDM-52 Neutron Total and Scattering Cross Sections of ^{6}Li in the Few MeV Region by P. Guenther, A. Smith and J. Whalen, February 1980.

ANL/NDM-53 Neutron Source Investigations in Support of the Cross Section at the Argonne Fast-Neutron Generator by James W. Meadows and Donald L. Smith, May 1980.

ANL/NDM-54 The Nonelastic-Scattering Cross Sections of Elemental Nickel by A. B. Smith, P. T. Guenther and J. F. Whalen, June 1980.

ANL/NDM-55 Thermal Neutron Calibration of a Tritium Extraction Facility using the $^{6}Li(n,t)^{4}He/^{197}Au(n,\gamma)^{198}Au$ Cross Section Ratio for Standardization by M. M. Bretscher and D. L. Smith, August 1980.

ANL/NDM-56 Fast-Neutron Interactions with ^{182}W, ^{184}W and ^{186}W by P. T. Guenther, A. B. Smith and J. F. Whalen, December 1980.

ANL/NDM-57 The Total, Elastic- and Inelastic-Scattering Fast-Neutron Cross Sections of Natural Chromium, Peter T. Guenther, Alan B. Smith and James F. Whalen, January 1981.

TABLE OF CONTENTS

REVIEW OF MEASUREMENT TECHNIQUES FOR THE NEUTRON RADIATIVE CAPTURE PROCESS*

by

W. P. Poenitz
Applied Physics Division
Argonne National Laboratory
9700 South Cass Avenue
Argonne, Illinois 60439, USA

ABSTRACT

The experimental techniques applied in measurements of the neutron capture process are reviewed. The emphasis is on measurement techniques used in neutron capture cross section measurements.

The activation technique applied mainly in earlier work has still its use in some cases, specifically for measurements of technologically important cross sections (^{238}U and ^{232}Th) with high accuracy. Three major prompt neutron radioative capture detection techniques have evolved: the total gamma radiation energy detection technique (mainly with large liquid scintillation detectors), the gamma-energy proportional detectors (with proportional counters or Moxon-Rae detectors), and the pulse-height weighting technique. These measurement techniques are generally applicable, however, shortcomings limit the achievable accuracy to a ≈5-15% uncertainty level.

*This work supported by the U.S. Department of Energy.

REVIEW OF MEASUREMENT TECHNIQUES FOR THE NEUTRON RADIATIVE CAPTURE PROCESS

I. Introduction

The neutron capture process results in a variety of effects and related quantities which are of interest in understanding its physical nature and must be known for practical applications. The intent to measure a specific quantity which describes a process, occurring in nature or initiated in the laboratory, requires first considering which effects of the process are observable and which processes could interfere with possible detection schemes. The measurement of a specific quantity involves several auxiliary conditions which must be considered in the selection of measurement techniques and the judgment of their applicability. It is the intent of this introduction to review briefly the measurable effects of the capture process and to survey neutron sources commonly used in capture studies. Neutron flux measurements required in such experiments will also be considered. More detailed information on the latter two subjects is available elsewhere.*

I.1. The Neutron Capture Reaction

The neutron capture process is defined by

$$n + E_n + A \rightarrow (A + 1) + \sum_i \gamma_i + E_A \qquad (1)$$

where a neutron, n, with energy, E_n, interacts with a target nucleus of mass A; a nucleus of mass A + 1 is formed, and one or several gamma-rays are emitted (see Fig. 1). E_A is the recoil energy which is negligible for most nuclei. Thus the effects resulting from a capture event which might be detected are:

Absorption (the loss of a neutron),

Transmutation (the creation of a nucleus with a mass larger by one AMU than the mass of the target nucleus),

and

Radiation (the emission of electromagnetic energy, e.g. γ rays).

The radiative capture process results in a radioactive nucleus for about one third of all stable target nuclei. This provides one more opportunity for the detection of capture events:

---

*See for example: Nuclear Energy Agency Nuclear Data Committee (OECD) series on "Neutron Physics and Nuclear Data in Science and Technology" Pergamon Press.

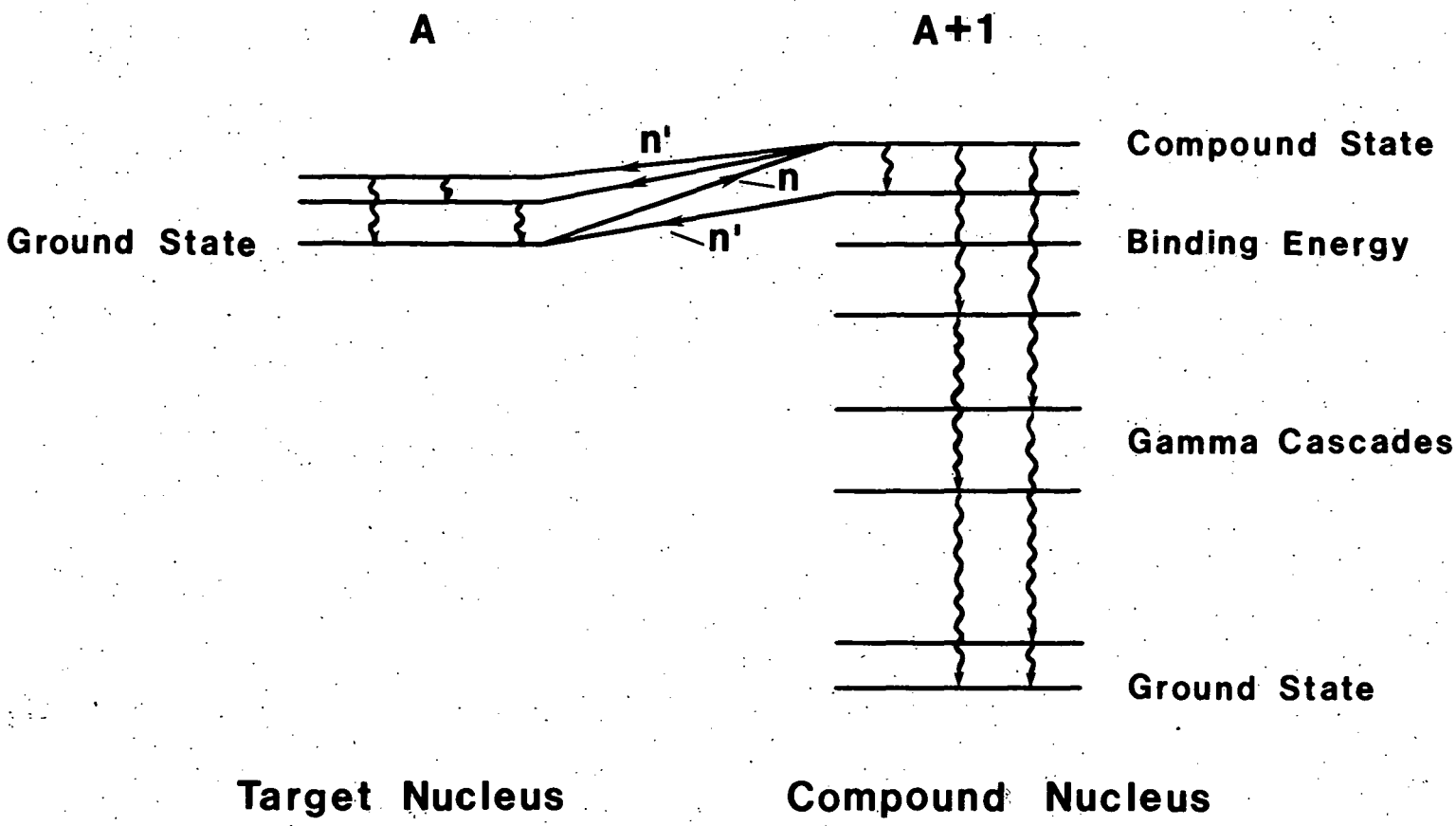

Fig. 1. Schematic of the Neutron Capture Process. (n;γ,n') and (n;n,γ) Reactions are also Indicated.

Activation (the creation of a radioactive nucleus).

The emission of prompt γ rays in a neutron-capture process makes direct measurement techniques possible whereas the other effects provide for indirect measurement techniques. The energy of the reaction is given by the sum of the center-of-mass energy of the incoming neutron and the neutron-binding energy, B_n, of the nucleus of mass A + 1. Most of this energy is emitted in form of electromagnetic radiation. The neutron binding energy is typically in the range of 5-9 MeV.

The quantities which are descriptive of the various effects of the capture process as represented with Eq. (1) and Fig. 1 are:

The interaction probability for the (n,γ) process, which besides its physical information is often of technological importance, and is expressed as a cross section;

The γ-ray spectrum which results from the neutron capture process. It is determined by the level structure of the nucleus with mass A + 1, and has physical as well as applied importance;

The probability for specific transitions in the de-excitation of the compound nucleus which help to define properties of the levels involved;

The population probability of some of the low-lying states of the compound nucleus, and

The multiplicity of the γ cascades in the decay of the compound nucleus.

The quantity of primary interest is the probability of the radiative capture process taking place, which is expressed with the cross section, $\sigma_{n,\gamma}$, defined by the equation:

$$C_\gamma = \sigma_{n,\gamma} \bullet N \bullet \phi \quad , \qquad (2)$$

where C_γ is the number of capture events resulting from the irradiation of a sample containing N nuclei with a neutron flux, ϕ.

The energy dependence of the neutron-capture cross section and features of available neutron sources are criteria for the selection of specific detection techniques. A plot of the capture cross section as a function of the neutron energy, as it is observed for most medium and heavy mass nuclei, is shown in Fig. 2. At low energies ($\lesssim$1 eV) the capture cross section often varies as a function of energy with $1/\sqrt{E}$. Perturbations of this "law" are due to the existence of bound levels close to the neutron-binding energy or the proximity of the first positive-energy resonance. The cross section at low energies is often relatively large. The structure in the resolved resonance energy range is due to compound-nuclear phenomena and for neutron angular momentum $\ell = 0$ (s-wave), can be described in terms of the single-level Breit-Wigner resonance formalism (see, for example, Blatt and Weisskopf,[1]):

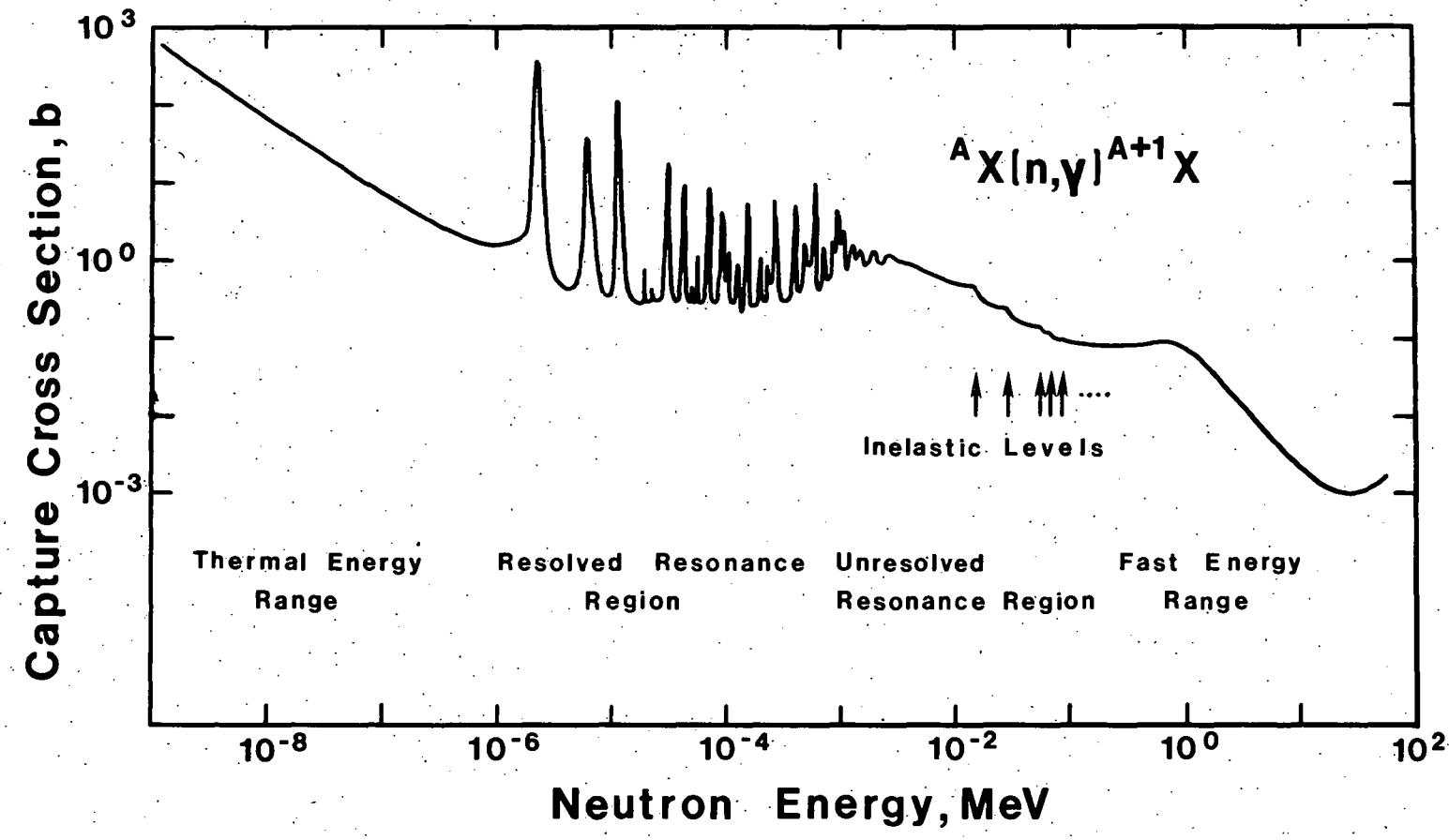

Fig. 2. Schematic of the Energy Dependence of the Neutron Capture Cross Section for a Typical Medium or Heavy-Mass Nuclei.

$$\sigma_{n,\gamma}(E) = 4\pi \lambda\!\!\!^{-2}\, g_J \frac{\Gamma_n \Gamma_\gamma}{(E-E_R)^2 + (\Gamma/2)^2} \quad , \tag{3}$$

as long as these resonances have total widths, $\Gamma = \Gamma_n + \Gamma_\gamma$, small compared with their average level spacing, D. Here $\lambda\!\!\!^{-}$ is the neutron wave length divided by 2π, g_J is a statistical weight factor $((2J + 1)/2\cdot(2I + 1))$ given by the spin of the compound resonance, J, and the spin of the target nucleus, I. E_R is the resonance energy, and Γ_n and Γ_γ are the partial widths of the resonance for neutron and γ-ray emission which relate to its decay probabilities with Γ_n/h and Γ_γ/h. The $1/\sqrt{E}$ behavior of the cross section at low neutron energies can, of course, be deduced from the Breit-Wigner derivation of the resonances with $E << E_R$, $\Gamma_n \sim \sqrt{E}$, $\lambda\!\!\!^{-2} \sim 1/E$, and $\Gamma_\gamma \sim$ const. At higher energies, attainable experimental neutron-energy resolution becomes insufficient to resolve the resonance structure and/or the density and the widths of the resonances increases such that overlap occurs and a smooth average cross section is observed (unresolved-resonance range). In the MeV-energy range, the capture cross section decreases rapidly with increasing neutron energy as other competing decay channels open (mainly inelastic scattering) and finally above ~10 MeV capture is nearly entirely determined by direct capture processes. Direct capture might also be observed between compound resonances where contributions from the compound process are small.

The structure in the resolved-resonance-energy range requires the use of the prompt-detection techniques for the measurement of the capture cross section in order to achieve the best neutron-energy resolution. The prompt detection of the emitted electromagnetic radiation is, of course, also applicable at lower and higher neutron energies though with restrictions on the latter due to competing reactions. The smooth variation of the cross section with neutron energy in the thermal-energy range and at higher energies permits the use of the activation technique. Restrictions on the applicability of absorption and transmutation measurements to the areas of smooth cross sections or to evergy-averaged quantities are again due to resolution but mainly due to the requirement for intense-neutron sources and problems with competing reactions.

Knowledge of the γ-ray spectra, cascade multiplicity, low-level-population probability, and transition strengths provides information about the reaction mechanism of the capture process, the energies, spins, and parities of the levels, and the statistical behavior of the compound states. The total-radiative width varies little from one compound resonance to another as it is the sum of many possible decay probabilities to lower-lying states. However, the width of an individual transition follows a chi-square distribution with one degree of freedom which results in marked differences of the observed γ-ray spectra for different resonances. Such pronounced spectral differences were observed for many nuclei for example by Chrien and co-workers (e.g. Lone et al.[2], Mughabghab et al.[3], Mughabghab and Chrien[4], Lion et al.[5]). Figure 3 shows as an example the γ-ray spectra obtained for several resonances of the ^{177}Hf(n,γ) process recently reported by Stefanon and Corvi[6]. Changes of the γ spectra for different energies must also be expected, if averaged over many

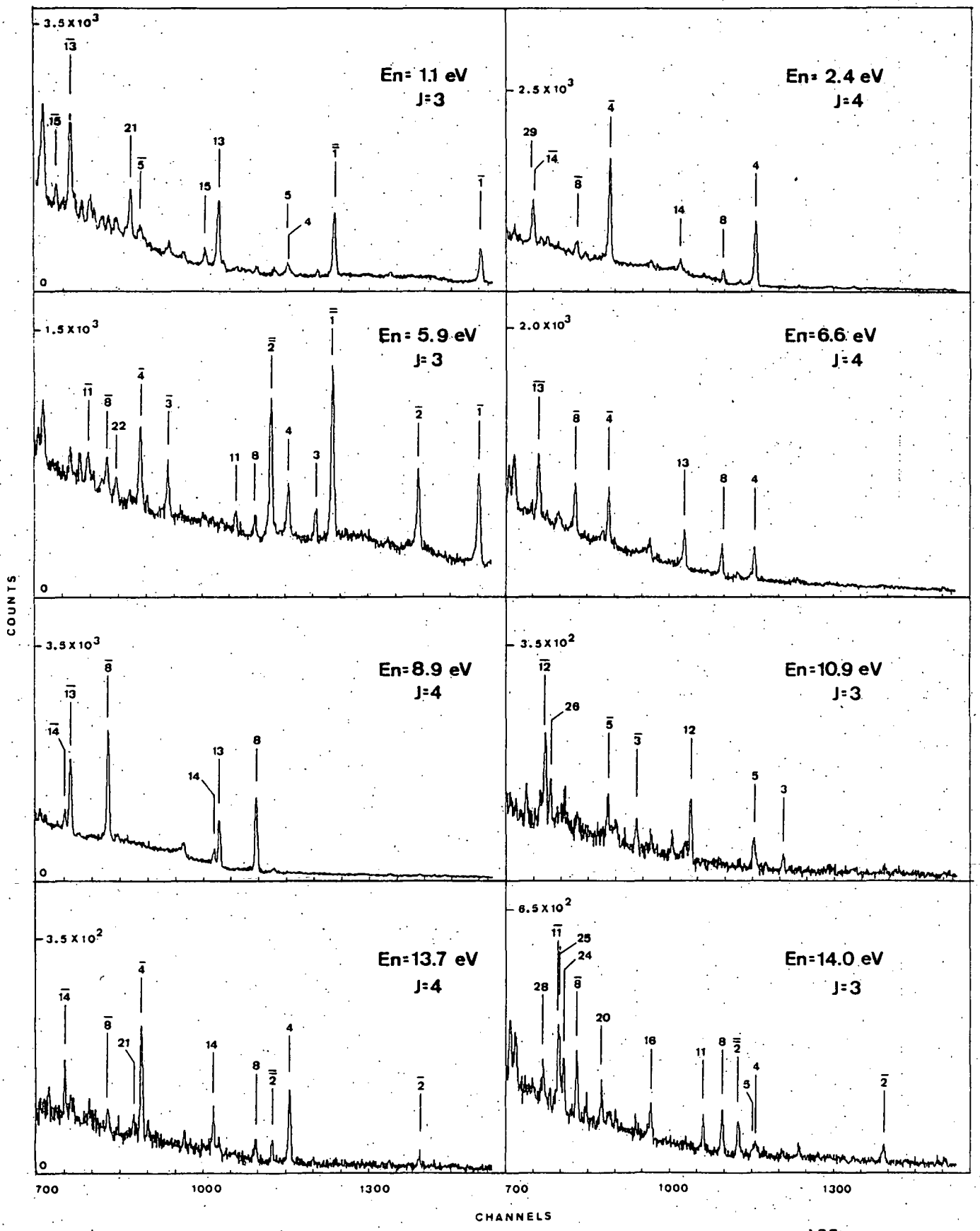

Fig. 3. Gamma-ray Spectra Obtained in Different Resonances of the ^{177}Hf (n,γ) Reaction.[6]

resonances, as angular-momentum-selection rules cause additional variability. This can be seen in Fig. 4 where γ spectra of $^{156}Gd(n,\gamma)$ averaged over many resonances obtained with average energies of ~2 KeV and ~24 KeV are compared (Reich[7]). The observed spectral changes require that techniques employed for the detection of capture events be spectra insensitive.

Other reactions which must be considered because they result in effects similar to the capture process and thus might disturb the measurement of true capture events are of the type:

$$n + E_n + A \rightarrow B + x + E_x + \sum_i \gamma_i \quad . \tag{4}$$

B is a nucleus of the same or similar mass to that of the target nucleus, A, and x is a reaction product (e.g. an α particle or a proton) which might also be a neutron with less energy than the primary neutron (inelastic scattering). The γ rays from such reactions will have different energy spectra and multiplicities. The processes defined in Eq. (4) always compete with the measurement of the neutron absorption, except for inelastic scattering events. Of major concern is the emission of γ rays in competing $(n;n;\gamma)$ and $(n;\gamma,n')$ processes which interfere with the detection of capture events by the method of measuring the promptly emitted electromagnetic radiation. Figure 1 shows the major difference between capture and inelastic scattering events as far as the emitted γ rays are concerned. The maximum total γ-ray energy of the inelastic process is equal to the center-of-mass energy of the primary neutron, whereas the capture process results in a total γ-ray energy equal to the sum of the center-of-mass energy of the primary neutron and the neutron-binding energy. The reaction thresholds for the inelastic-scattering process are usually in the higher keV or the MeV-energy range (see Fig. 2) but might be substantially lower for heavy and odd-mass nuclei (a few keV).

The fission process is another reaction which, for some heavy-mass nuclei, interferes with the detection of capture events by means of measuring the prompt-γ radiation:

$$n + E_n + A \rightarrow B_1 + B_2 + \nu \cdot n + \sum_i \gamma_i \quad . \tag{5}$$

The emission of ν neutrons also excludes the use of the absorption for the detection of capture events. The γ radiation emitted during the fission process has a maximum total energy which usually exceeds that of the capture process.

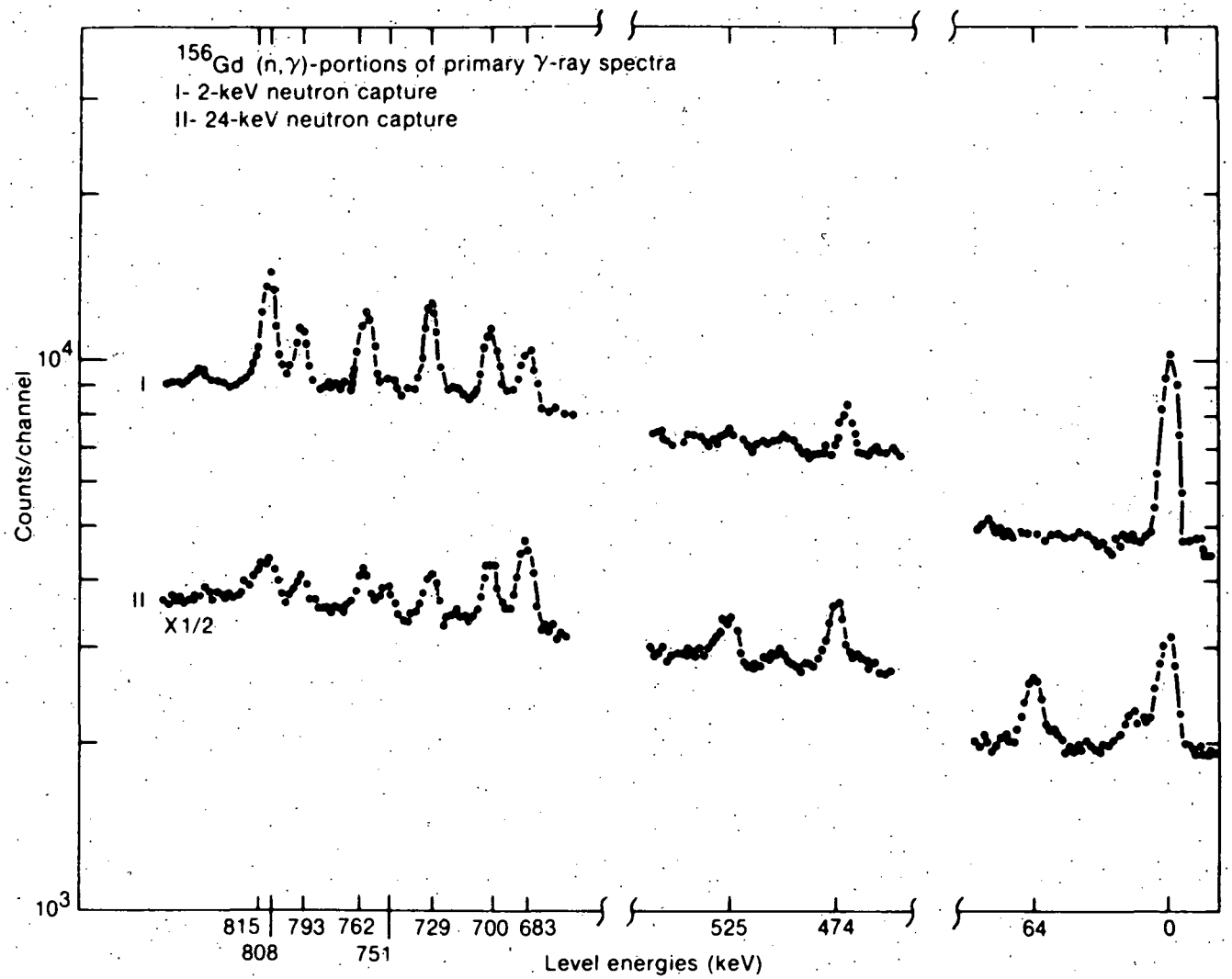

Fig. 4. Differences in Resonance-Averaged Gamma-Ray Spectra Obtained with the ^{156}Gd (n,γ) Reaction.[7]

I.2. Neutron Sources

There are several neutron sources available which are used in the investigation of capture processes or the measurement of important related quantities. Neutrons generated with linear-electron accelerators (LINAC's), cyclotrons, electrostatic accelerators, and reactors are presently the main sources for neutron-capture measurements. In the past, photoneutron, spontaneous-fission sources, and betatrons were also used.

LINAC's and cyclotrons with suitable targets (often heavy metals like Ta or U for the former, but sometimes light nuclei like Be for the latter) provide neutron bursts in the keV to MeV-energy range. Using small moderators near or surrounding the target permits the shifting of the primary source spectra to lower energies and neutrons are obtained with continuous spectra ("white"-spectrum sources) extending from the low-eV to the MeV-energy range. The white-spectra nature of these sources requires the separating of the neutrons with different energies. This is possible with the time-of-flight technique due to the pulsed operation of the accelerator. LINAC's provide most of the data in the resolved-resonance range due to their high source intensity and corresponding good energy resolution. The neutron-flight paths consist of evacuated or He-filled tubes of 10-200 m length. Figure 5 shows as an example the Oak Ridge Linear Electron Accelerator Facility (ORELA)[8] with a large-liquid scintillator for capture measurements stationed at a 40-m-flight path. A smaller capture detector utilizing the pulse-height-weighting technique is also used at this facility at another 40-m-flight-path station. Spectral γ-ray measurements can be carried out at a shorter flight path of $\approx$10-20 m.

Electrostatic accelerators, utilizing neutron-source reactions like the $T(p,n)^3He$ or $^7Li(p,n)^7Be$ reactions can be used to produce monoenergetic neutrons with thin targets, or, with thick targets, pseudo-white neutron spectra. These accelerators can be operated in a pulsed or a continuous time-mode and capture data have been obtained in the keV and MeV energy range. The time-of-flight technique is usually employed for background suppression and/or energy determination.

Reactors are used to measure neutron-spectrum-averaged quantities or, with additional devices (fast-mechanical choppers, crystal spectrometers, and resonance-interference filters), measurements at specific energies are possible. The neutron intensity obtained with a mechanical chopper in the low-eV range at a high-flux reactor (HFR), e.g. as available at Brookhaven National Laboratory or the Laue - Langerin Institute at Grenoble, is usually higher than that obtained with a LINAC. Figure 6 shows the beam-tube layout of the HFR at Grenoble and the neutron-flux intensities for different energy ranges (Moessbauer[9]). More recently, resonance-interference filters have been frequently used to provide monoenergetic-neutron beams utilizing reactors or LINAC's as primary sources. Average energies of 2 keV and 24 keV have been obtained with scandium and iron filters, respectively. Most reactors operate in a steady-state mode, however, a pulsed reactor at Dubna has been the site of significant resonance-neutron capture studies. A new reactor

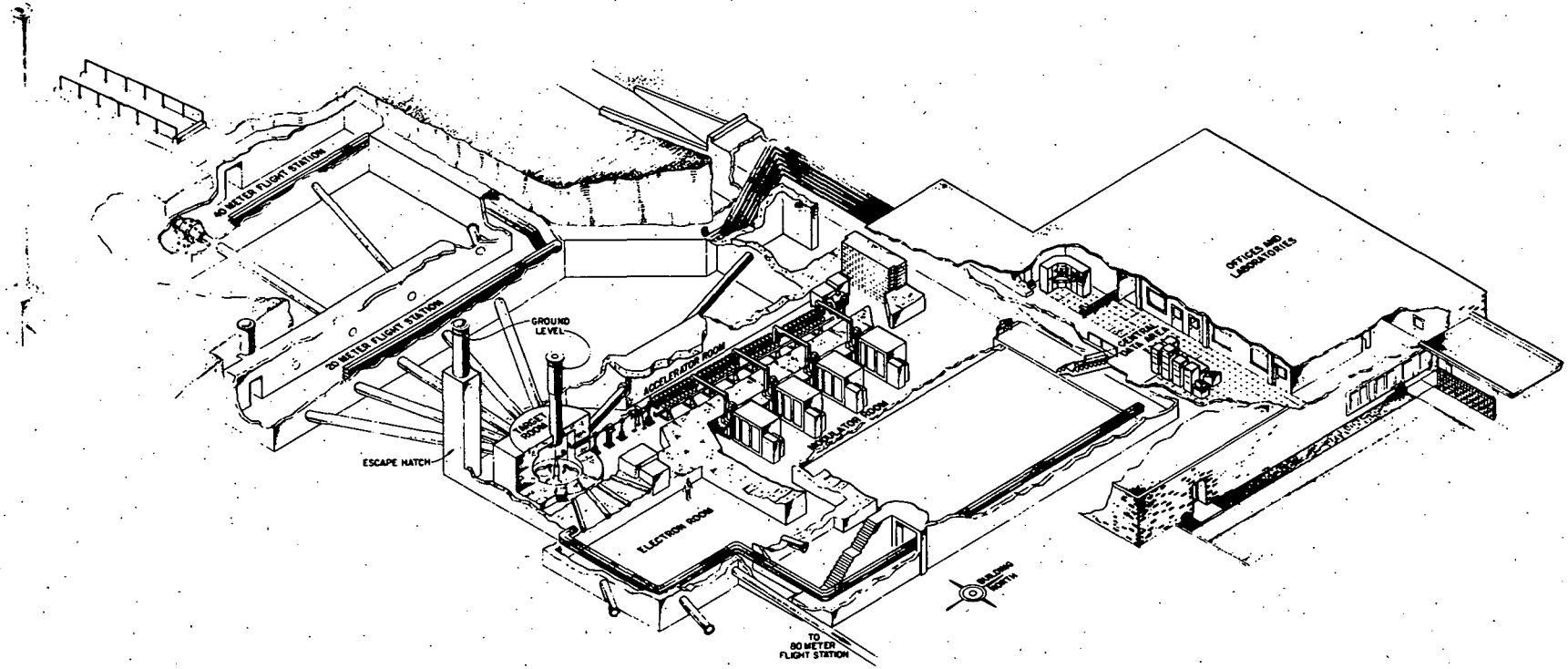

Fig. 5. The Oak-Ridge-Linear-Electron-Accelerator Facility (ORELA), Showing the Target and various 20 and 40 m Flight Path Stations. The Large Liquid-Scintillator-Detector is Indicated at a 40-m-Flight Path.

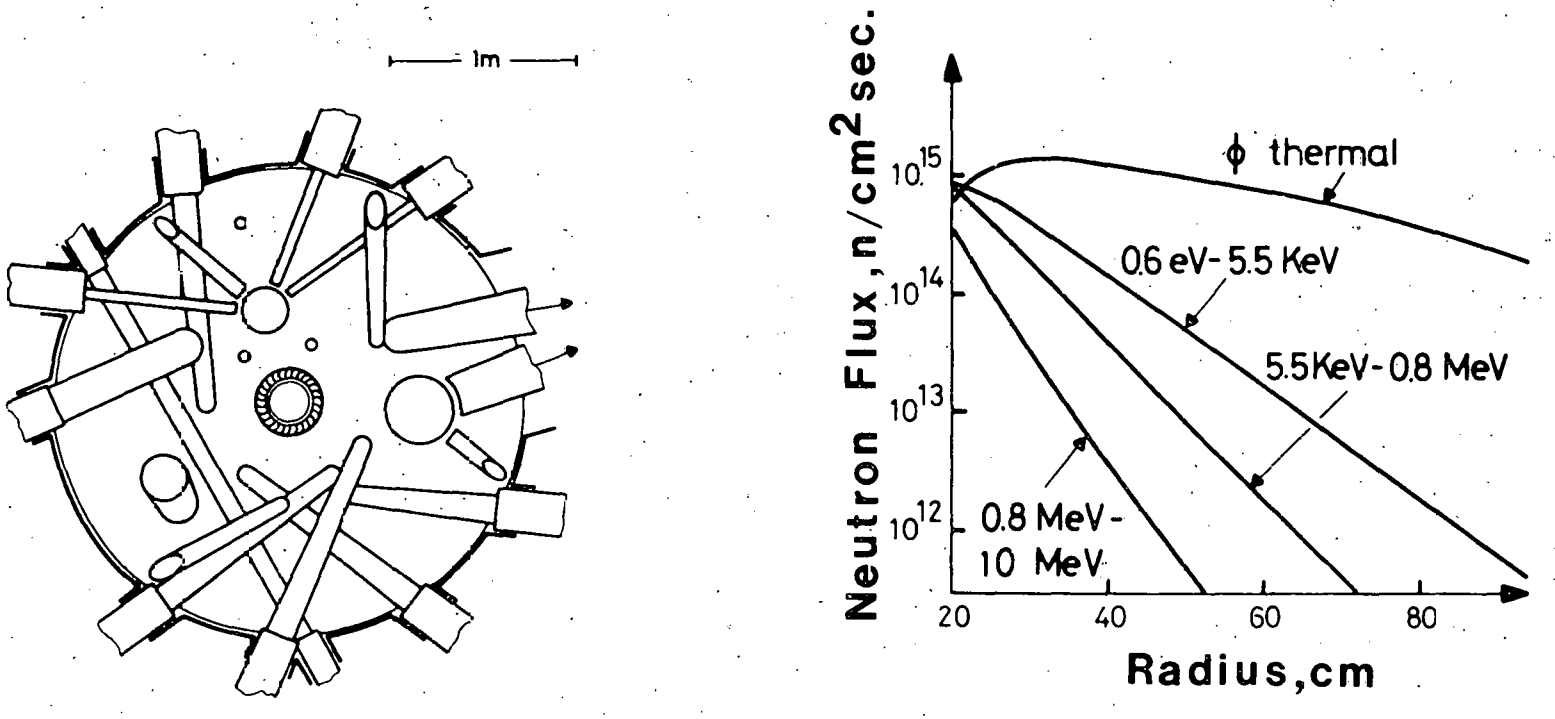

Fig. 6. Beam-Tube Layout and Neutron-Flux Intensities Outside the Core of the High-Flux Reactor at Grenoble.[9]

of this type constructed at Dubna is shown in Fig. 7. It is designed to produce pulses with ≈100 μsec width and a peak thermal-neutron flux of $\approx 10^{16} - 10^{17}$ n/cmlsec (Schabalin[10]). The figure shows a mechanical chopper on one of the flight paths.

In several instances, underground-nuclear explosions have been used in capture-cross-section measurements (Diven[11]). The high-intensity one-event pulse has the advantage of low background and thus permits the measurement of highly radioactive samples. However, detectors and recording devices have to be adapted to this completely different experimental situation.

A special device used in neutron-capture-cross-section measurements is the lead-slowing-down spectrometer. It consists of a large pile of lead (e.g. 1.6 x 1.6 x 1.6 m, Mitzel and Plendl[12]) into which bursts of fast neutrons are injected with a primary source (LINAC or electrostatic accelerator). The slowing-down neutron field in the pile is used as a neutron source with the energy determined by the time dependence of the moderation:

$$\overline{E_n(t)} = a(t + b)^{-2} \qquad (6)$$

where t is the time after neutron injection, and a and b are constants. The intensity of the neutron field follows from age-theory:

$$\ell n[n(t)] = c \cdot \ell n[t] - t/T + d \qquad (7)$$

where n is the neutron density, T is the average neutron life-time in lead, and c and d are again constants. Both relationships are usually experimentally confirmed. The time-dependence of the average neutron energy can be confirmed with known resonance energies and the neutron intensity is measured with a well known cross section, e.g. the $^{10}B(n,\alpha)$ reaction. Although energy resolution is poor for lead-slowing-down spectrometers, they are a valuable source of energy-averaged quantities like resonance integrals or average cross sections in the lower-keV-energy range.

The white-neutron spectra obtained with LINAC's or cyclotrons restrict these sources to use with prompt-γ-ray detection techniques, whereas at electrostatic accelerators the absorption and the activation technique can be employed in addition. The neutron intensity is high enough only in reactors to utilize transmutation for spectrum-averaged measurements. Spectral-γ-ray measurements can be carried out using all types of sources. However, the higher neutron intensity obtained with reactors and LINAC's is favorable for these devices.

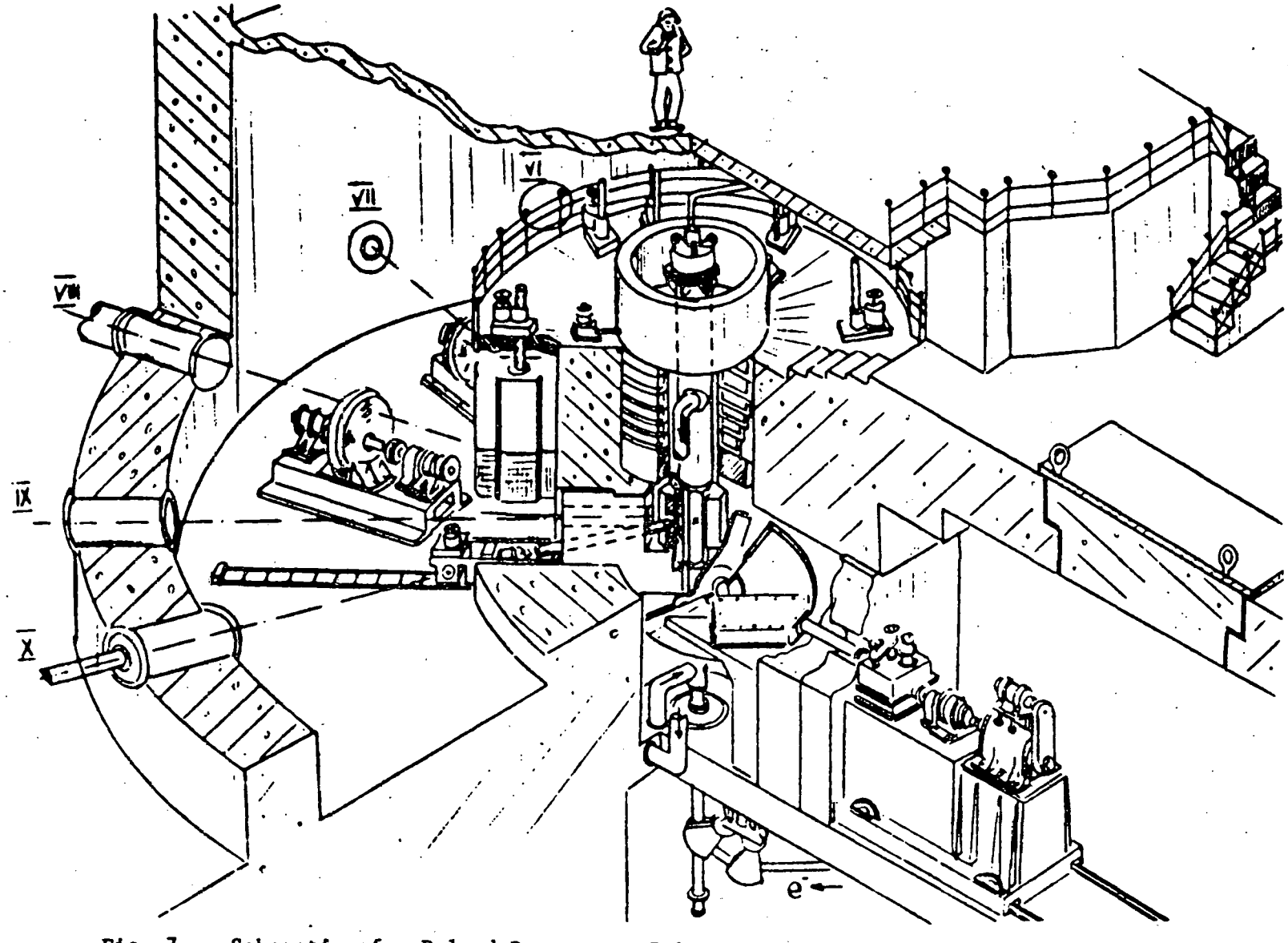

Fig. 7 Schematic of a Pulsed Reactor at Dubna. A Mechanical Chopper is Shown at One Flight Path.[10]

I.3. Neutron-Flux Measurements

The determination of the neutron-flux intensity is required in most cases for the analysis of capture-yield data and their reduction to cross-section values. The flux measurement can be avoided if the measurement is made relative to another capture cross section which is well known. This procedure not only eliminates the need to determine the neutron flux but also reduces, in some cases, the systematic uncertainties caused by the efficiency of the detector as well as corrections required for other measurement effects. The capture cross section of gold is now accepted as the standard for capture measurements and is often used in the thermal and fast-energy range. The cross sections for In(n,γ), Ag(n,γ), I(n,γ) and Ta(n,γ) have been occasionally used as references in the past.

Resonance structure in the resolved-resonance range and cross-section fluctuations in the unresolved-resonance-energy range make measurements relative to a capture cross section impractical and reactions with smooth cross sections are utilized. The cross section of the ^{10}B(n,α) reaction is often used, with ionization chambers as detectors. The ^{10}B(n,α) cross section varies smoothly with energy, is large, and has a $1/\sqrt{E}$ dependence below a few keV. The use of the ^{10}B(n;α,γ) cross section; detecting the γ ray with the same detector as employed for the measurement of the capture events, has the advantage of canceling the geometry factor of the detection probability. More recently, the ^{6}Li(n,α) cross section was utilized, with lithium - glass detectors providing a convenient instrument. The cross section for this reaction also varies with energy as $1/\sqrt{E}$ up to $\approx$10 keV. A resonance at 240 keV determines its shape in the keV-energy range.

At higher energies, the well known H(n,n) cross section or neutron monitors calibrated with various other techniques are occasionally used in capture cross section measurements; however, more often the well known ^{235}U(n,f) cross section is utilized as a reference.

II. Capture-Event Detection Techniques

II.1. Indirect Detection Techniques

II.1.1. Absorption and Transmutation Measurements

Elastic scattering and neutron capture are often the only possible reactions below the first inelastic scattering threshold. Some exceptions are nuclei for which the (n,p) or (n,α) reactions or the neutron-fission process are possible. For much of the low-energy range, and for many nuclei, the capture cross section is larger than the scattering cross section ($\sigma_{n,\gamma} > \sigma_{n,n}$, and $\Gamma_\gamma > \Gamma_n$), and it can be obtained as the difference between the total cross section and the elastic-scattering cross section. At thermal energies this is a simple cross section difference, however, in the resolved-resonance range the analysis is more complicated and will be discussed below. Specifically, for $\sigma_{n,\gamma} \approx \sigma_{tot}$ ($\Gamma_\gamma \approx \Gamma$), the uncertainty of determining the capture events via the neutron absorption (which is measured as a difference between the total cross section and the elastic-scattering cross section) can be expected to be less than with a direct measurement of the capture cross section. This is because the total cross section is determined with the self-normalizing transmission technique, and the uncertainty of the scattering-cross-section measurement becomes less important if it is only a small fraction of the total. The determination of the capture cross section is of specific interest below the threshold for coherent scattering where the total cross section consists only of the absorption cross section, the incoherent scattering and the thermal-inelastic-scattering cross section which goes to zero for zero temperature.

There are several other techniques which permit the determination of accurate thermal-neutron-absorption cross sections. The measurement of the "danger coefficient" for a sample introduced into a reactor core involves the determination of the change in the multiplication constant which is caused by the neutron absorption in the sample material. This method has been superseded by the pile-oscillator technique which proved more sensitive to the measurement of absorption and less dependent on long-term drifts of the reactor power. The fluctuation of the neutron field due to the oscillating sample is observed and gives a measure for the sample absorption relative to a standard (e.g. gold or boron). Another technique for determining the absorption cross section is the measurement of the decay constant of a neutron pulse injected into a moderating medium which contains the absorber. These techniques were very important for the determination of accurate thermal cross sections and are discussed in detail by Hughes[13] and Beckurts and Wirtz.[14] They fall into the subject area of neutron fields, and will not be further discussed here. However, it should be mentioned that the absorption measurement with a pulsed-neutron field was also applied for measurements of capture cross sections at 30 keV (Miessner and Arai[15]). The result in this case is an effective-absorption cross section which includes the resonance-self-shielding effect.

The spherical-shell-transmission method was employed to measure the absorption cross section at higher energies where $\sigma_{n,n} > \sigma_{n,\gamma}$, in particular at 23 KeV with Sb - Be(γ,n) sources. A typical arrangement is shown in Fig. 8 (Schmitt and Cook[16]). In these measurements the neutron source or the detector are surrounded with a spherical shell of the sample material. The count rate of the detector with the shell around the source is reduced by the neutrons absorbed and scattered in the sample material between the source and the detector; however, all losses due to scattering are substituted by neutrons in scattered from other parts of the spherical shell. The advantage of this method is that it has the self-normalization feature of the transmission technique. Unfortunately, rather thick spherical shells must be used and require substantial corrections for capture events of multiple scattered neutrons and for resonance self-shielding effects. Some of the original measurements (Macklin et al.[17], Schmitt and Cook[16], and Belanova et al.[18,19]) were recently reanalyzed with Monte-Carlo techniques (Bogart and Semler[20], Miller and Poenitz[21], and Froehner[22]) resulting in substantial changes of the originally reported cross sections. The Monte-Carlo calculations are still sensitive to input parameters (as, for example, the neutron-strength function and level spacings), and the uncertainties of results obtained with this technique are usually not less than $\approx$5%. Figure 9 shows the original result obtained by Schmitt and Cook[16] for the absorption cross section of ^{197}Au at 23 keV, an analytical reinterpretation by Schmitt[23], as well as the results from several Monte-Carlo analysis of this experiment. Also shown are two more recent measurements using the activation technique at the same neutron energy (Ryves et al.[24], Pauw[25]). However, the independence of the spherical-shell-transmission method from neutron-flux measurements and detector efficiencies provides an incentive to utilize this technique for the measurement of important cross sections which are difficult to measure with other techniques, e.g. ^{238}U(n,γ) (Dietze[26]).

Some other measurements were made in order to determine the absorption cross section even where $\sigma_{n,n} >> \sigma_{n,\gamma}$. These experiments were designed to achieve identical efficiencies for the detection of the scattered and the transmitted neutrons from a sample (Langsdorf[27], Pavlenko and Gridak[28]). However, the basic problems of secondary-neutron capture and resonance self-shielding is similar to that for the spherical-shell-transmission technique.

The transmutation technique is infrequently used due to the insensitivity of the isotopic-mass analysis. The fraction of nuclei which is captured in a sample irradiated in a neutron flux ϕ for one year is $\approx 3 \cdot 10^7 \cdot \phi \cdot \sigma_{n,\gamma}$. The reproducibility of the isotopic-mass analysis is $\approx$0.1 - 0.3%. Requiring a minimum uncertainty of $\approx$1% leads to the requirement $\phi \cdot \sigma_{n,\gamma} > 5 \cdot 10^{-9}$ which, even for a high flux reactor with $\phi \approx 10^{15}$, results in a restriction for the applicability of this measurement technique to cross sections with $\sigma > 500$ b. Smaller cross sections can, of course, be determined with a larger uncertainty.

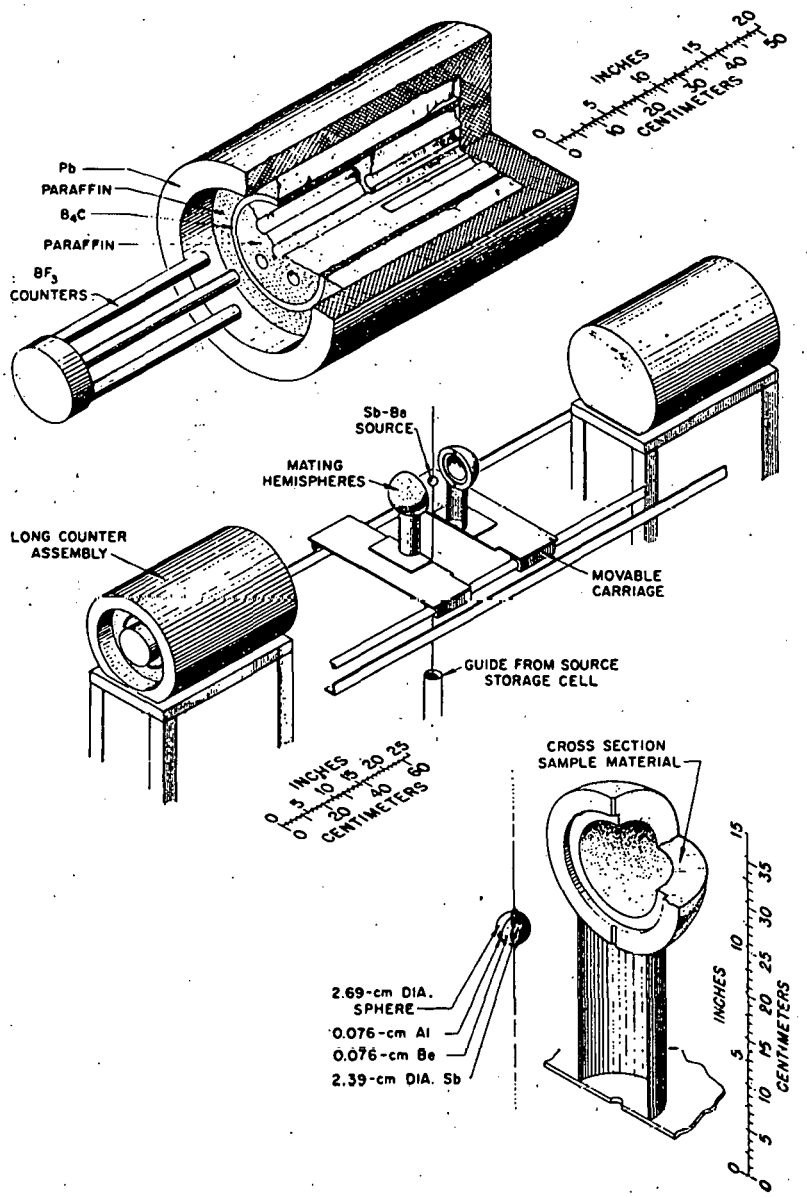

Fig. 8. Experimental Arrangement for the Measurement of Neutron-Absorption Cross Sections by the Spherical-Shell-Transmission Technique.[16]

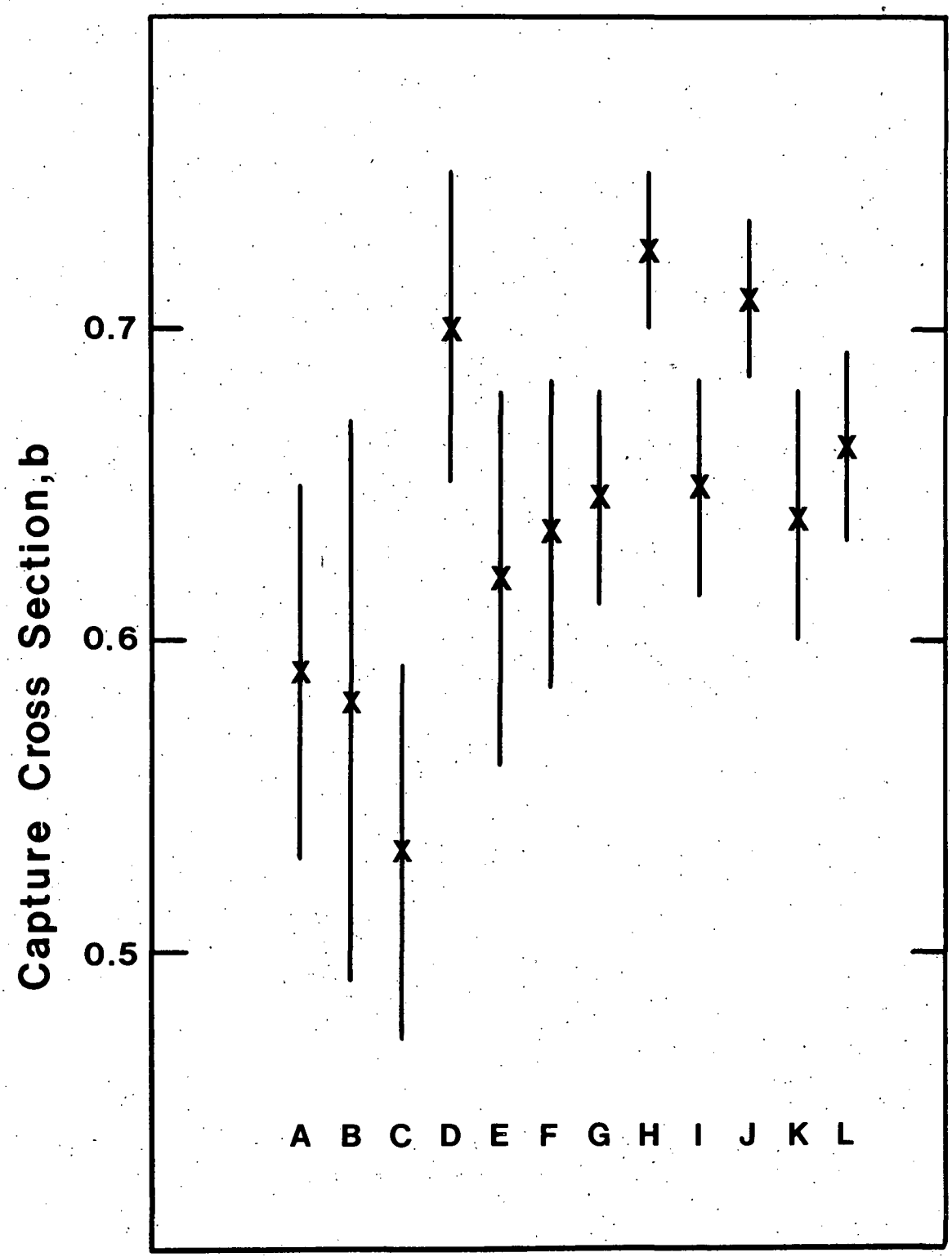

Fig. 9. The Original Results for the ^{197}Au (n,γ) Cross Section Obtained by the Spherical Shell Transmission Technique (A,B,Ref. 16), An Analytical Reinterpretation (C,Ref. 23), Monte-Carlo Interpretations (D-J, Refs. 20, 22), and Values Obtained in Activation-Cross-Section Measurements (K,Ref. 24,L,Ref. 25).

II.1.2. The Activation Technique

The application of the activation technique to the measuement of capture events is restricted to about one third of all stable nuclei. This fraction is further reduced due to the very short or long half-lives of some of the radioactive nuclei which result from the neutron-capture process. The restriction for the measurement of short half-lives can be overcome to some extent by the use of fast-sample-transport systems between the irradiation site and the activity detector, e.g. pneumatic tubes and rotating or stepping wheels. In some cases, the γ-ray cascades which de-excite the compound nucleus end on an isomeric state which then decays with a different half-life to the ground state and/or to the daughter nuclei. In this case, the measured activity yields only a partial capture cross section. The isomeric-cross-section ratios derived from these partial-capture cross sections are of some interest, however, in order to obtain the total-capture cross section all the partial cross sections must be measured and summed in accordance with the decay branches. For some nuclei it is more convenient to measure the decay of the daughter nuclei resulting from the primary decay.

The experiment usually consists of irradiating a sample for a time, T, in a neutron flux, ϕ, transferring it to a detector with a time, t, elapsing between the end of the irradiation and the beginning of a counting period, Θ. The number of counts obtained in Θ is then given by

$$C = \varepsilon_k \cdot n \cdot \phi \cdot \Sigma \sigma_i \Sigma b_{ik} K_{ik} \quad ,$$

where ε is the efficiency for counting specific β's or γ's occurring in the decay of the daughter, grand-daughter, etc., nuclei, and σ_i is the cross section for forming an isomer (i = m) or ground state (i = g) nuclei in the capture process. The b_{ik}'s are the frequencies with which the observed radiation occurs per decay of the activated isomeric or ground state. The K_{ik} are time factors which can be obtained from the differential equations discribing radioactive-decay chains (Evans[29]) and appropriate boundary conditions:

$$K_1 = F_1$$

$$K_2 = a_{21}F_1 + a_{12}F_2$$

$$K_3 = a_{21}a_{31}F_1 + a_{12}a_{32}F_2 + a_{13}a_{23}F_3$$

$$\vdots$$

with $F_i = \frac{1}{\lambda_i}\,(1 - e^{-\lambda_i \tau})\, e^{-\lambda_i \tau}\,(1 - e^{-\lambda_i \Theta})$

and $a_{ik} = \frac{\lambda_i}{\lambda_i - \lambda_k} = \frac{T_i}{T_k - T_i}$, $\lambda_i = \frac{\ell n 2}{T_i}$

T_i is the half-life of a particular unstable state with i = 1 for the activated nuclei, i = 2 for its daughter, i = 3 its grand-daughter, etc.

Although it had widespread use in the past, the activation technique is now less frequently employed owing to the development of reliable prompt detection techniques. It still has its justification in some important cases. Measurements of capture rates in neutron multiplying or moderating media can be easily carried out with higher accuracy, while other techniques would be less sensitive (transmutation) or disturb the geometry of the field (prompt detection techniques). For some nuclei, the capture rate can be determined with the activation technique with substantially less uncertainty than with the prompt-detection techniques. An example is the standard capture cross section of $^{197}Au(n,\gamma)^{198}Au$ where the ^{198}Au activity can be determined with probably 0.1% accuracy and certainly with less than 0.5% uncertainty by means of the $4\pi\beta - \gamma$ - coincidence technique (Champion[30]). Another example is the technologically important ^{238}U-capture process. The ^{239}U nuclei formed in the neutron-capture process decay with a half-life of 23.5 min to $^{239}Np(T_{1/2} = 2.355$ d) which is also formed in the decay of $^{243}Am(T_{1/2} = 7380$ y) (see Fig. 10). Detectors which are used to measure the decay of ^{239}Np (usually high-resolution Ge(Li)-detectors) can easily be calibrated with ^{243}Am sources which are in equilibrium with ^{239}Np - decays. The absolute ^{243}Am-α-decay rate can be accurately determined by low-geometry α counting. The same scheme can be employed for the measurement of $^{232}Th(n,\gamma)$ reaction rates. These techniques offer the potential of achieving an overall accuracy of $\lesssim$1%. The uncertainties for the determination of capture rates using prompt-detection techniques are larger by factors of 2-10. Other advantages of using the activation technique are complete isotopic selectivity and high sensitivity for counting decay-rates. The latter permits the use of

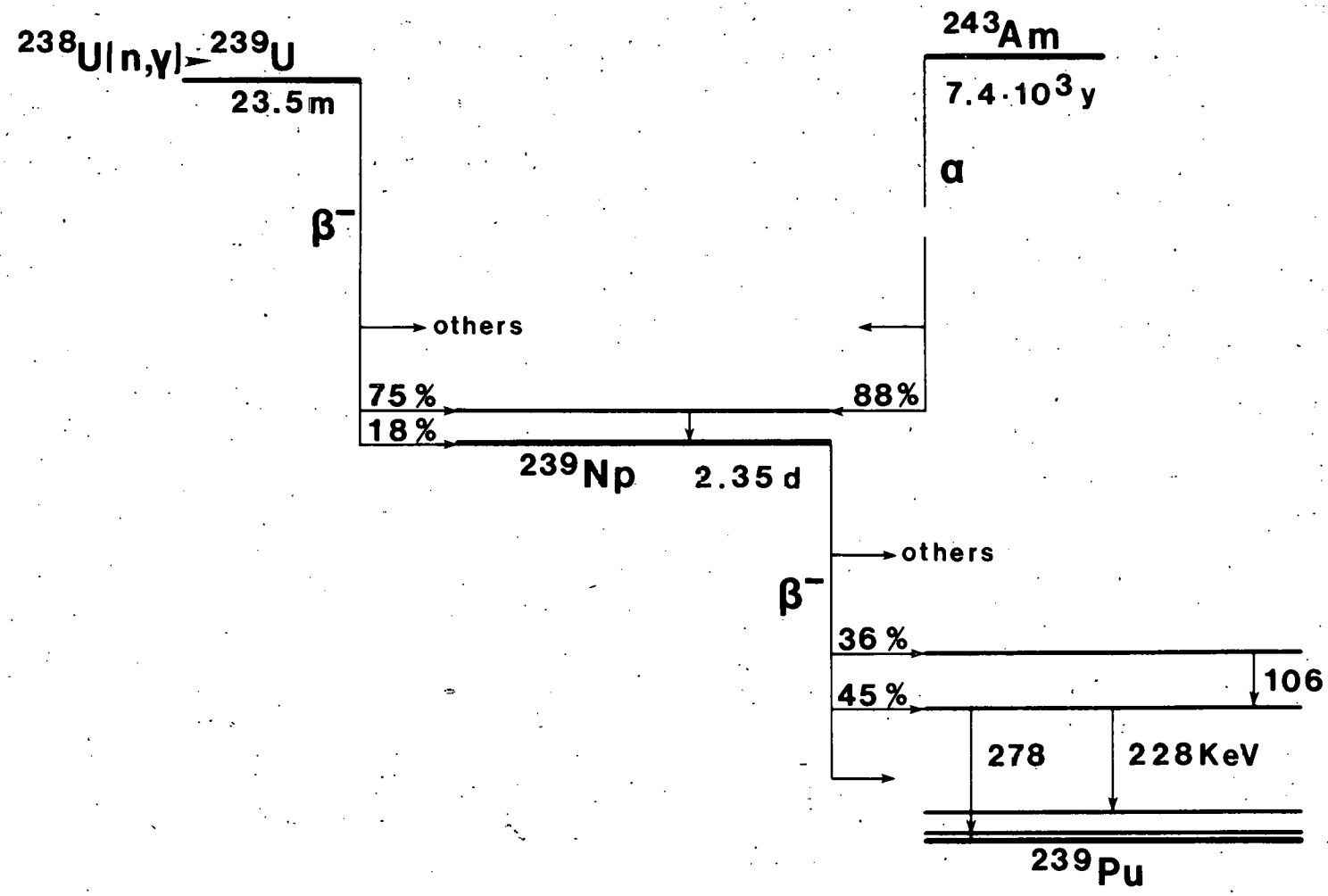

Fig. 10 Schematic of the Decays of ^{239}U and ^{243}Am via ^{239}Np to ^{239}Pu.

small samples, which reduces required corrections, and makes the measurement of small cross sections (≈μb) possible.

Measurements with the activation technique are restricted to spectrum-averaged quantities or require the use of monocromatic neutron sources. Thus, most data have been obtained in the thermal-energy range or in the fast-neutron-energy range. However, some measurements have been made in the resolved-resonance region, e.g. LeRigoleur et al.[31] found a previously-unobserved resonance at ≈35 keV in Na using the activation technique. A considerable advantage of this technique is that it provides independent data which might be used for the normalization of values obtained with the prompt detection technique. Therefore, measurements are often carried out only at selected neutron energies, utilizing specific sources. The Sb-Be(γ,n) source, the Fe-filtered-neutron beam from a reactor, and the kinematically-collimated-forward-neutron cones obtained close to the thresholds of the $^{7}Li(p,n)^{7}Be$ and the $T(p,n)^{3}He$ reactions provide such opportunities (e.g. Macklin et al.[32], Chrien et al.[33], Poenitz[34]). Irradiations at higher neutron energies are usually carried out at zero degree reaction angle using the neutron-source reactions $^{7}Li(p,n)^{7}Be$ or $T(p,n)^{3}He$ (e.g. Cox[35], Grench and Menlove[36]), or simultaneously at several angles utilizing the energy spread obtained in these reactions (e.g. Lindner et al.[37]). The use of the $^{51}V(p,n)^{51}Cr$ or $^{45}Sc(p,n)^{45}Ti$-neutron-source reactions offers the advantage of a direct neutron-flux determination by utilizing the associated ^{51}Cr- or ^{45}Ti-activities. The energy spread of these reactions is substantially less than for light-nuclei-(p,n) reactions, and activation cross sections can be measured by surrounding the source with the sample in a 4π-spherical geometry (e.g. Harris et al.[38]).

The decay of the radioactive nuclei produced in the neutron capture process can be measured by detecting the emitted β and/or γ rays. β rays are usually detected with 2π- or 4π-proportional counters. γ transitions between levels of the daughter nuclei may be detected with NaI(Tl)-scintillation counters or Ge(Li) detectors. The high resolution obtained with the latter has favored these in more recent applications. These measurements require corrections for β- and γ-self-absorption in the samples which can be avoided if the activity of the daughter nuclei is measured after chemical separation from the sample. In some cases, the emitted β rays can be measured directly as a current in an appropriately constructed counter; a method which finds application in reactor flux measurements with the $^{103}Rh(n,\gamma)^{104}Rh$ reaction (Warren et al.[39]). Measurements of the induced activity without any self-absorption effects are possible if the sample nuclei are part of the detector, as for example Na and I in a NaI(Tl)-scintillator detector (Bame and Cubitt[40]).

It is a substantial advantage for measurements in the fast-neutron-energy range, if accurate thermal cross section values are known from prior activation or absorption measurements. In this case, a similar sample of the β- or γ-counting equipment (Johnsrud et al.[41]). Results for the cross sections for the activation of the isomeric and ground states of ^{116}In by neutron capture in ^{115}In are shown in Fig. 11. These data were obtained using different reference cross sections ($^{235}U(n,f)$, $^{10}B(n,\alpha)$, $^{197}Au(n,\gamma)$), and are in good agreement.

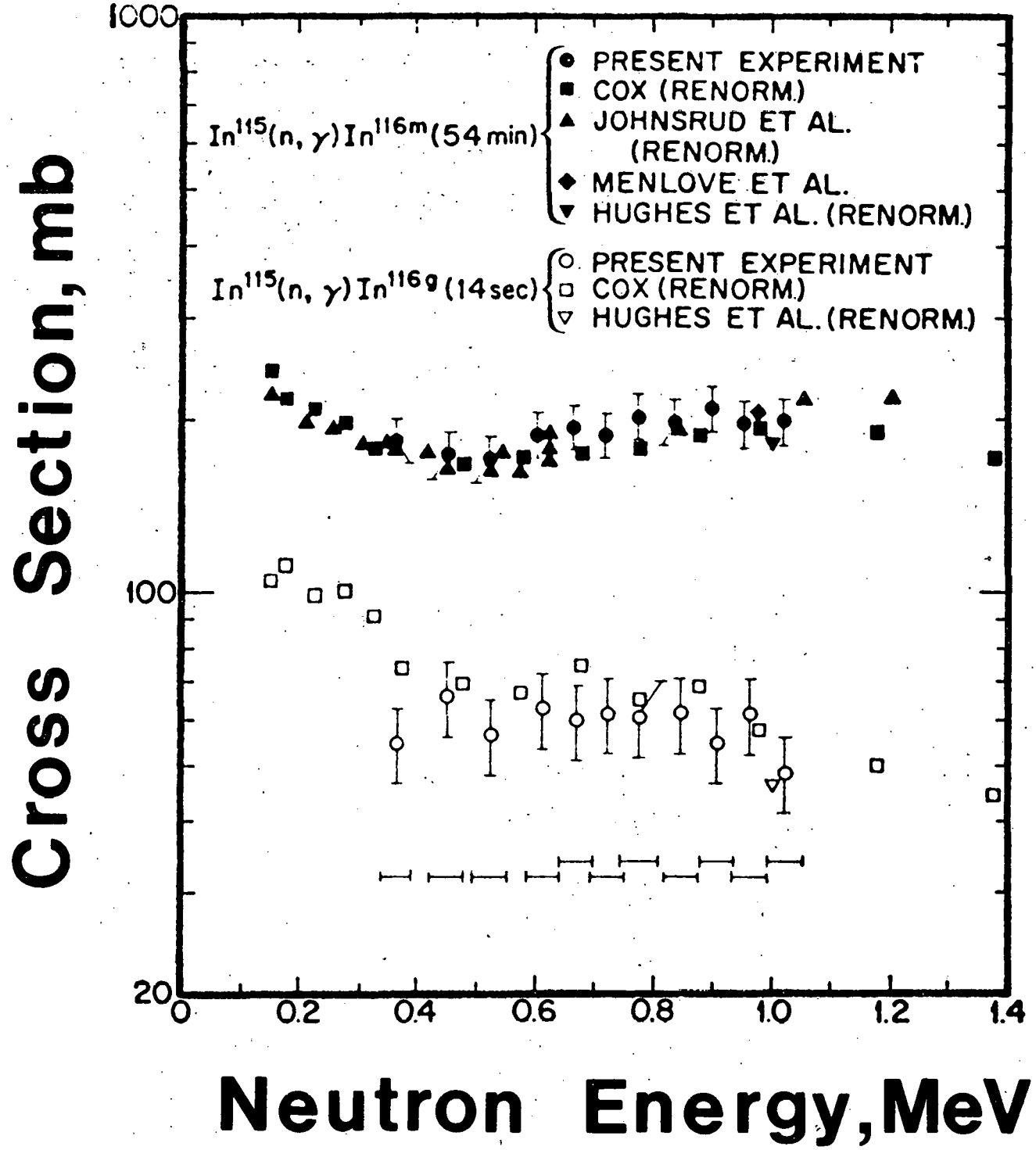

Fig. 11. Results for the Activation Cross Sections of ^{115}In Between 130 and 1400 keV.

II.2. Prompt-Radiation-Detection Techniques

The most generally applicable technique for the measurement of capture events is the detection of the electromagnetic radiation emitted promptly after the capture of the neutron. A number of different detection schemes and detectors have been developed over the years. They are favorable in some applications but have shortcomings in others. The majority of the available data has been obtained with these prompt detection techniques, particularly in the resolved-resonance-energy range. Historically, the detection of the prompt γ radiation was first made with rather small detectors, organic or inorganic crystals (e.g. Meservey[42], Albert and Gaerttner[43], Rae and Bowey[44]). Such detectors were sensitive to variations of the γ-ray spectra with neutron energy, e.g. from resonance to resonance, as discussed above. Later developments resulted in three major groups of detectors: i) total-γ-energy-absorption detectors, ii) γ-energy-propertional detectors, and iii) small spectral-sensitive detectors. The latter have been used in conjunction with appropriate procedures which compensate for the spectral sensitivity of the measured data.

II.2.1. Total-Radiation-Energy-Absorption Detectors

The principle of these detectors is to collect all prompt-γ-radiation energy emitted in the capture process. An ideal detector of this type would have a 4π-geometry around the capture sample; would be very large, and result in a δ-function response signal corresponding to the sum of the neutron-binding energy and the center-of-mass energy of the primary neutron. Capture events could be well separated from inelastic scattering events ((n;n,γ) and (n;γ,n')) because of the difference in the total amounts of γ-radiation energy released. The size of the detector required to absorb essentially all γ radiation from the capture sample is determined by the primary γ spectrum on the one hand, and by the interaction probability of the γ rays in the absorbing material on the other hand. In practice, the principle of such a detector is realized with a scintillator material which converts the γ rays to electrons and subsequently to light which is detected at the scintillator surface with photomultipliers. Most often, a liquid scintillator is used. The radius of a typical liquid scintillator required to achieve an intrinsic efficiency (probability that an interaction of the γ ray takes place in the scintillator) of 99% would be ≈3m, assuming the emission of a single γ ray of ≈10 MeV. A detector of this size would have a volume about 30 times larger than the largest detector built so far for neutron-capture-cross-section measurements. It would be impractical, costly and suffer from many problems, e.g. high background. Fortunately, the γ-ray multiplicity is larger than unity for most capture-γ-ray cascades and the intrinsic efficiency of much-smaller detectors can be expected to be sufficiently high. Figure 12 shows the intrinsic efficiency calculated by Kompe[45] for a detector with a radius of 55 cm, for γ-ray-cascade multiplicities of n = 1,2, and 3. These calculations were carried out using the simplifying assumption that the γ-ray energies are equal for any specific cascade. The figure shows that a sufficiently large intrinsic efficiency can be obtained for a multiplicity of 3. The average γ-ray multiplicity for medium and heavy mass nuclei is 3 to 4. However, light nuclei, e.g. Ni, may have a large fraction of transitions to the ground state or other low-lying states, and consequently a lower cascade multiplicity. This will result in a lower intrinsic efficiency and differences in the observed γ-ray-pulse-height spectrum at different energies as shown in Fig. 13 (Ernst et al.[46]).

In practice, a detector will consist of a large volume tank filled with liquid scintillator. Various liquid scintillators can be used; however, cost and safety considerations suggest pseudocumene (1,2,4-trimethylbenzene) as a solvent which has a reasonably safe flash-point and is available with sufficient purity at comparatively low costs. A scintillator, e.g. p-therphenyl, and a wavelength shifter are added to the solvent. The inside of the tank is painted with a light reflector and photomultipliers mounted on the surface of the tank view the scintillation light. A channel through the tank provides for the transmission of the neutron beam and the insertion of the capture samples.

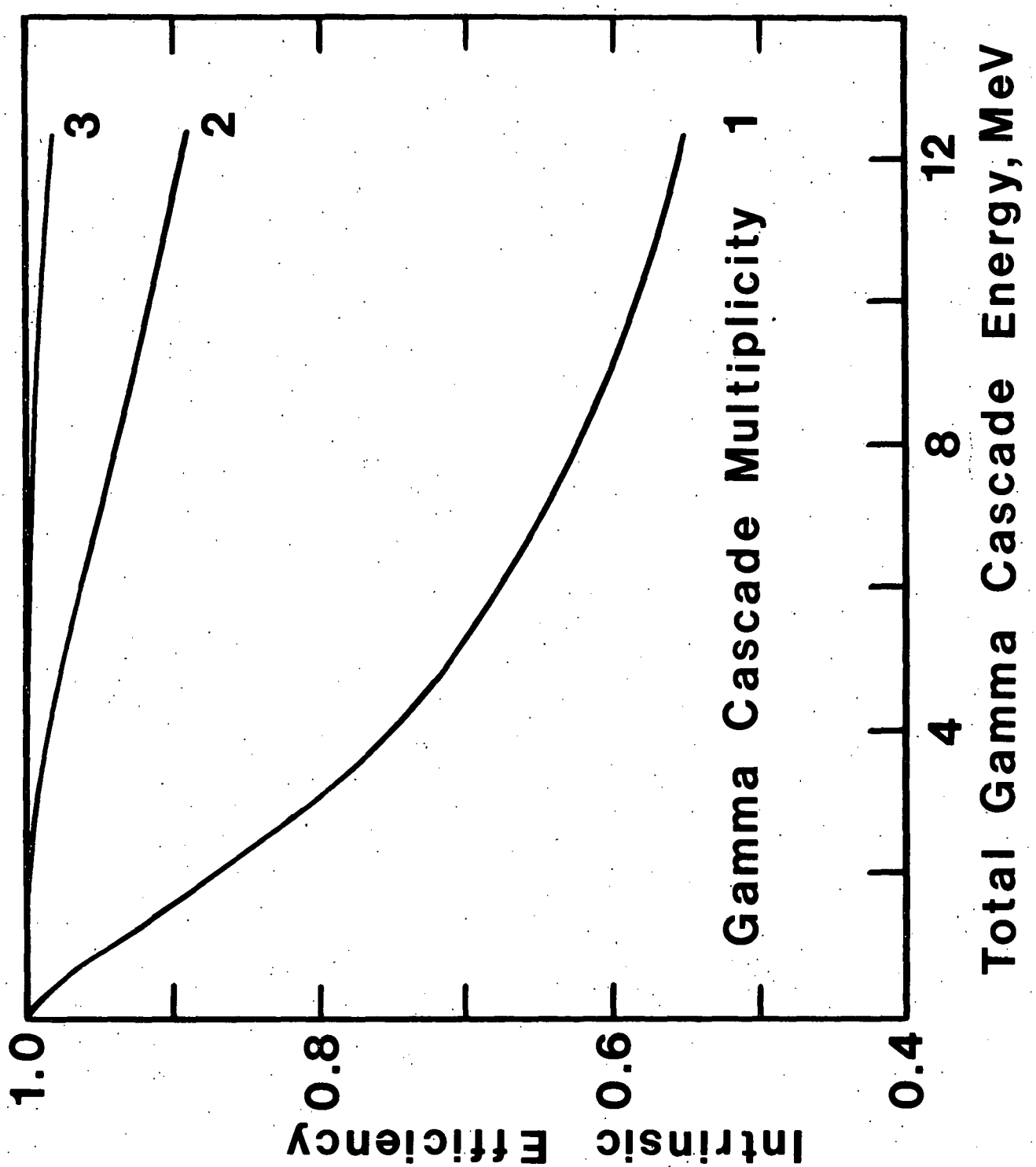

Fig. 12. Calculated Intrinsic Efficiency of a 800 liter Large Liquid Scintillation Detector.[45]

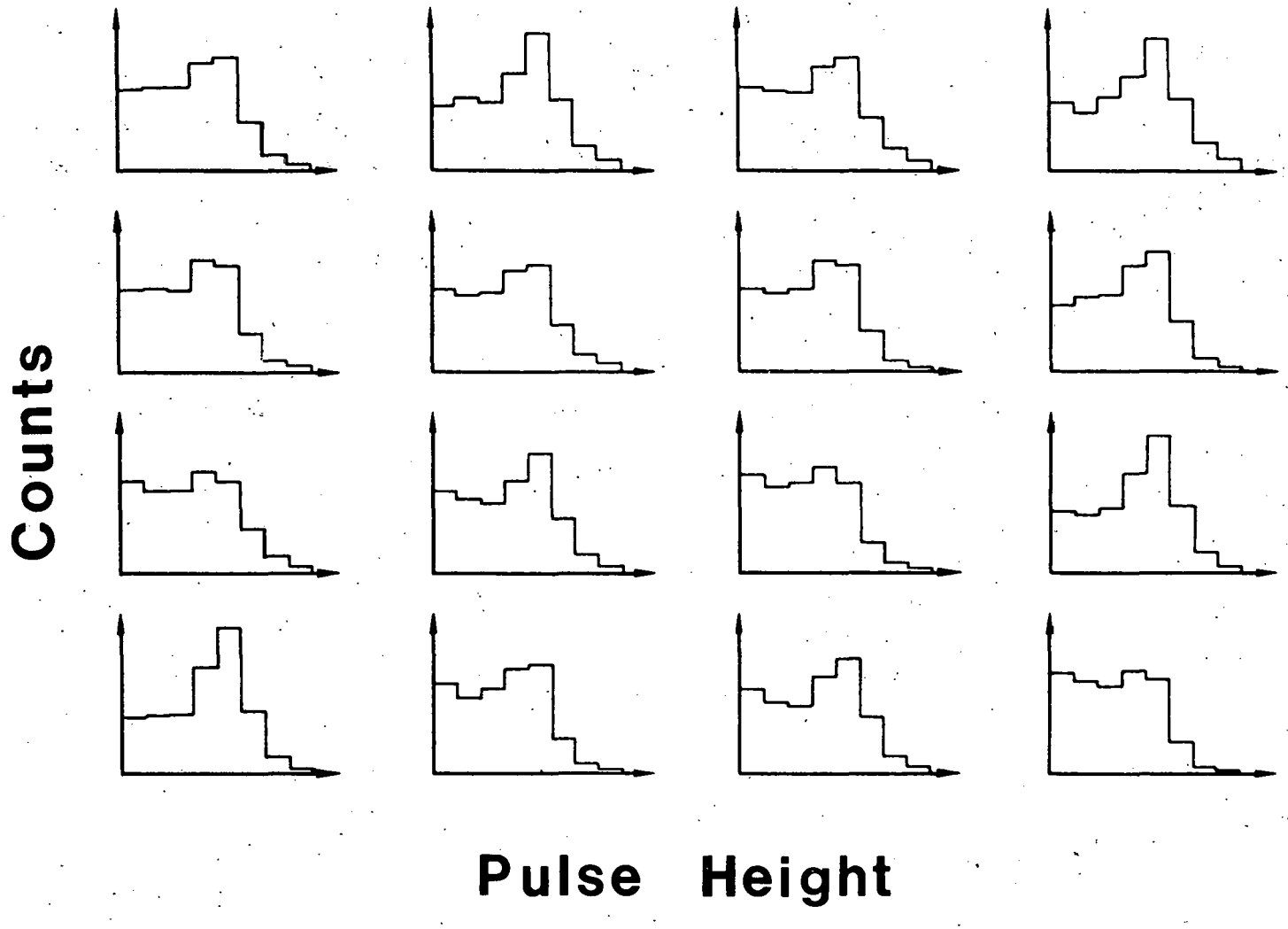

Fig. 13. Variations of the Pulse-Height Spectra Obtained with a Large Liquid-Scintillation Detector at Different Neutron Energies for the Ni(n,γ) Reaction.[46]

The background of such a detector is the major limiting factor for choosing a large detector size with a correspondingly high intrinsic efficiency. Background is caused by a variety of sources. Cosmic rays and environmental radiation are expected to be ambient and proportional to the cross section and the volume of the detector. Figure 14 shows the background from these sources for the ≈800-liter-liquid-scintillator tank by Kompe.[45] Though appropriate shielding can substantially reduce the background caused by environmental radiation, it is still very large at low energies and requires the setting of a threshold for the detection of events, corresponding to γ energies of 1-3 MeV. Background from cosmic radiation can be substantially reduced with an anticoincidence shield, however, the total count rate is not very large, and the corresponding detector pulses are usually beyond of the range of the capture γ-ray spectrum due to the energetic nature of the cosmic rays.

Some of the non-ambient background is caused by neutrons scattered from the sample. These neutrons are slowed down in the scintillator and captured in hydrogen producing 2.2-MeV-γ rays which are detected with high efficiency. In order to reduce this background, methylborate is added to the liquid scintillator which causes these moderated neutrons to be captured by the $^{10}B(n,\alpha)$ reaction. Capture-γ rays are also produced by the scattered neutrons in the through-tube material and for measurements at low neutron energies ^{6}LiH liners can be inserted in the tube in order to reduce the amount of scattered neutrons reaching the tube and the scintillator. Other non-ambient background is due to source neutrons which are captured or inelastically scattered in the surrounding materials of the room, or, directly penetrate the detector shielding.

Taking into account the threshold required to reduce the background-count rate and to eliminate inelastic events, the efficiency, η, of the detector for counting capture events can be expressed as a product of the intrinsic efficiency, ε, and the spectrum fraction, s,

$$\eta = \varepsilon \cdot s \quad . \tag{8}$$

The spectrum fraction is determined by a variety of effects. The final size of the detector causes some of the γ rays of a cascade to escape from the tank, or they escape after only a partial energy loss in a Compton-scattering event. Light absorption and the nonlinearity of the light production in the scintillator are other factors which result in pulses smaller than those corresponding to the δ-function expected from an ideal detector. Figure 15 shows experimental spectra obtained for two different large liquid-scintillator detectors of similar size (1100 liter and 1300 liter). The low-energy threshold is usually fixed in a specific experiment. It is chosen to reduce of the size of the background, and is set above the maximum γ-ray energy resulting from the inelastic processes. The spectrum fraction is determined by extrapolation to zero pulse height. This extrapolation is very uncertain because measurements of the spectrum shape below 1 MeV are usually not feasible due to the high background. The problem is, of course, much greater for nuclei with a low neutron-binding energy (like ^{238}U) because the spectrum fraction is then smaller. The spectrum fraction is a function of the

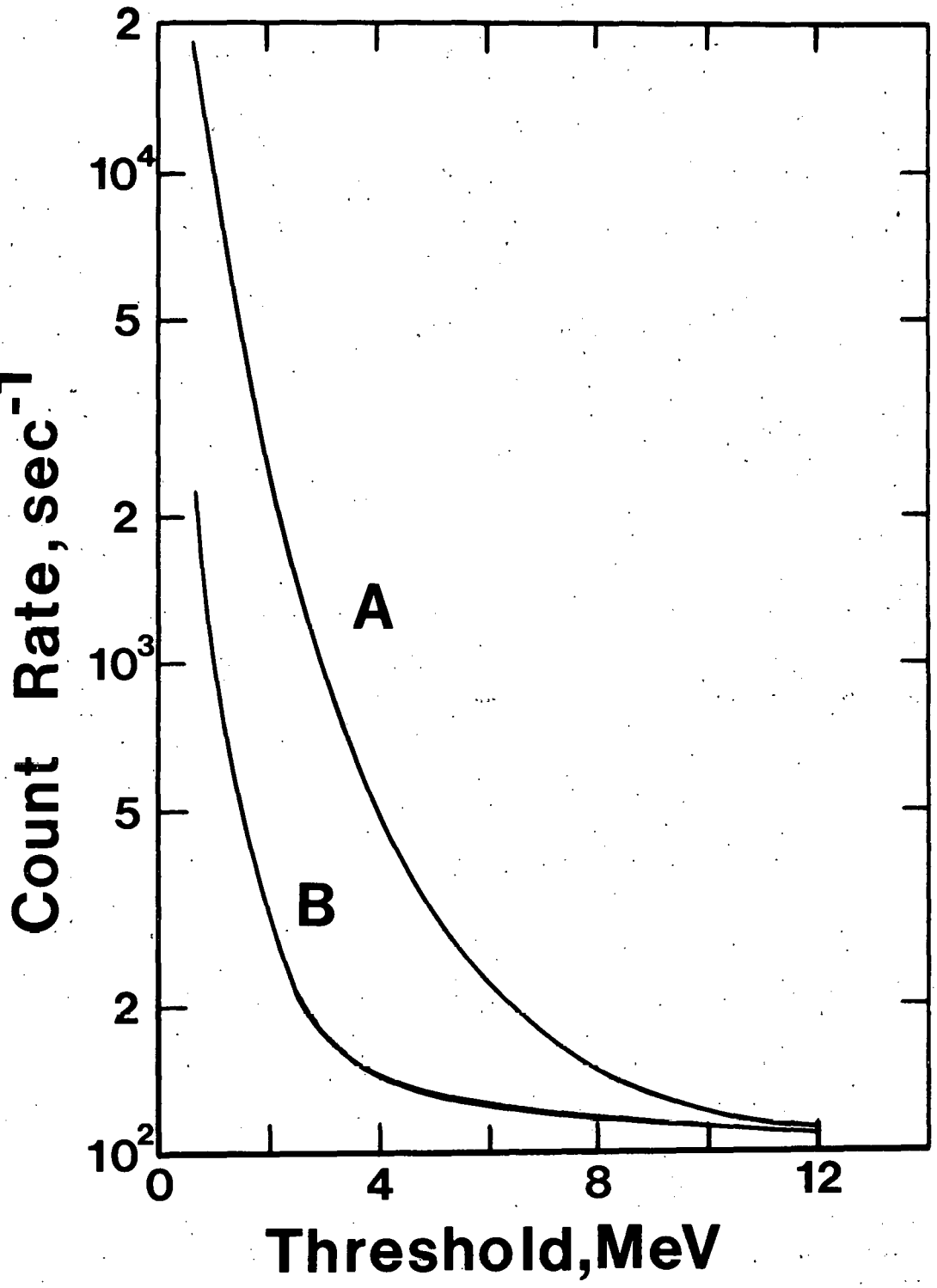

Fig. 14. Background Count Rates Obtained with an 800-liter-Liquid-Scintillation Detector. A is without, B with a 10-cm-thick 4π - Lead Shield.[45]

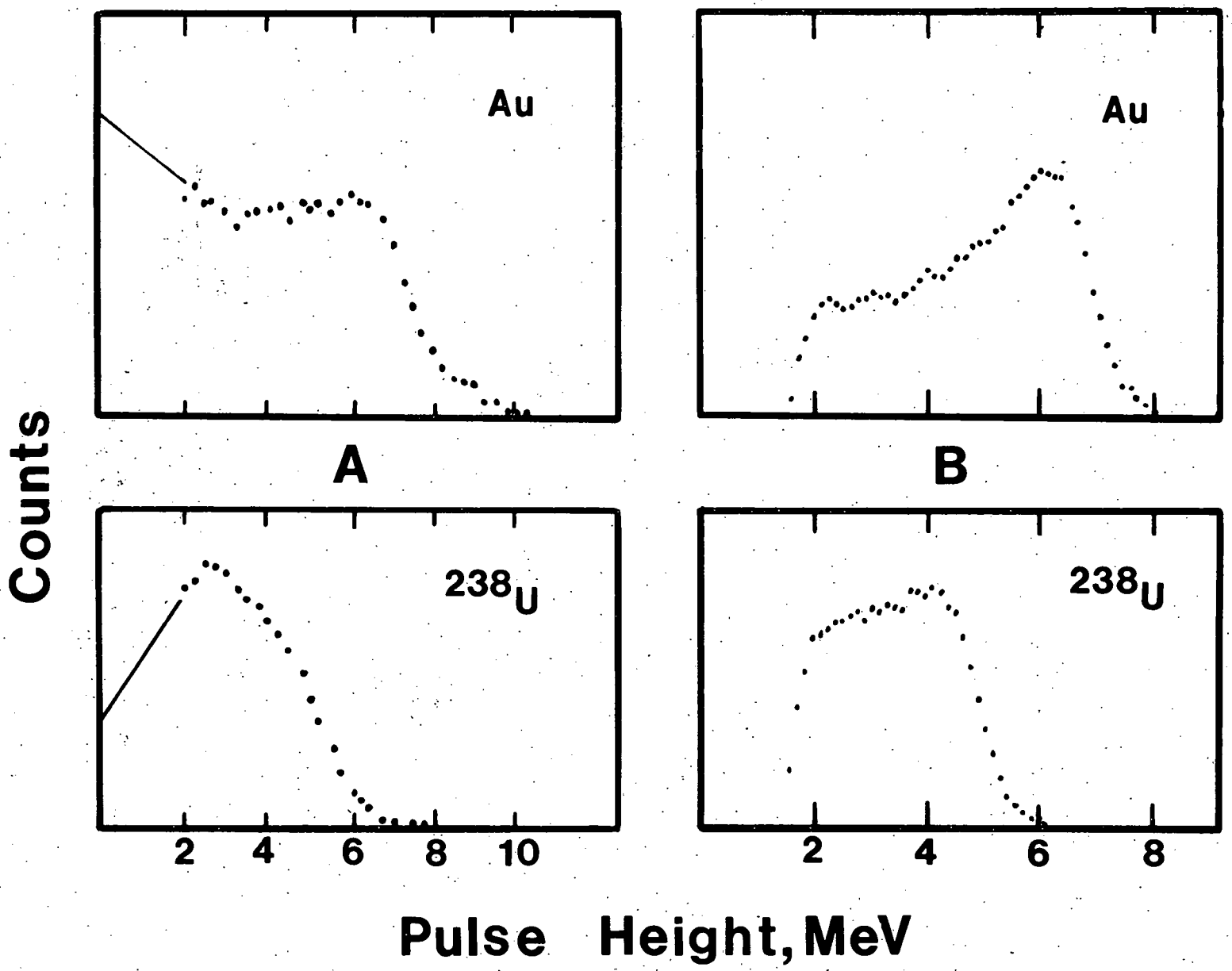

Fig. 15. Pulse-Height Spectra Obtained with (A 1100 liters, B 1300 liters) Large Liquid-Scintillation Detectors for ^{197}Au (n,γ) and ^{238}U (n,γ).

primary neutron energy because a larger fraction of pulses will be above the detection threshold for a higher total γ-cascade energy.

There are several advantages of the large liquid-scintillator detector over other prompt γ-ray detectors. It has a discrimination feasibility against inelastic-neutron-scattering events without compromising its basic principle. It also does not require a normalization as long as the intrinsic efficiency and the spectrum fraction are large enough. The major disadvantages are the costs of the detector, its size, and the large background with related shielding requirements. As a result of these disadvantages few large liquid scintillators were built in the last ten years, although many such detectors are still in operation. Only a few of them will be mentioned here.

The first large liquid-scintillator detectors were designed by Diven et al.[47] The two tanks had cylindrical shape and volumes of ≈60 and ≈525 liters. Twenty-eight 5" - photomultipliers were mounted in four rows of seven each at the outside of the cylinder surface of the larger tank. The counting efficiencies of these detectors were ≈50% and ≈75%, respectively, with a bias corresponding to 3-MeV γ-ray energy. Pulse-height spectra were measured using 400 keV neutrons and the time-of-flight technique for background suppression. Figure 16 shows spectra obtained by Diven et al. for a silver sample with these two detectors. The smaller tank does not fulfill the objective of summing up the total-radiation energy released in the capture events. With the larger detector, Diven et al. measured the capture cross sections of 28 elements between 175 and 1000-keV-neutron energy, using monoenergetic neutrons obtained with a Van-de-Graaff accelerator.

A very large liquid-scintillator detector was built by Haddad et al.[48] It has a total volume of 4000 liters, and is thus the largest existing detector of this type. The detector consists of a smaller cylindrical tank of ≈600 liters which surrounds the capture sample. Forty-four additional long-, cylindrically-shaped-plexiglas containers with photomultipliers at each end were positioned around the inner tank (see Fig. 17). A decaline-base scintillator was used which is compatible with the plexiglas containers. Measurements of the γ-energy spectra with this high-efficiency detector show a substantial improvement for the summation of the total radiation energy released in the capture events compared with detectors of a smaller size. A Monte-Carlo calculation for monoenergetic γ rays (cascade multiplicity of one) predicted an intrinsic efficiency of ≈80% for 8 MeV compared with only ~63% for the 800 liter tank built by Kompe (see Fig. 12). The modular construction of this detector permits its use with different sized configurations, thus varying the background level. A smaller-size detector will prove adequate for measurements of nuclei which have a high γ-cascade multiplicity. Measurements were carried out with this detector at a LINAC facility using three different configurations: a minimal 600-liter size, a median size of 2400 liters, and the full-sized detector of 4000 liters. Data were obtained for a large number of isotopic and elemental samples in the resolved-neutron-resonance region and in the keV-energy range.

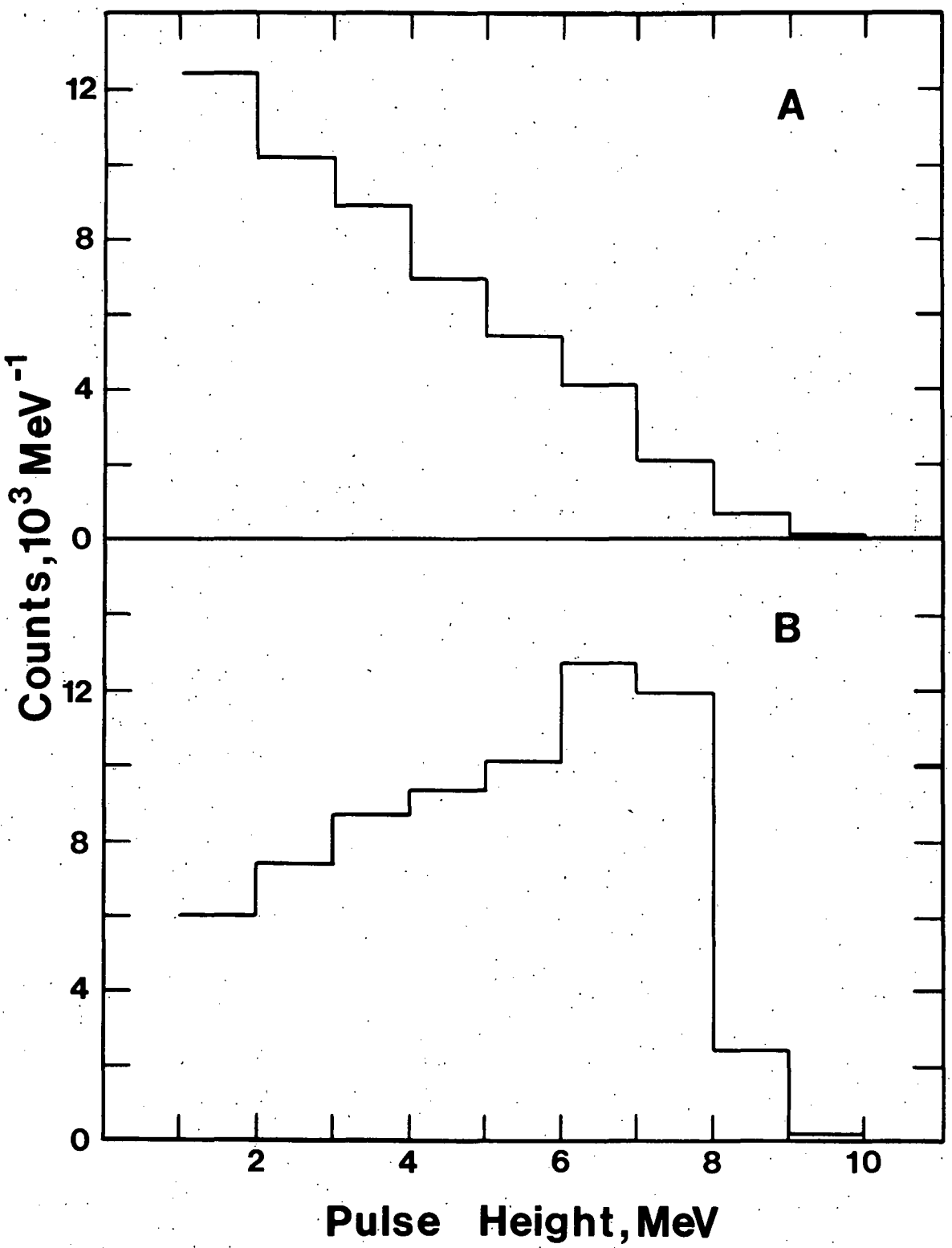

Fig. 16. Pulse-Height Spectra Obtained with (A, 60 liters, B 525 liters) Large Liquid-Scintillation Detectors for Ag (n,γ). The Volume of the 60-liters Detector is Insufficient to Achieve the Required Gamma-Energy Summation.[47]

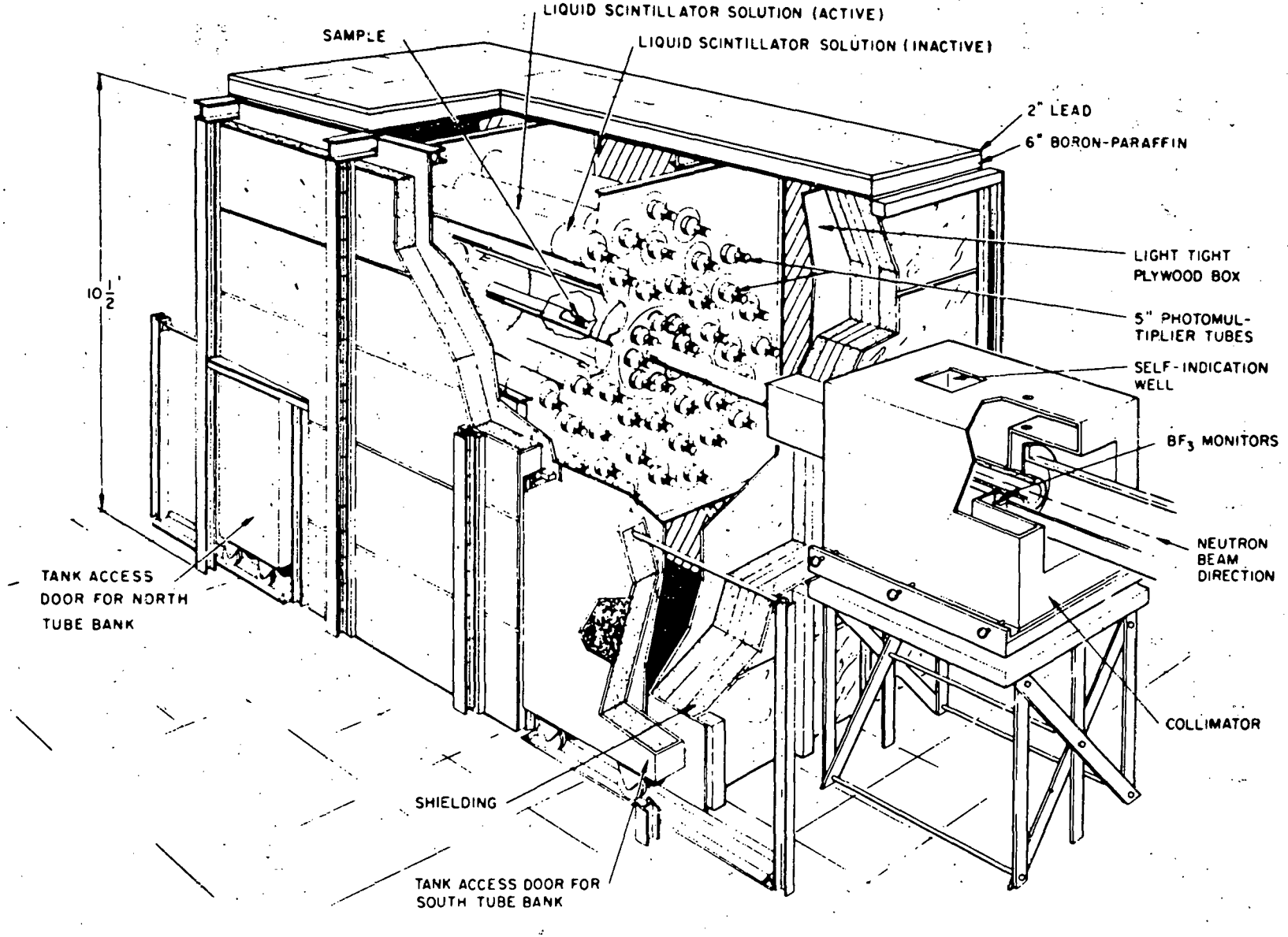

Fig. 17. The 4000-liters Large Liquid-Scintillation Detector by Haddad et al.[48]

An 800-liter tank was constructed by Kompe[45] at Karlsruhe. The tank approximates a sphere in shape and was used in capture-cross-section measurements in the keV-energy range for many elements and isotopes. A time-resolution of ≈3 nsec was achieved with this detector by using 12 fast photomultipliers (57 AVP) which were distributed equally spaced over the surface of the tank. The time resolution of this detector was recently further improved to ≈2 nsec by using even faster photomultipliers (60 AVP). It is now the fastest of all large-liquid-scintillator detectors with a time-resolution close to the limit given by the time-of-flight at the light in the tank. Substantial fluctuations in capture cross sections were found with this detector in the keV-energy range where they were previously observed to vary smoothly with energy. A similar detector was built at Argonne National Laboaratory (Poenitz[49]), however, with a larger volume (1300 liters). The time resolution of this detector is ≈3 nsec and was achieved by matching of the individual photomultiplier timing, and the application of an on-line-computer rise-time correction. This detector was used for the measurement of the capture cross sections of ≈30 elements in the energy range from 0.4-4.0 MeV. An anticoincidence shield was used to reduce cosmic-ray background.

Another large-volume detector (≈3000 liters) was built at Oak Ridge National Laboratory (Silver et al.[50]). The tank has an elongated shape consisting of a central cylinder and two truncated cones which increase the interaction probability for γ rays emitted in the direction of the neutron-beam channel (see Fig. 18). Thirty-two fast photomultipliers (RCA 4522) are mounted on the outside surface of the tank. The time-resolution of the detector was found to be ≈6 nsec and the energy resolution was ~28% for the ^{60}Co sum-peak and ≈24% for the ^{24}Na peak. A Helmholtz-coil pair was used for eliminating the vertical component of the earth's magnetic field. A ^{6}LiH-liner in the beam tube reduced the amount of scattered neutrons which otherwise produce background. An aluminized-mylar barrier divided the tank into two halves and permits the use of the coincidence technique which reduces background by about a factor of 8. The relative count rates obtained with and without the coincidence requirement for ^{238}U(n,γ) are shown for a part of the time-of-flight spectrum in Fig. 19. The substantial improvement in the count-to-background ratio is most obvious between the compound resonances and it is beneficial for the measurement of small p-wave resonances. However, a coincidence requirement affects the counting efficiency by reducing the counting probability for low-multiplicity γ cascades. This would specifically apply to direct-capture between compound resonances. DeSaussure et al.[51] found agreement between the data taken with and without the coincidence requirement within ≈7%.

Gupta et al.[52] used a Gd-loaded-liquid-scintillator detector for capture-cross-section measurements in the higher-energy range. Gadolinium has a high thermal cross section and neutrons scattered into the scintillator will be captured in Gd after slowing-down collisons. Thus, observing coincidences between the originally prompt-γ event and a delayed-γ count permits discrimination against inelastic scattering events.

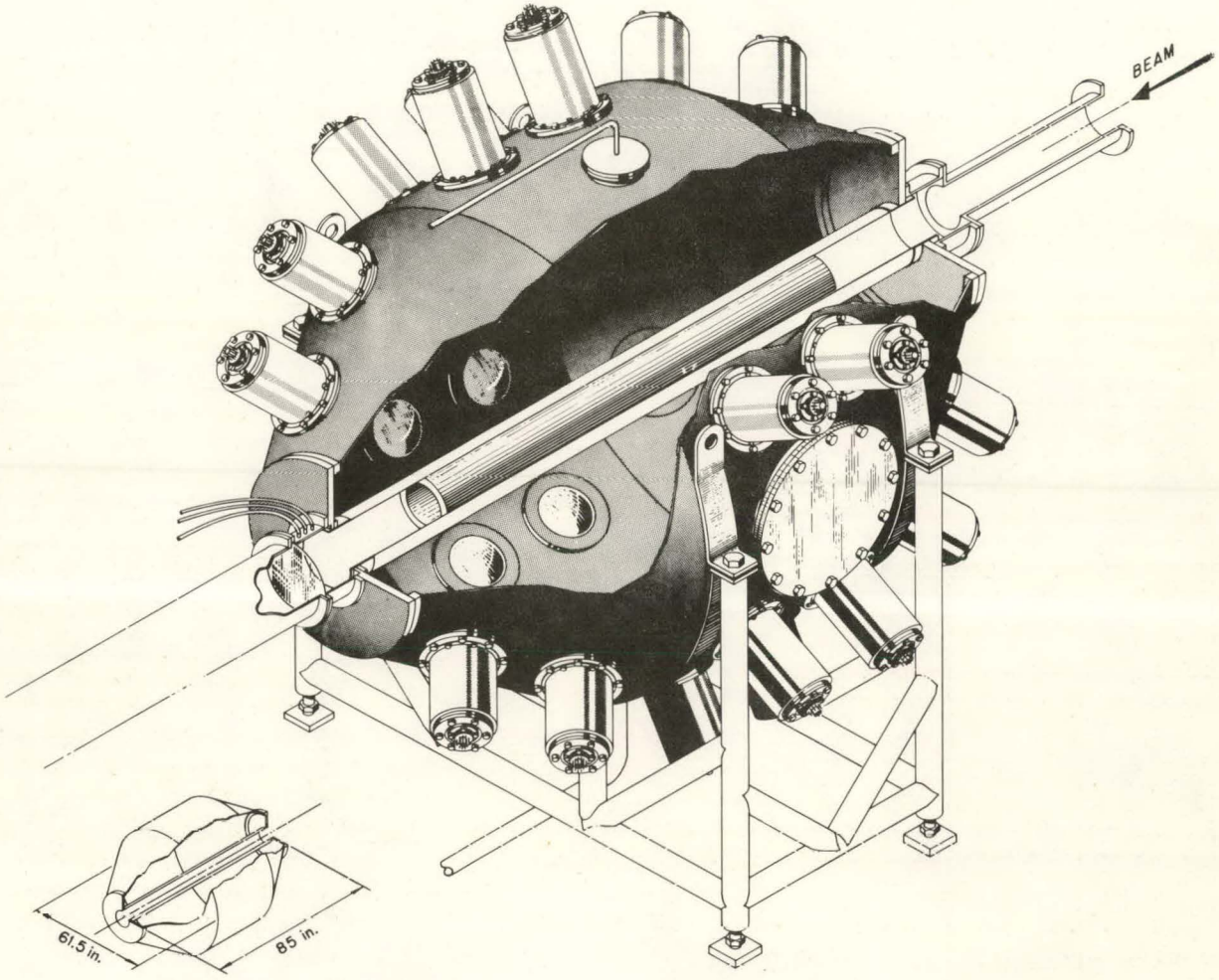

Fig. 18. The 3000-liters Large Liquid-Scintillation Detectors at Oak Ridge National Laboratory.[50]

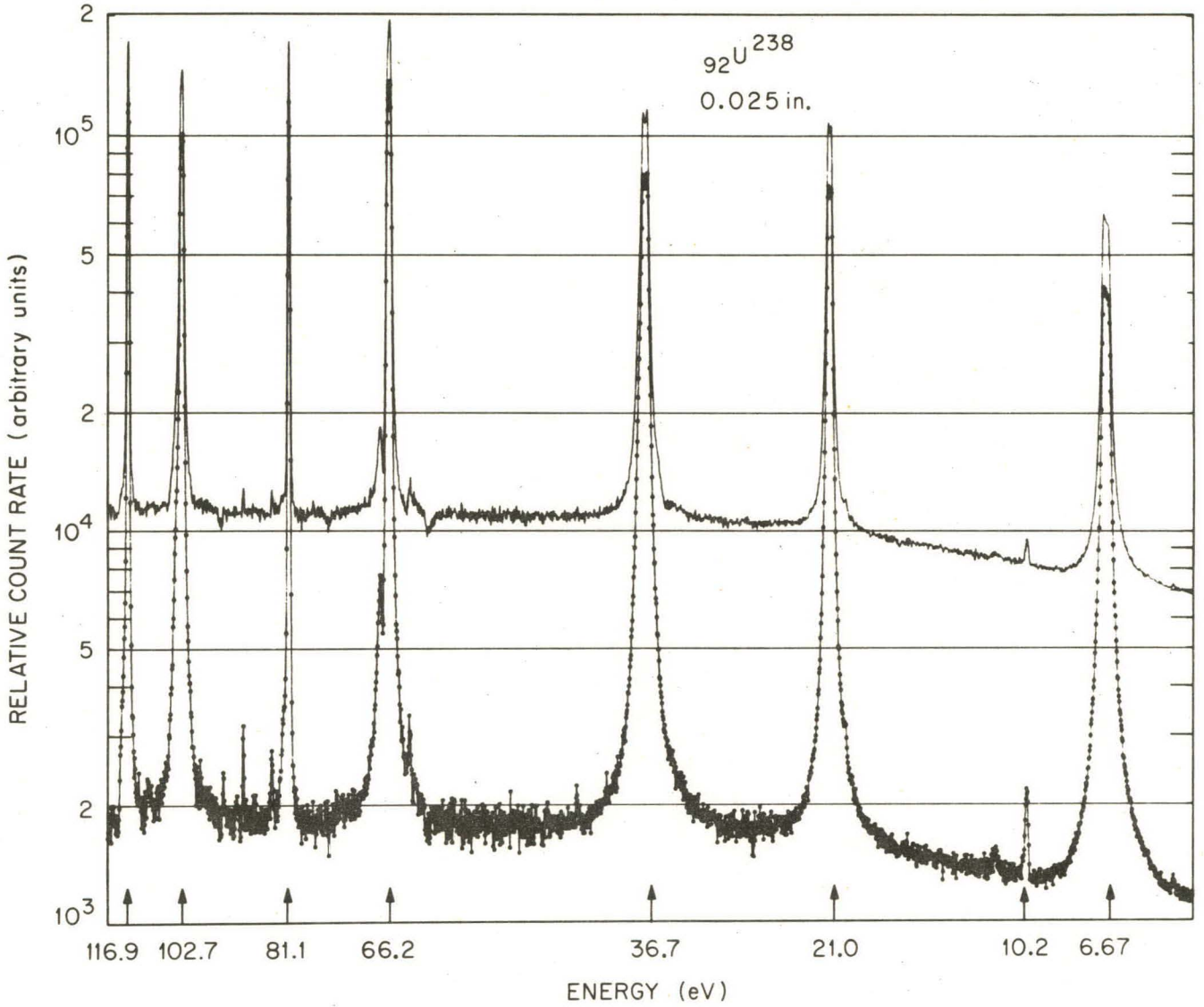

Fig. 19. Capture Rates Obtained without (upper data) and with (lower data) Coincidence Between Two Optically Separated Halves of the Oak Ridge National Laboratory Large Liquid-Scintillation Detector.[51]

A small detector of ≈270 liters has been built by Gayther et al.[53]. The efficiency of such small detector is expected to be spectral sensitive and Monte-Carlo calculations of the shape of the pulse-height spectra were carried out and compared with the observed γ-ray spectra (see Fig. 20). Such calculations lead to the determination of the spectrum fraction and the total efficiency; however, the calculations require the knowledge of the γ-cascade multiplicities. Some estimate for the latter could be obtained from the coincidence rate between the optically separated two halves of this detector.

The efficiency of a large liquid sctinillator for high-energy γ rays could be improved and/or the size of the tank reduced, if it would be possible to load the scintillator solvent with a high-Z material. A proposal in this direction has been made by Macklin.[54] A liquid scintillator could be mixed with small particles of a lead-loaded glass. In order to match the refractive indices, a liquid scintillator with a napthalene base was suggested. Such a scintillator would have a density of about 2.4 g/cm^3 and a light output reduced, possibly, to 20% of a common liquid scintillator. The volume of the detector could be reduced by a factor of about six which would be result in a substantial reduction in background.

A more straightforward approach to reducing the size of the scintillator by using a high-Z material was employed by Adamdchuk et al.[55] They built a 4π-detector with 12 sections of NaT(Tl) - crystals. The detector was used in measurements of the capture cross section of ^{238}U.

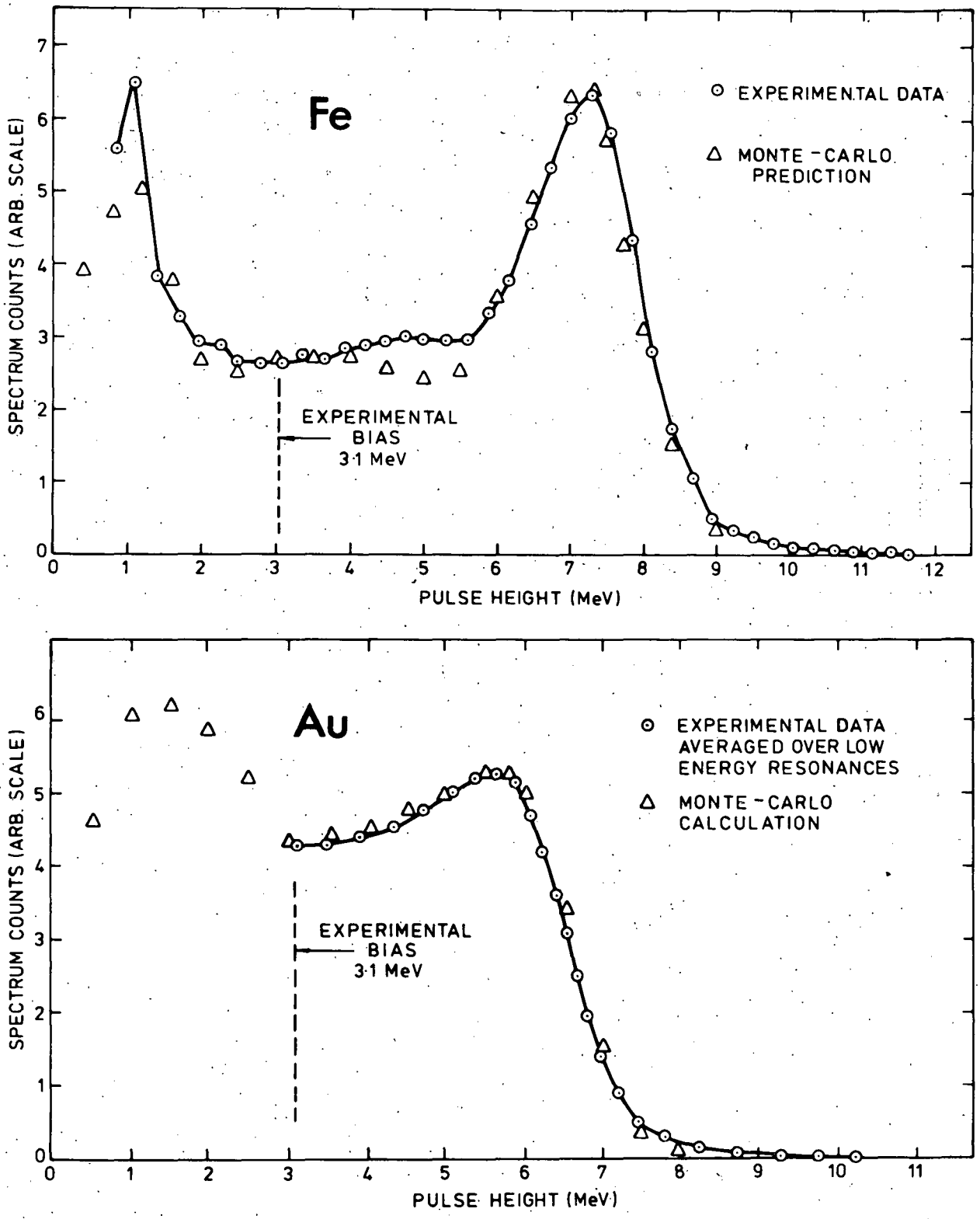

Fig. 20. Comparison of Experimental Pulse-Height Spectra of Fe (n,γ) and Au (n,γ) with Monte Carlo Calculations for a 270-liter Large Liquid-Scintillators Detector.[53]

II.2.2. Gamma-Energy Proportional Detectors

Large 4π-detectors achieve γ-spectra insensitivity by summation of the total radiative energy emitted in a capture event. A detector which has an efficiency proportional to the γ energy of an individual transition, $\eta(E_{\gamma i})$, and detecting only one quantum per event, can be shown to have a total efficiency proportional to the total γ-ray energy of the cascades and thus, also independence of the γ-spectrum:

$$\eta = \sum_{i=1}^{n} \eta(E_{\gamma i}) \quad , \tag{9}$$

and with $\eta(E_\gamma) = c \cdot E_\gamma$, where c is constant

$$\eta = c \sum_{i=1}^{n} E_{\gamma i} = c \cdot E_{tot} \quad , \tag{10}$$

where E_{tot} is given by the neutron binding energy and the center-of-mass energy of the neutron.

This principle is realized with Geiger counters having with a wall thicker than the range of the secondary electrons of the highest γ-ray energy (Brandt et al.[56] and Fowler et al.[57]). However, the dead-time of such counters is very large and thick-walled proportional counters were used in capture-cross-section measurements instead. Kashukeev et al.[58] investigated the linearity of the thick-walled proportional counter and found a linear dependence up to γ-ray energies of ≈4 MeV (see Fig. 21). The sample usually surrounds the cylindrical proportional counter with the wall being the converter. Measurements were made for many nuclei, elemental and isotopic, from thermal energies to ≈30 keV in a lead slowing-down spectrometer (e.g. Isakov et al.[59], Konks et al.[60]). Kashukeev et al.[58] also carried out measurements with a 2-mm-Bi converter and a 9-mm-thick-GaF_2 scintillation detector. However, due to the thickness of the scintillator, this detector resulted in an efficiency which was not proportional to the γ-ray energy (see also Fig. 21).

Instead of the thicker scintillator attempted by Kashukeev et al., Moxon and Rae[61] used a thin plastic scintillator for the detection of the secondary electrons produced in a graphite or an aluminum converter. Such a detector is not only proportional to the primary-γ energy but it also has a fast time-response and became known as a Moxon-Rae detector. Figure 22 shows this detector schematically in a typical time-of-flight experiment at a LINAC. The thickness of the converter must be greater than the maximum range of the secondary electrons in order to achieve proportionality of the detector response with γ-ray energy. Moxon and Rae considered a maximum γ-ray energy

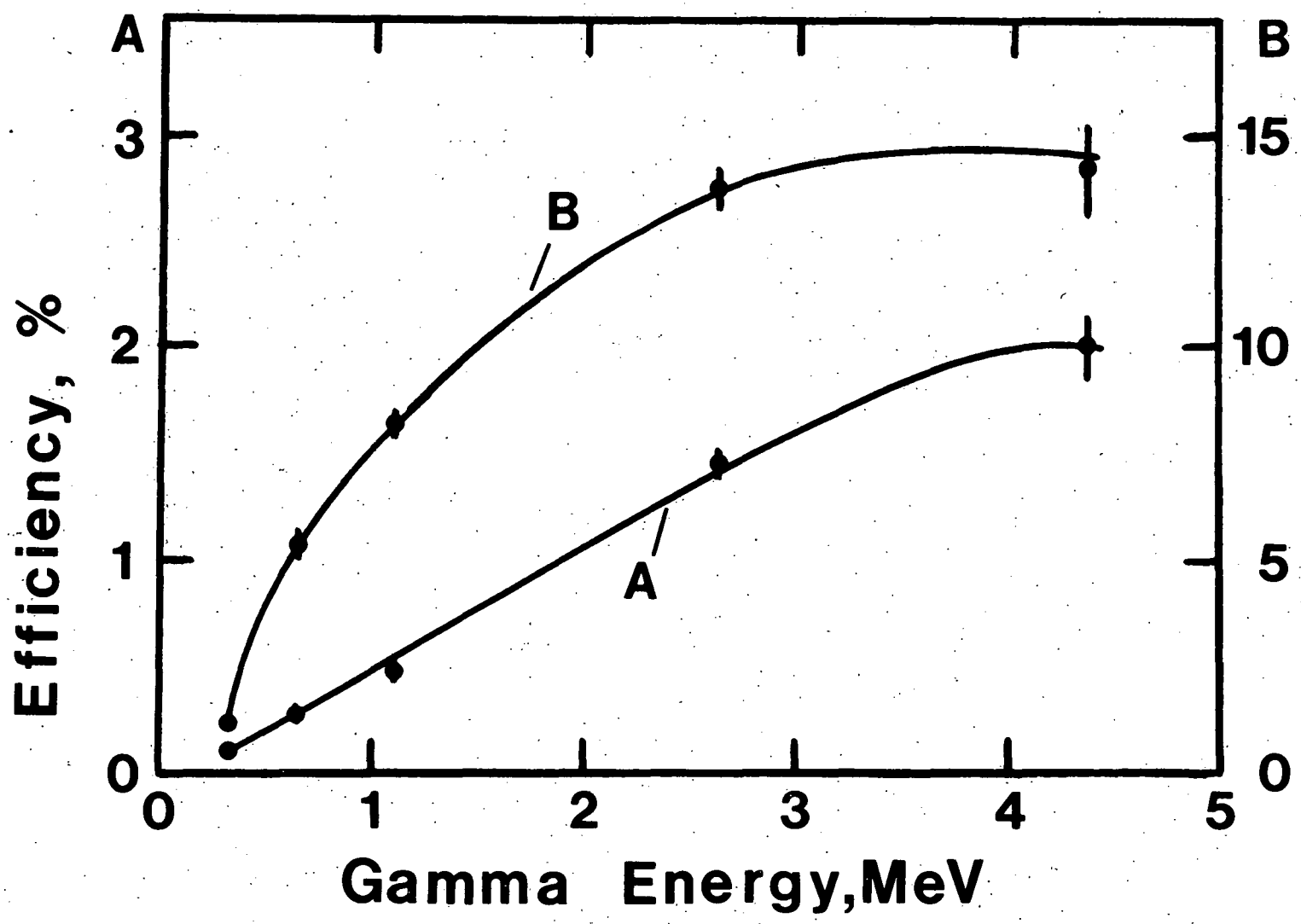

Fig. 21. Linearly of the Efficiency of a Thick-Walled Proportional Counter with Gamma Energy (A), and Nonlinearily of a 2-mm-Bi Converter with a 9-mm-GaF_2-Scintillation Detector.[58]

of 12 MeV; which requires a thickness of 3.2 cm of graphite.

In order to derive Eq. (10), it was assumed that c is constant. The variation of c, the efficiency per MeV of γ-ray energy, was calculated and investigated experimentally by several authors, most recently by Iyengar et al.[62] (see Fig. 23). The value of c was found to increase from zero to nearly a constant value above 1-2 MeV γ-ray energy. The value of c for low-Z-material converters reaches a maximum around 2 MeV and then decreases with energy. High-Z-material converters already reach a high value at ≈1 MeV but then increase with increasing γ-ray energy. The value of c is larger for high-Z materials than for low-Z materials by about a factor of 2. Converters with Z ≈50 show a nearly constant value for the efficiency per MeV of γ-ray energy above 1-2 MeV. This can also be achieved by mixing a high-Z material with a low-Z material. Figure 24 compares values of c calculated by Macklin et al.[63] for graphite and graphite mixed with lead (40%).

The scintillator of a Moxon-Rae detector is choosen to have a high efficiency for the detection of the converted electrons and a low efficiency for γ rays and neutrons. The recoil protons resulting from neutron collisons in the scintillator have a much lower light yield than the electrons, thus the neutron efficiency of the detector is very low up to several hundred-keV-neutron energy. The capture of scattered neutrons in the converter and photomultiplier cause some additional background. The efficiency of a Moxon-Rae detector for capture-γ rays is ≈4-5%, about a factor of 20 lower than the efficiency of a large liquid scintillator. However, the background of the Moxon-Rae detector is lower by about a factor of 100, resulting in an improvement of the signal-to-background ratio by about a factor of five. The small size of the scintillator in a Moxon-Rae detector results in good timing characteristics which were once considered to be another advantage of this detector over a large liquid-scintillator detector, but the use of fast multipliers with the latter has resulted in comparable time resolutions of 2-3 nsec. A major advantage of the Moxon-Rae detector, besides its lower background, is the low cost of such a detector and the reduced amount of required shielding material. Among the disadvantages are the need for normalization of the measured capture rates, the sensitivity to inelastic-scattering γ rays, the drop of the "constant" c below 1-2 MeV and its λ-energy-dependence above, as well as the low overall efficiency.

An attempt to overcome the low efficiency of the Moxon-Rae detector was made by Weigmann et al.[64] They designed a detector which consists of a stack of six optically-isolated sheets of plastic scintillator of 3.5-cm-thickness each, which were alternately viewed by two photomultipliers. By requiring coincidences between the two photomultipliers, one effectively makes one of the plastic sheets a converter and the adjacent one the detector for the secondary electrons. The efficiency of such a detector is increased (n-1)-fold if n scintillator sheets are used. The linearity of the detector efficiency with γ-ray energy was measured with several calibrated-γ-ray sources and with neutron capture in different Ag and Mo resonances. The result is shown in Fig. 25. The linearity appears to be good above ~2 MeV but a drop-off seems to occur below 1 MeV similar to that observed for Moxon-Rae detectors. The coincidence requirement reduces the probability for

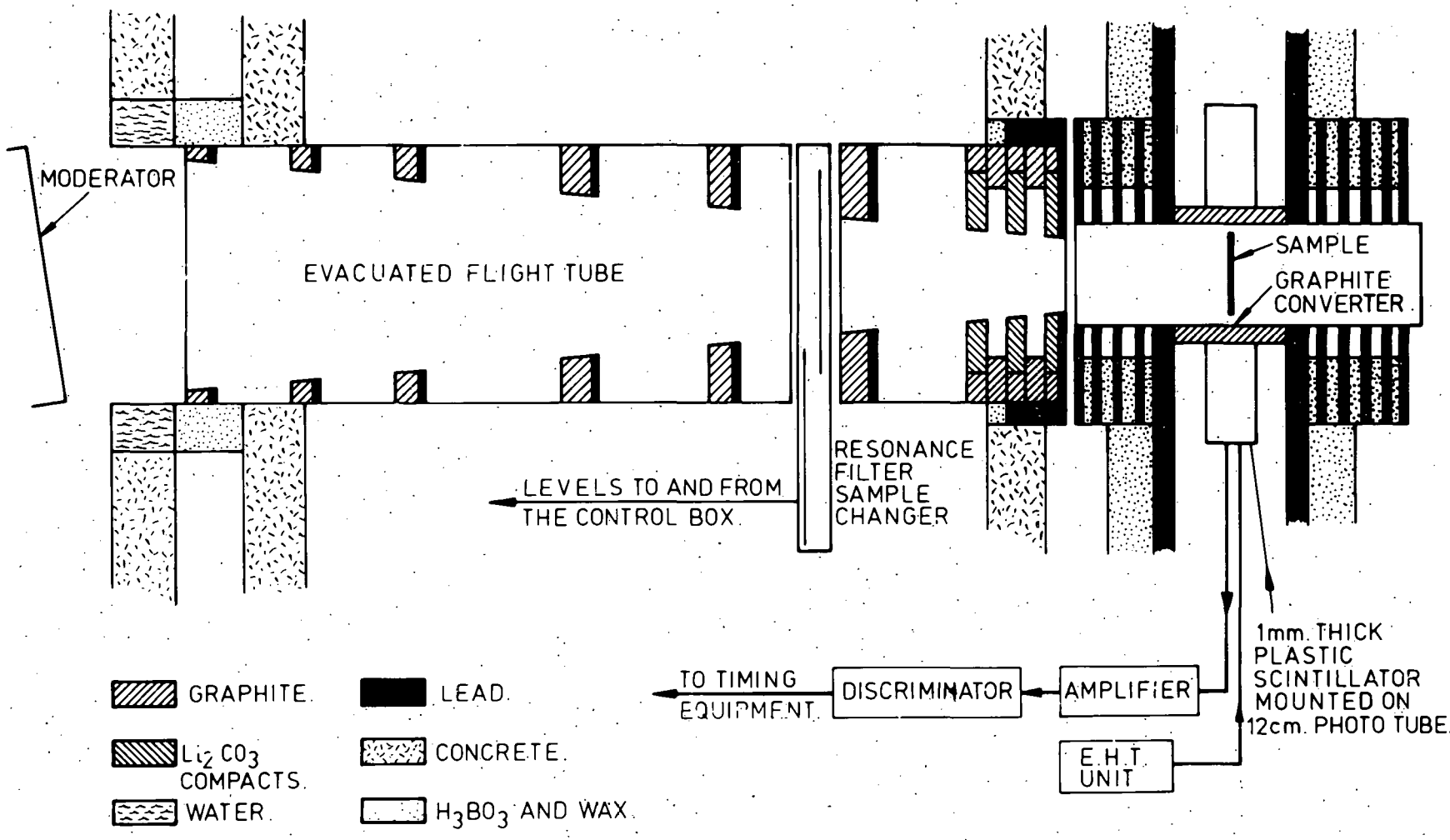

Fig. 22. Experimental Arrangment for Measurements of Neutron-Capture Cross Sections with a Moxon-Rae Detector.[61]

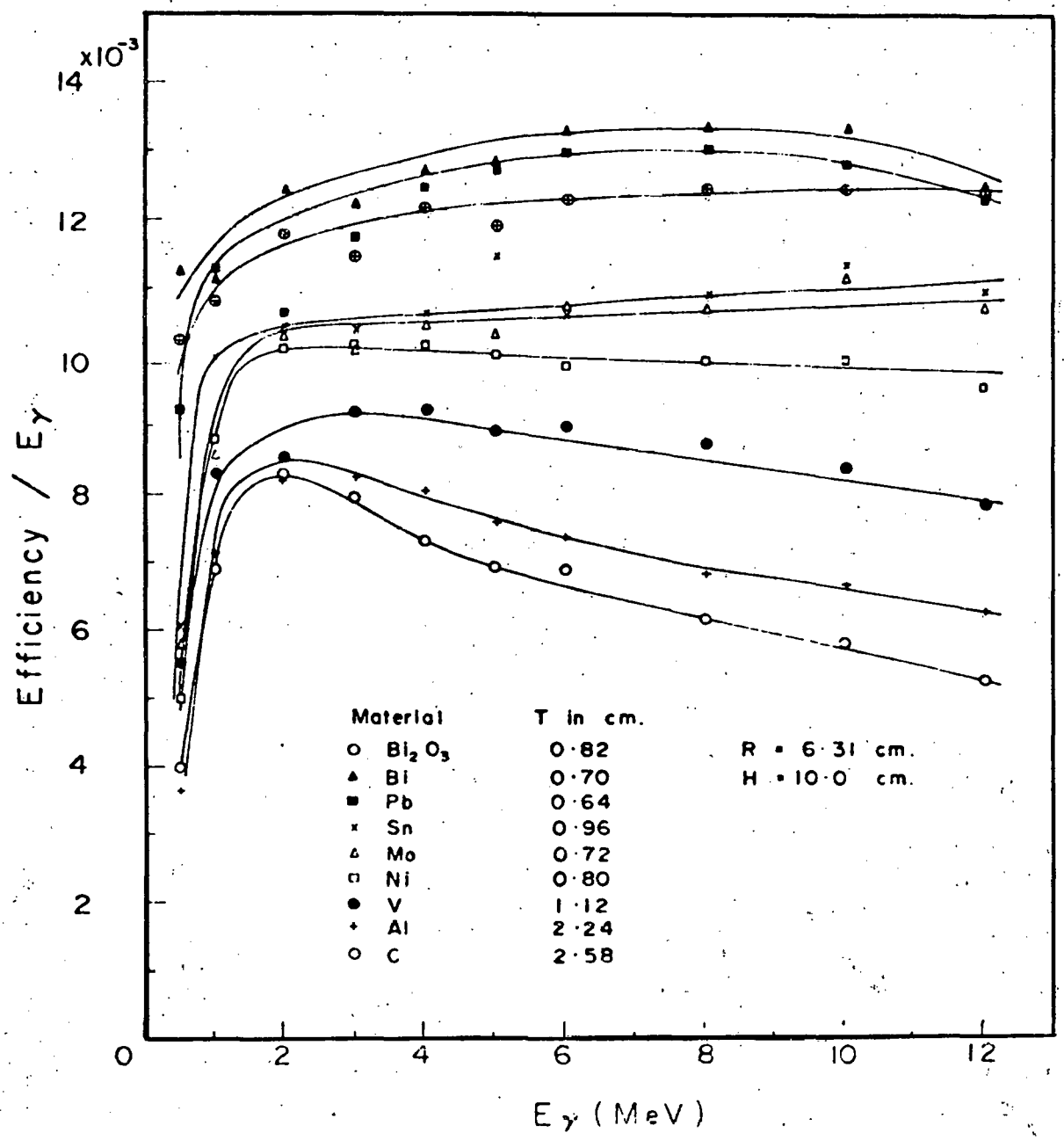

Fig. 23. The "Constant" Efficiency per MeV Gamma-Ray Energy for Various Z Materials.[62]

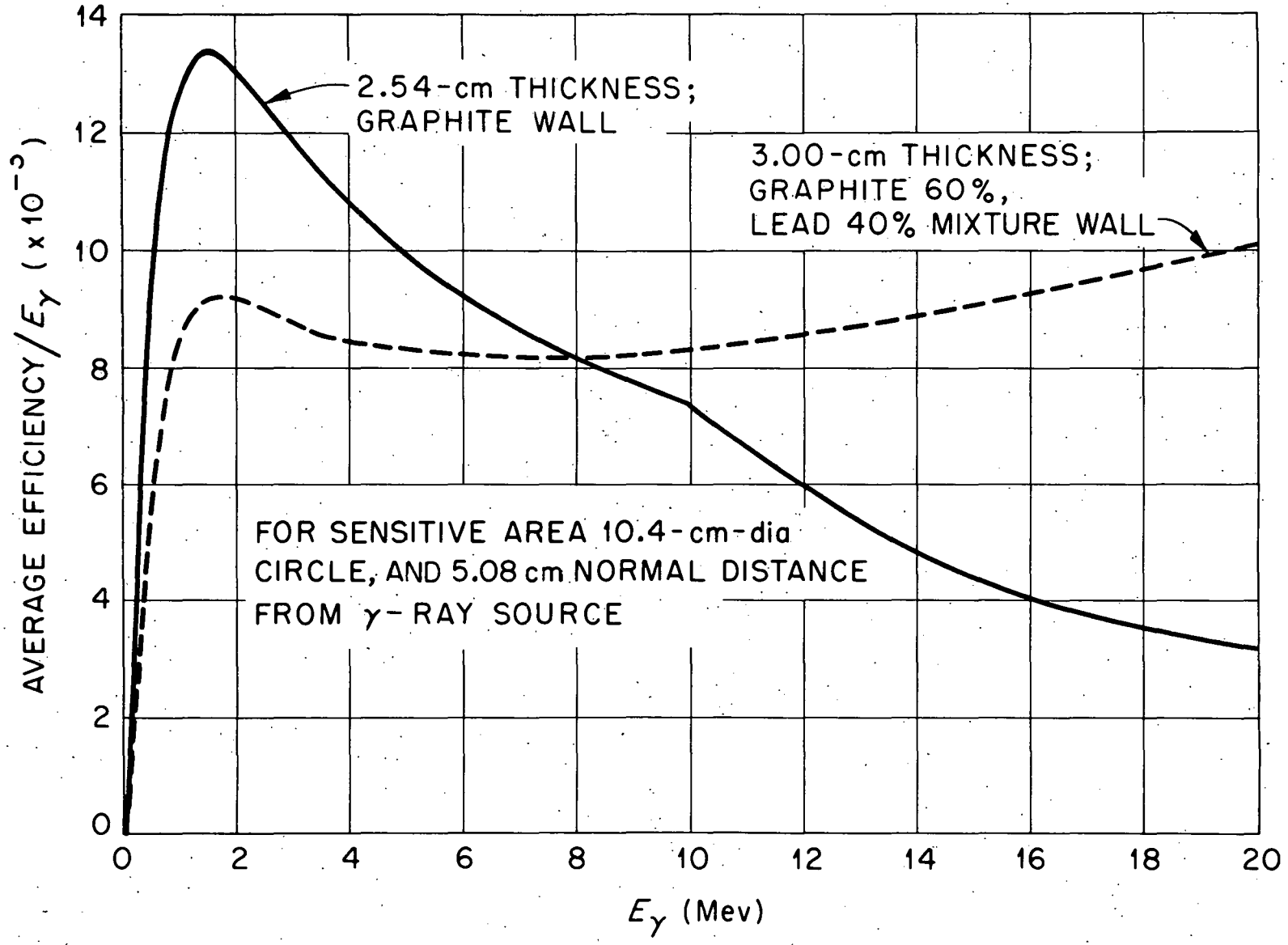

Fig. 24. The Efficiency per MeV Gamma-Ray Energy for a Graphite and a Graphite-Lead Converter.[63]

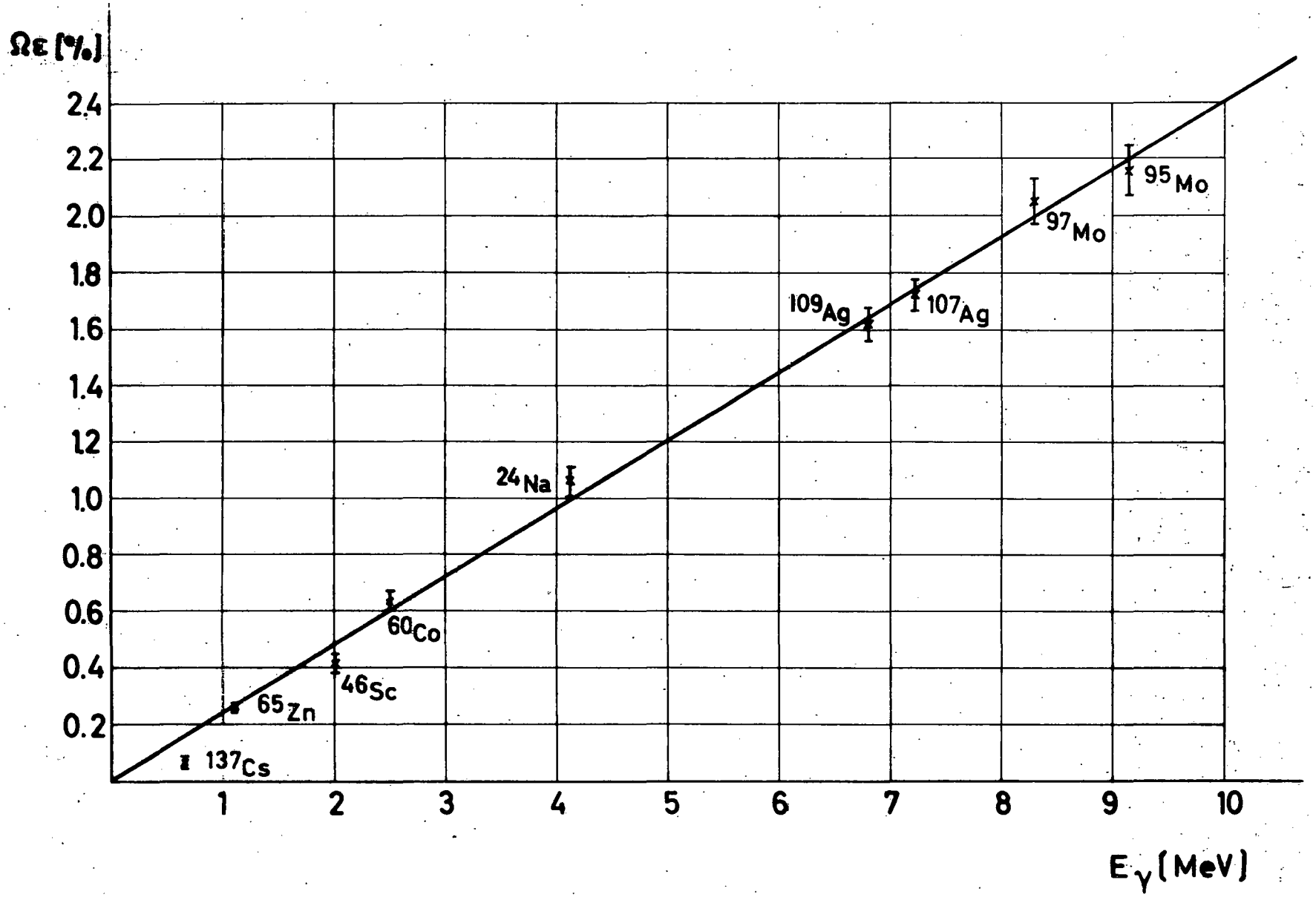

Fig. 25. The Linearity of the Efficiency with Gamma-Ray Energy for a High-Efficiency Moxon-Rae-Type Detector Designed by Weigmann et al.[64]

detecting neutrons at higher energies and thus extends the range for the use of a Moxon-Rae type detector to higher neutron energies.

Another variation of the Moxon-Rae detector was used to measure capture cross sections of radioactive samples in time-of-flight experiments carried out with a nuclear explosion as a neutron source (Diven[11]). A solid-state electron-detector was used for the detection of the secondary electrons instead of the plastic scintillator employed in most Moxon-Rae detectors.

II.2.3. Pulse-Height-Spectrum-Weighting Technique

A detector which was not specifically designed to have a linear response function, like the thick-walled proportional counter or the Moxon-Rae detector, will have a total-detection efficiency

$$\eta_\gamma = \sum_{i=1}^{n} F(E_{\gamma i}) \quad , \tag{11}$$

where n is the number of γ rays emitted in a specific cascade, $E_{\gamma i}$ is the energy of the i^{th} γ ray, and F is the probability that this γ ray will be detected. The total number of capture events, N_γ, is then derived from the observed number of detector counts

$$C_\gamma = \eta_\gamma \, N_\gamma \quad . \tag{12}$$

For a space angle, Ω, small enough that sum coincidences are very improbable ($\Omega \ll 4\pi$), we can write

$$\eta_\gamma = \frac{\Omega}{4\pi} \sum_{i=1}^{n} f(E_{\gamma i}) \quad . \tag{13}$$

Let us now assume that we can observe the pulse-height spectra which are denoted by $C_\gamma(E_\gamma,P)$. The detector response $f(E_{\gamma i})$ can be factored into the interaction probability for the detector material, $Q(E_\gamma)$, and a factor, $G(E_\gamma)$, which represents the probability of registering this interaction. This factor, $G(E_\gamma)$, can now be manipulated by applying an operator or weighting function, W(P), on the observed pulse height distribution

$$G(E_\gamma) = \int_0^{E_\gamma} C_\gamma(E_\gamma,P) \cdot W(P) \, dP \tag{14}$$

in order to obtain again a linear response

$$f(E_\gamma) = R(E_\gamma) \cdot G(E_\gamma) = c \cdot E_\gamma \quad . \tag{15}$$

These relations were outlined by Hurst and Ritchie[65] as a generalized concept for radiation dosimetry. Maier-Leibnitz[66] recommended the application of this concept for neutron capture measurements and Macklin and Gibbons[67] first applied it to cross section measurements in the 30-220-keV-energy range.

It can be easily seen that the γ-energy-proportional detectors are a simplified version within this group of detectors where $Q(E_\gamma) \sim E_\gamma$ due to the principle of the converter and $G(E_\gamma)$ is constant due to the design of

the scintillator (Czirr[68]). A need for recording the pulse-height spectrum exists for the more general case but results in considerable freedom to select a detector with high efficiency, good time resolution and low background sensitivity.

The weighting function is choosen such that $f(E_\gamma) \sim E_\gamma$ and therefore η_γ becomes, as for the energy-proportional detector, independent of the specific γ-cascade features. This independence permits the calculation of the weighting function using measured or calculated pulse-height spectra, $C(E_\gamma,P)$, from a system of equations or the corresponding matrix equation which follows from Eq. 15. A detector for which $Q(E_\gamma) = 1$, e.g., a large NaI(Tl) detector with a collimator channeling the γ rays to the bottom of a well in the crystal (Macklin and Gibbons[67]), the pulse-height spectrum $C(E_q,P)$ becomes equal to 1 for $P = E_\gamma$ and equal 0 elsewhere; therefore the weighting function becomes proportional to E_γ. Czirr[68] pointed out that when using a detector for which the response $Q(E_\gamma)$ is such that the weighting function is linear; the necessity to count only one γ ray per cascade is no longer required and larger space angles, Ω, can be used.

In practice, a rather simple NaI(Tl) detector or plastic scintillator is used, and the weighting function is determined from calculated pulse-height distributions. The use of fluorocarbon or deuterated-liquid scintillators has the advantage of reduced response from scattered neutrons. Figure 26 shows the weighting function calculated by Macklin and Gibbons[67] for a pair of cylindrical-plastic scintillators with a radius of 5.8 cm and a height of 7.6 cm which are placed 2.6 cm from the capture sample. The weighting function is nonlinear and gives the rather frequently occurring small pulses a low weight and the less frequently occurring larger pulses a high weight. This results in an increase of the statistical uncertainty of the measured data. Figure 27a shows a typical measured pulse-height spectrum and Fig. 27b shows the weighting function and the resulting spectrum (Macklin and Allen[69]) for ^{103}Rh(n,γ). Measurements of capture cross sections between 30 and 310 keV neutron energy (by Macklin and Gibbons[56]) resulted for many nuclei, specifically In and Ta, in essentially the same cross section values, regardless of whether the weighting function was applied or not. This suggests that, for some detectors, the pulse-height-spectrum changes are compensated by efficiency changes or that the primary γ-spectra changes are not as substantial as one might expect for neutron-angular-momentum changes from $\ell = 0$ to $\ell = 1$ or 2.

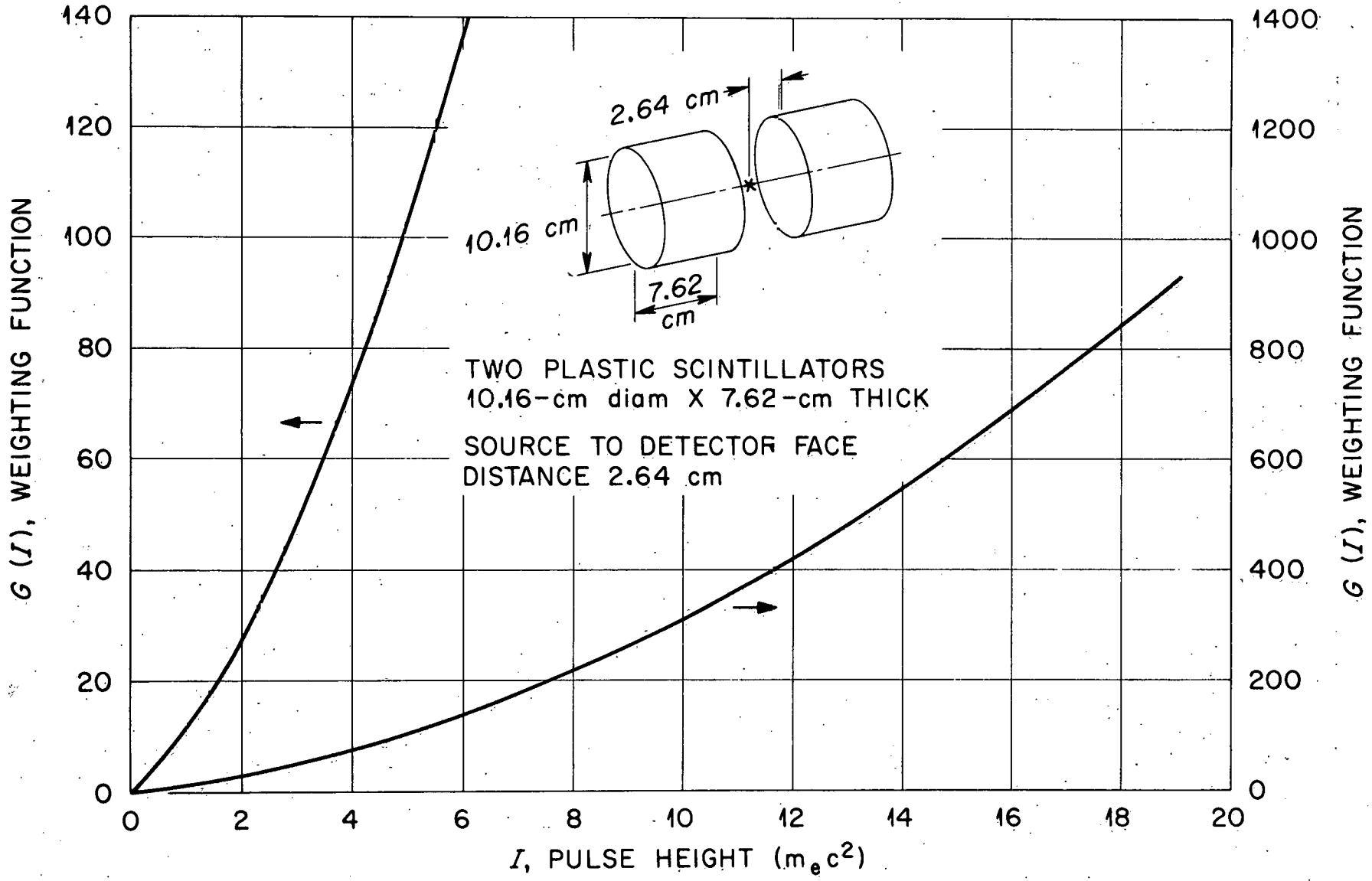

Fig. 26. The Weighting Function Calculated for a Pair of Plastic Scintillators as a Function of the Pulse-Height.[67]

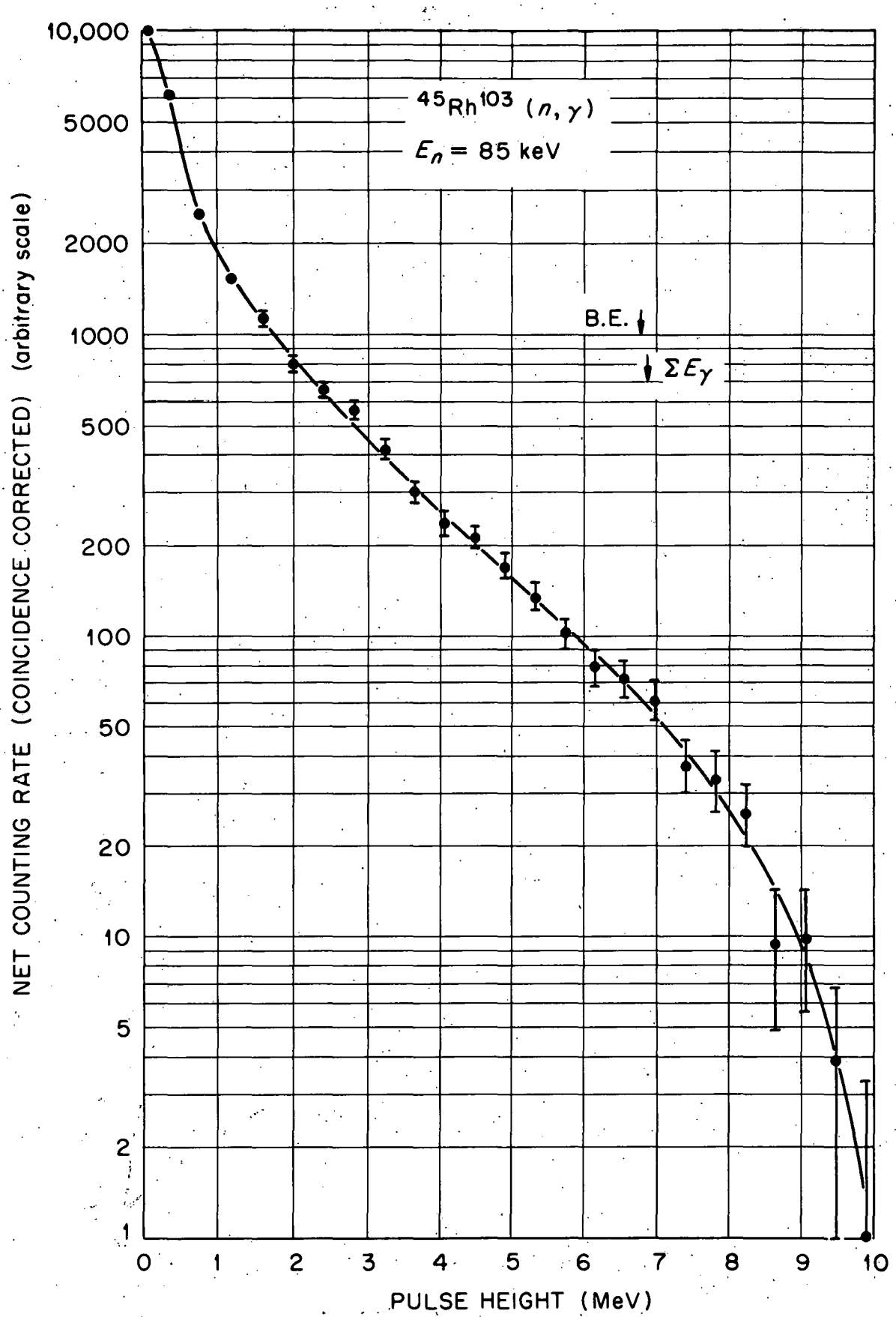

Fig. 27a Pulse-Height Spectra Obtained for the ^{103}Rh (n,γ) Reaction with a Small Spectrum-Sensitive Detector.[69]

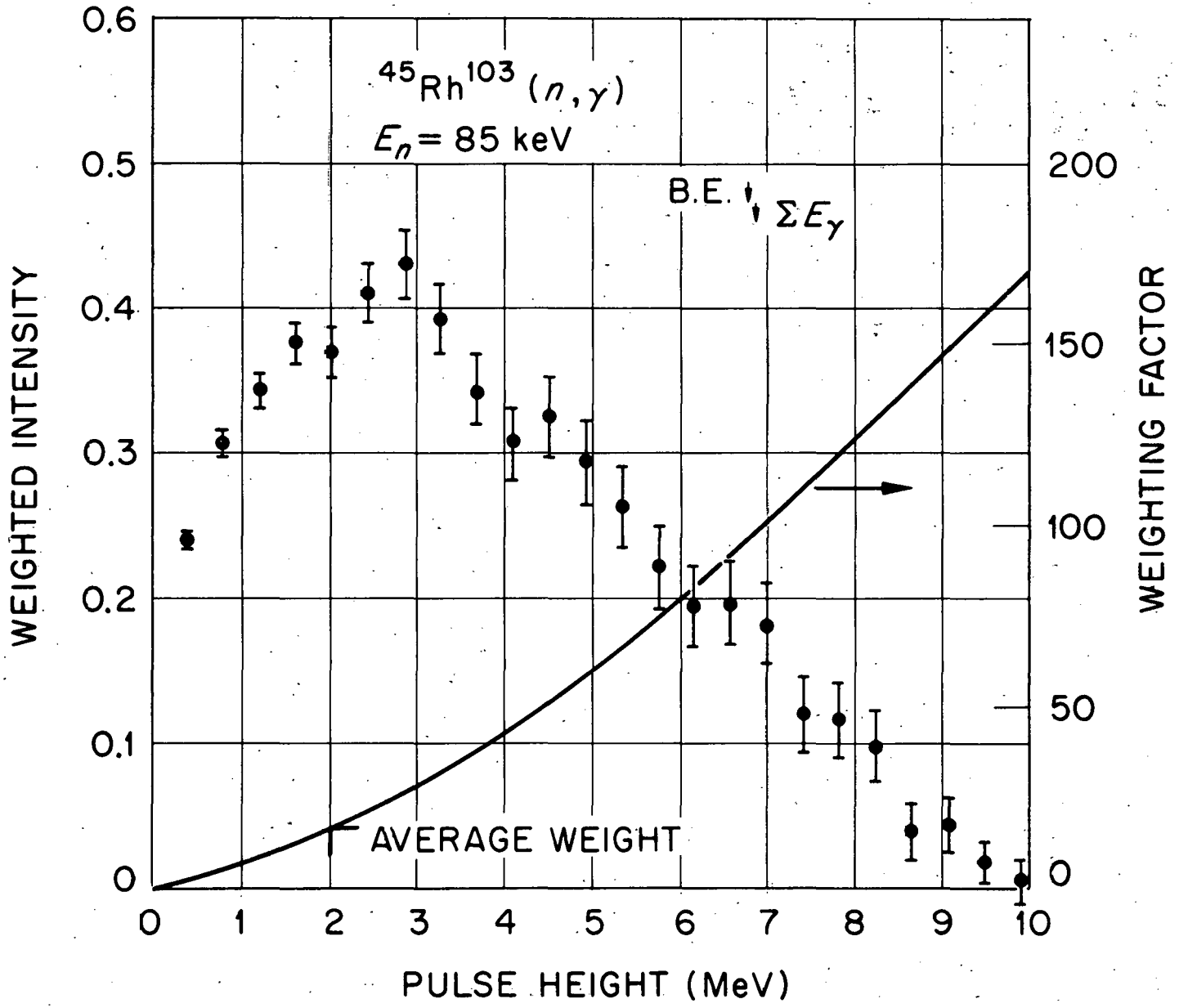

Fig. 27b Weighting Function and Resulting Pulse-Height Spectrum for the Data in Fig. 27a.

II.3. γ-Spectrum-Measurement Techniques

The large thermal flux in a reactor makes it a suitable neutron source for γ-spectra investigations. Initially, NaI(Tl) detectors were used. They have a high efficiency but suffer from poor resolution and a complicated response function. Such measurements provided only limited information on the energy levels of the compound nucleus because of the complexity of the spectra resulting from the (n,γ)-process. A substantial amount of spectral data was obtained with magnetic pair or Compton spectrometers which have reasonably good resolution ($\approx 10^{-3}$) but rather low efficiencies ($\approx 10^{-5}$) (Groshev et al.[70]). Considerable improvement was achieved with the introduction of Ge(Li)-detectors. These not only have a good energy resolution (≈0.05%) but also a much higher efficiency than the magnetic spectrometers, and thus make measurements with time-of-flight neutron-energy selection, e.g. neutron-resonance γ spectroscopy, feasible. However, the spectral response is again, as for NaI(Tl) detectors, rather complicated and involves single- and double-escape peaks, and Compton background. This problem can be overcome in part with the use of anti-coincidence spectrometers (e.g. Michaelis and Horsch[71]) or double-escape-coincidence spectrometers (e.g. Michaelis et al.[72]). Figure 28 compares the resolution obtained with a magnetic-Compton spectrometer, an early Ge(Li)-detector, and the performance of a more modern Ge(Li)-detector. The doublet from the de-excitation to the ground state and the first excited state of $^{56}Fe(n,\gamma)$ is shown (Chrien[33]). Even better resolution and lesser energy uncertainties were achieved more recently for measurements of low-energy-γ rays with curved-crystal spectrometers (≈150 eV resolution and 2-eV-energy uncertainty at 0.5 MeV, see Kane[73]). This performance is surpassed with flat-crystal spectrometers but at the cost of several orders of magnitude lower efficiency (Kessler et al.[74]). The use of crystal spectrometers has the advantage of simplified spectra interpretation and the precision needed for the composition of the level schemes with the help of the Ritz-combination principle. The required high source strength for these spectrometers is achieved by in-pile targets which limits the application to measurements averaged over the thermal spectrum. Little can be learned from these measurements at thermal energies besides the energies of the levels, however, Ge(Li) detectors and NaI(Tl) detectors were used to measure angular correlations between coincident transitions (e.g. Schmidt and Heck[75]) or from polarized targets and beams (Abrahams[76]). Of substantially greater interest are measurements of γ spectra as a function of neutron energy. Such measurements are usually made in a two-dimensional mode (γ energy vs. neutron time-of-flight) at reactors with a chopper or at LINAC's. Spectra obtained in this manner are shown in Fig. 3.

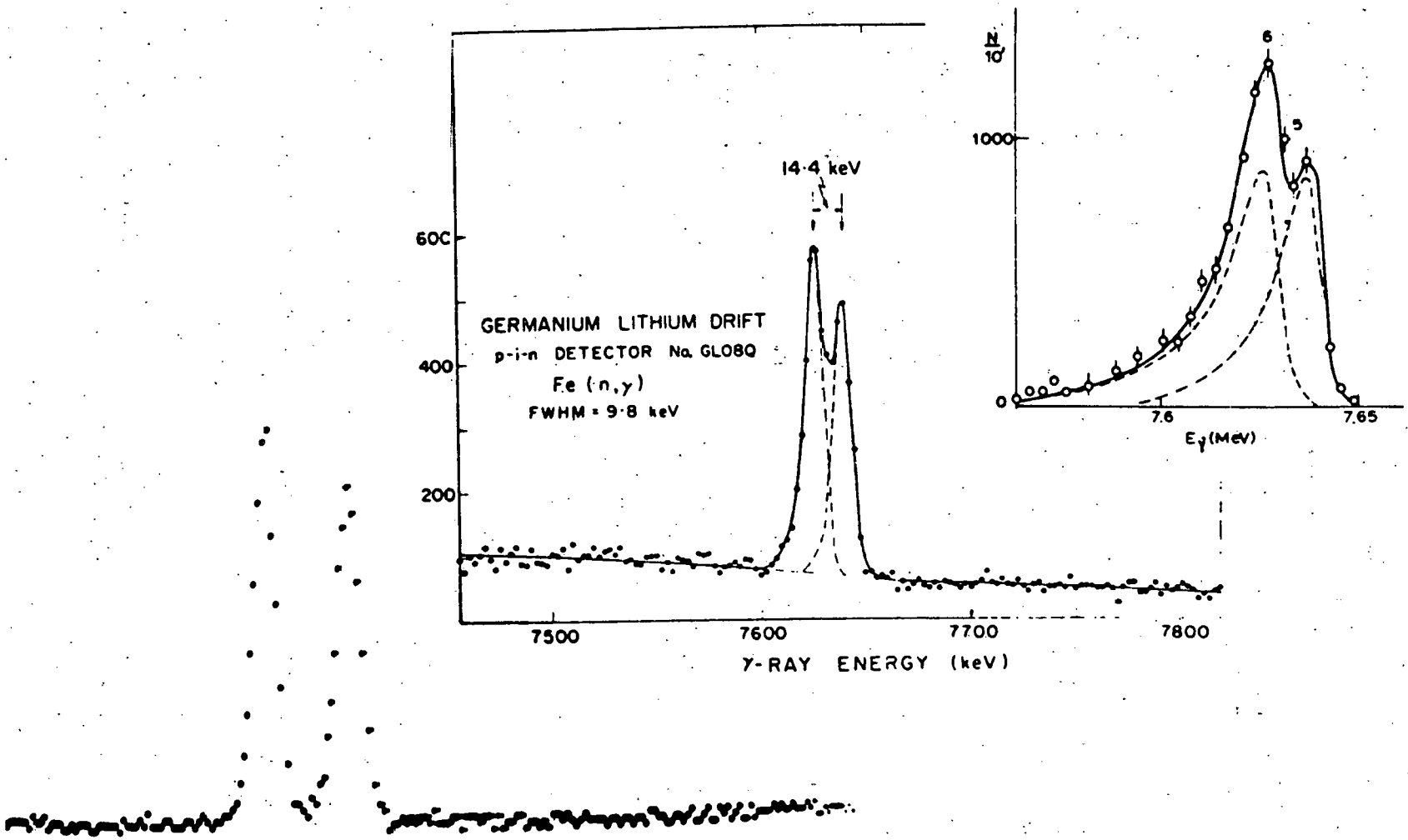

Fig. 28. Comparison of the Resolution of a Gamma-Ray Doublet with a Magnetic-Compton Spectrometer and an Earlier and more Recent Ge(Li) - Detector.

III. Measurement Analysis and Results

The analysis of measured data depends on the neutron-energy range of the measurement and is expected to be most complicated in the resonance-energy range. A large amount of data has been measured over the years and subsequently published in scientific journals and conference proceedings. Cross-section data, resonance parameters and spectral measurements are referenced in an index to the literature on microscopic neutron data (CINDA[77]).

III.1. Thermal and Fast-Neutron-Energy Range

The neutron-capture cross sections in the thermal and fast-neutron-energy range vary smoothly within the achievable resolution. Therefore, the analysis of capture-yield data is to some extent similar. The measured capture rate (per cm^2 and per sec) is given for a beam-type-geometry experiment by

$$C_\gamma = \varepsilon_\gamma \cdot N \cdot d \cdot \sigma \cdot \phi \quad , \tag{16}$$

where ε_γ is the detection efficiency, N is the number of nuclei per cm^3 and d is the thickness of the sample in cm. ϕ is the number of incident neutrons per cm^2 and per sec which strike the sample perpendicular to its face. The same equation applies for the measurement in an isotropic neutron flux because only $\phi/2$ neutrons strike the sample per cm^2 and per sec but the effective thickness of the sample is larger by a factor of two than its physical thickness. Whereas Eq. 16 is a good approximation for very thin samples ($Nd\sigma \ll 1$), a number of effects must be considered for the thicker samples used in practice. The first is the neutron-flux attenuation in the sample. In a beam geometry, the number of interactions within the sample for unit flux is $(1 - \exp(-\Sigma_{tot}d))$ where $\Sigma_{tot} = N \cdot \sigma_{tot}$.

The correction factor for neutron-flux attenuation applied to Eq. 16 is then simply $(1 - \exp(-\Sigma_{tot}d))/\Sigma_{tot}d$. The attenuation of the primary neutrons for an isotropic neutron flux must be integrated over all angles and is given by

$$\frac{\psi(\Sigma_{tot}d)}{2 \cdot \Sigma_{tot}d} = \frac{1 - 2 \cdot E_3(\Sigma_{tot}d)}{2 \cdot \Sigma_{tot}d} \tag{17}$$

where E_3 is one of the integral-exponential functions defined by

$$E_n(x) = \int_0^1 t^{n-2} \exp\left(-\frac{x}{t}\right) \tag{18}$$

For a measurement in a thermal-neutron field, a further integration over the Maxwellian-energy spectrum and energy dependence of the cross sections is required.

The underlying resonance structure causes strong variations of the neutron-flux attenuation within the unresolved-resonance-energy range and may vary from nearly unattenuated flux at interference minima to nearly total attenuation at resonance maxima of the cross section. The fine-energy variation of the resonance-self-shielding effect cannot be observed in the unresolved-resonance-energy range. However, the average effect is clearly visible if measurements with different sample thicknesses are made. Figure 29 shows measurements of the capture cross section for two different thicknesses of iridium samples obtained in a lead-slowing-down spectrometer. The resonance-self-shielding effect suppresses the measured cross section and much smaller values are obtained for thicker than for thinner samples. Measurements with different sample thicknesses can be used to extrapolate the values to zero sample thickness and thus obtain the infinitely-dilute cross section. However, it is usually preferable to calculate the required correction for the resonance-self-shielding effect.

The neutron fraction which results in a first-collision-capture event is given by $\sigma_{n,\gamma}/\sigma_{tot}$. Neutrons which are not absorbed are elastically or inelastically scattered. In a beam-type geometry, scattered neutrons usually have a much higher chance of being captured than the primary neutrons. At lower energies where scattering is elastic and isotropic, this increased capture probability results from the increase of the average path length of the scattered neutrons in the sample which may exceed a factor of ten. The problem is more complex at higher energies where $\sigma_{n,\gamma} << \sigma_{tot}$. The larger relative amount of scattered neutrons increases the probability of secondary capture events but scattering is anisotropic and forward directed, which decreases the average path-length of the scattered neutrons in the sample compared with the low-energy-isotropic scattering. Energy degradation due to inelastic scattering might become very significant because the capture cross section is usually much larger for the lower-energy inelastically-scattered neutrons.

The problems of resonance-self-shielding and capture events due to scattered neutrons are usually treated together. Analytical solutions were given by Schmitt[78], Dresner[79], and Macklin[80]. Monte-Carlo techniques were used by Froehner[81], and Poenitz[49]. The required corrections can be substantial, and can explain some of the observed data discrepancies (Devaney[02]).

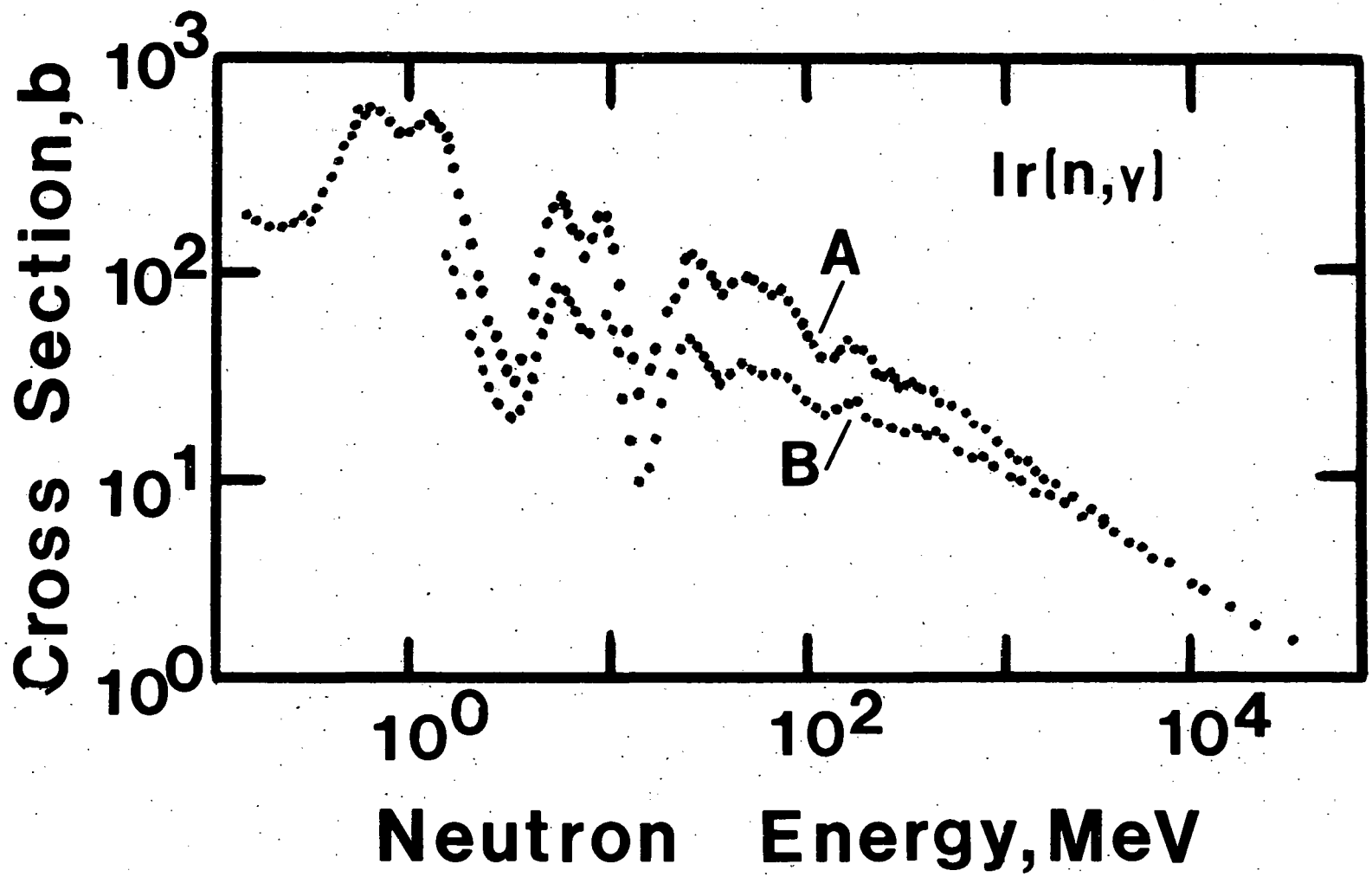

Fig. 29. Capture Cross Sections Measured with Two Differently Thick Samples. The Resonance-Self-Shielding Effect Results in Lower Cross-Section Values for the Thicker Sample (B).

III.2. Resonance-Energy Range

The total cross section of many nuclei in the resolved-resonance-energy range consists of the capture and the elastic-scattering cross section. This excludes some light nuclei with large (n,α) cross sections or heavy nuclei with (n,f) cross sections contributing to the total. Using the abbreviations $\sigma_o = 4\pi \lambda^2 g_J \Gamma_n/\Gamma$ and $x = 2(E - E_o)/\Gamma$ for the single-level-Breit-Wigner-resonance description of Eq. 3 yields

$$\sigma_{n,\gamma} = \sigma_o \frac{\Gamma_\gamma}{\Gamma} \frac{1}{1 + x^2} \quad , \tag{19}$$

$$\sigma_{n,n} = \sigma_o \frac{\Gamma_n}{\Gamma} \frac{1}{1 + x^2} + \sqrt{\sigma_o \sigma_p g_J \frac{\Gamma_n}{\Gamma}} \frac{2x}{1 + x^2} + \sigma_p \quad ,$$

where σ_p is the potential-scattering cross section. The objective in the resolved-resonance region is to obtain the resonance parameters E_o, g_J, Γ_γ Γ_n, and $\Gamma = \Gamma_\gamma + \Gamma_n$. A measurement of the infinitely-dilute-capture cross section, if it were possible, would yield the width, Γ, and, from the peak cross section, the value of $g_J\Gamma_\gamma\Gamma_n/\Gamma^2$. The thermal motion of the nuclei results in a Doppler broadening of the resonances and the terms $1/(1 + x^2)$ and $x(1 + x^2)$ of Eq. 19 must be substituted with the familiar Doppler-shape functions (e.g. Bethe and Placzek[83]):

$$\chi(x,\beta) = \frac{1}{\beta \sqrt{\pi}} \int_{-\infty}^{+\infty} \exp\left[-\left(\frac{x - t}{\beta}\right)^2\right] \frac{dt}{1 + t^2}$$

$$\psi(x,\beta) = \frac{1}{\beta \sqrt{\pi}} \int_{-\infty}^{+\infty} \exp\left[-\left(\frac{x - t}{\beta}\right)^2\right] \frac{t\, dt}{1 + t^2} \quad ,$$

$$\beta = \frac{4}{\Gamma} \sqrt{\frac{E\, KT}{A}} \quad . \tag{20}$$

KT is the effective temperature of the sample material. The Doppler broadening could be avoided if measurements were made with samples cooled down to temperatures close to zero. However, the experimental resolution still results in an increase of the width of the resonance, and a decrease of the peak cross section. The neutron-flux attenuation for sample thicknesses used in practice results in a further reduction of the observed peak cross section and requires the simultaneous measurement of the total cross section.

The computation of the area integrated over the extent of the resonance then becomes a simple method for extracting resonance parameters. The areas for the total cross section and the capture cross section are given by

$$A_{tot} = \int (1 - e^{-n\sigma'}) dE \quad ,$$

$$A_{n,\gamma} = \int (1 - e^{-n\sigma'}) \frac{\Gamma_\gamma}{\Gamma} dE = A_{tot} \frac{\Gamma_\gamma}{\Gamma} \quad , \tag{21}$$

where σ' is the Doppler- and resolution - broadened cross section. A plot of Γ_γ vs. Γ_n following from the measured A_{tot} and $A_{n,\gamma}$ for several sample thicknesses yields intersecting curves which provide Γ_n, Γ_γ values. The scattering cross section may be measured instead of the total cross section, and Fig. 30 shows an example for the area analysis of the 65.9 eV resonance of ^{238}U.

A further complication is caused by the capture of neutrons scattered elastically in the sample material. In contrast to the thermal and fast-energy range, the energy loss in an elastic scattering event becomes important. Neutrons which are scattered at the resonance energy lose sufficient energy to fall outside the resonance energy and cause few capture events. However, neutrons of somewhat higher energy which are scattered to ≈90 degrees and thus have a long average-path length in the sample may fall into the resonance and result in a substantial amount of secondary-capture events. Figure 31 shows this effect for the 1.15 KeV resonance in ^{56}Fe (Gayther et al.[84]). The total-capture area can then become much larger than the primary capture yield, and the analysis must include the scattering effect (see Fig. 32).

With the availability of fast and powerful computers, the shape analysis of measured capture and total-cross-section data by least-square-fitting procedures which include the Doppler effect, the resolution, the flux attenuation and the scattering of neutrons in the sample became possible. Figure 32 shows such a fit obtained with the code REFIT developed by Moxon.[85] Similar codes were developed at other laboratories, e.g., the code FANAC by Froehner.[87] The area analysis and the shape analysis of capture and total cross sections are sometimes insufficient to establish the resonance parameters and inclusion of self-indication data in the analysis is beneficial. Such data are obtained by inserting filters of the same material and various thicknesses into the neutron beam. Figure 33 shows as an example, the capture yield for the 6.67 eV resonance of ^{238}U obtained by Block et al.[87] for several filters and without a filter. The saturation of the capture yield obtained for a strong resonance with $\Gamma_\gamma >> \Gamma_n$ can be used for the calibration of the measured data. The product $\varepsilon_\gamma \phi$ of Eq. 16 is determined with the saturated-capture yield and only the energy dependence of ε_γ and ϕ need to be measured for other energies ("Black Resonance Technique").

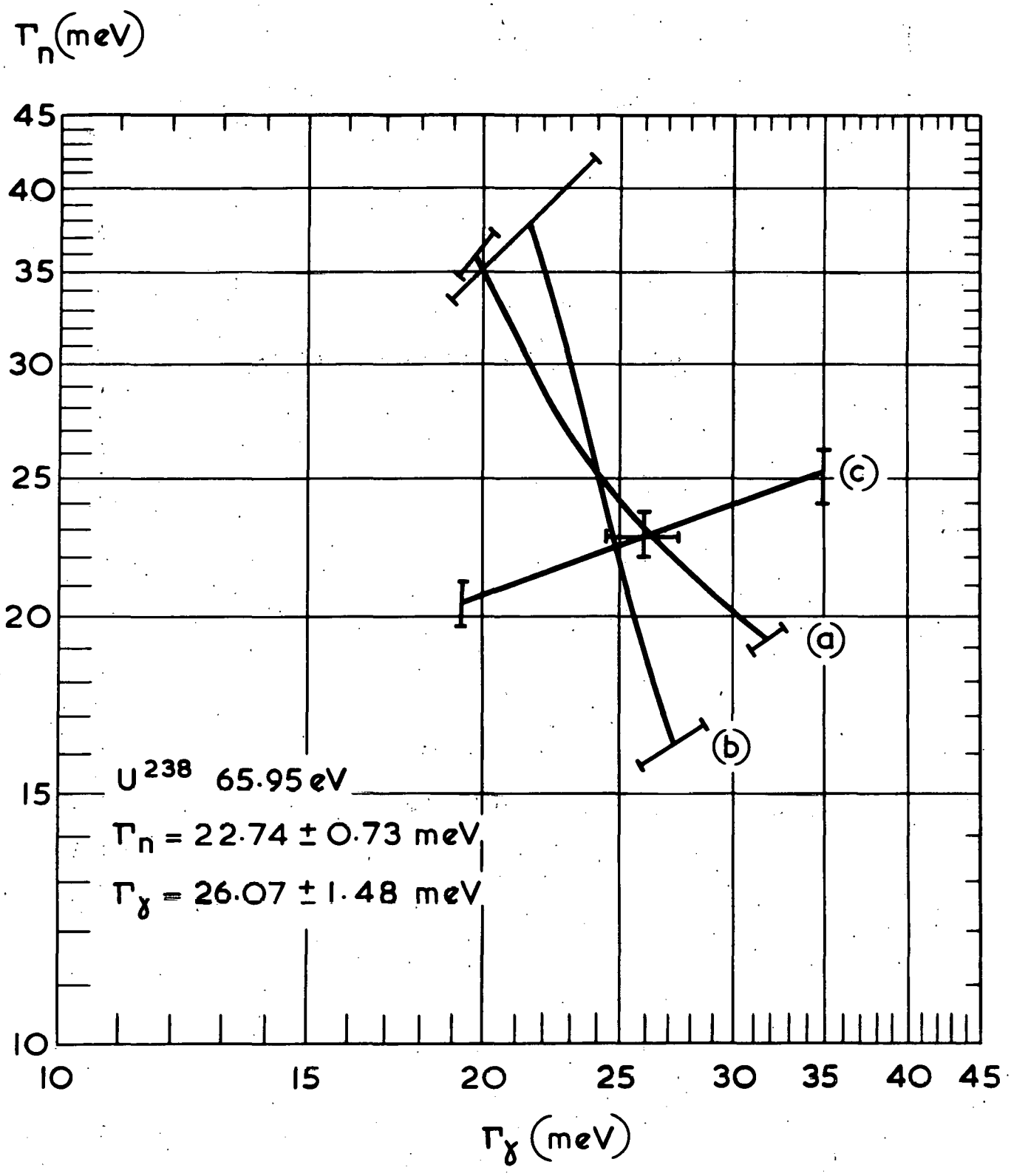

Fig. 30. Area Analysis of the 65.9 eV Resonance of ^{238}U (n,γ).

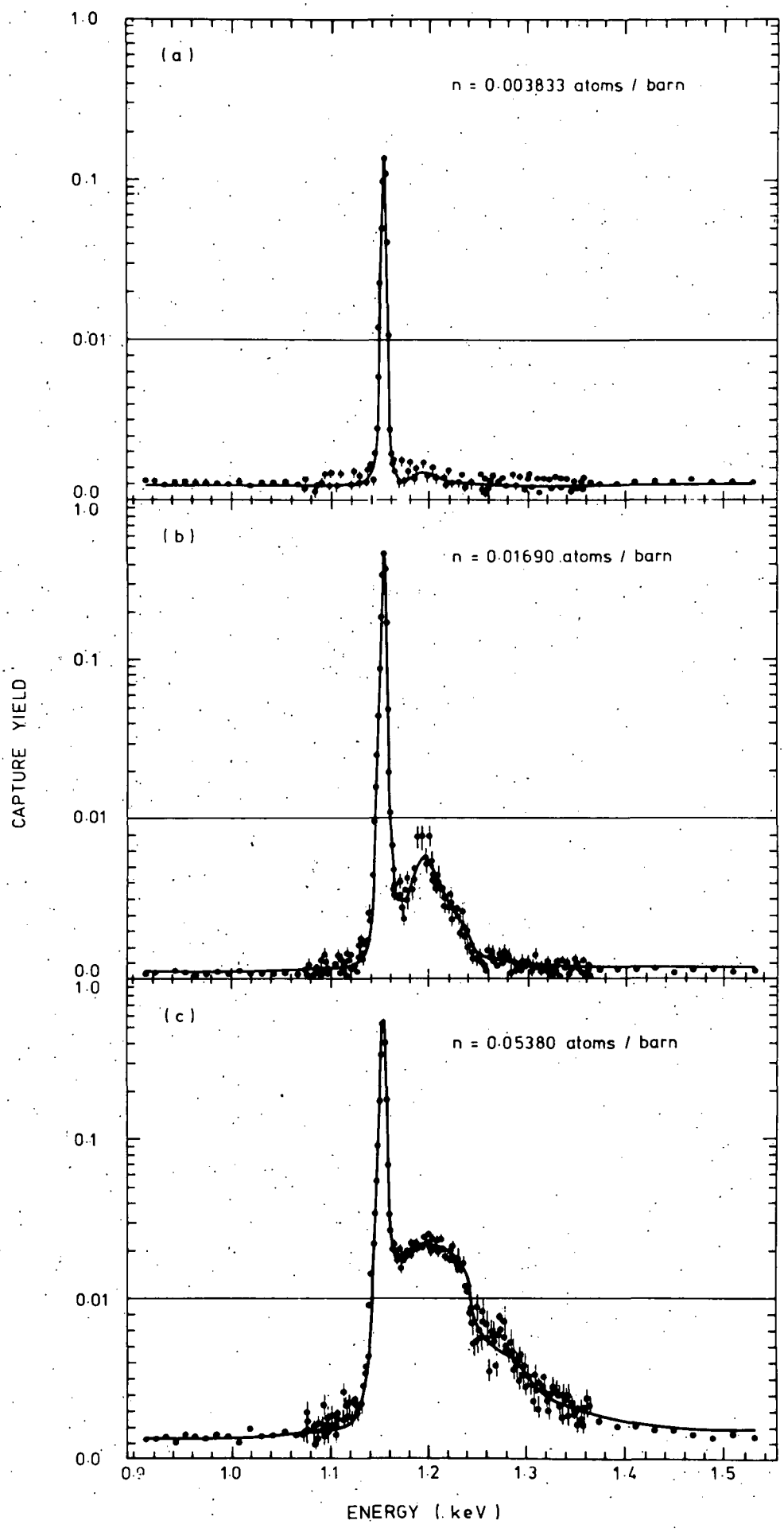

Fig. 31. The Effect of the Capture of Scattered Neutrons on Resonance-Capture-Cross-Section Measurements.

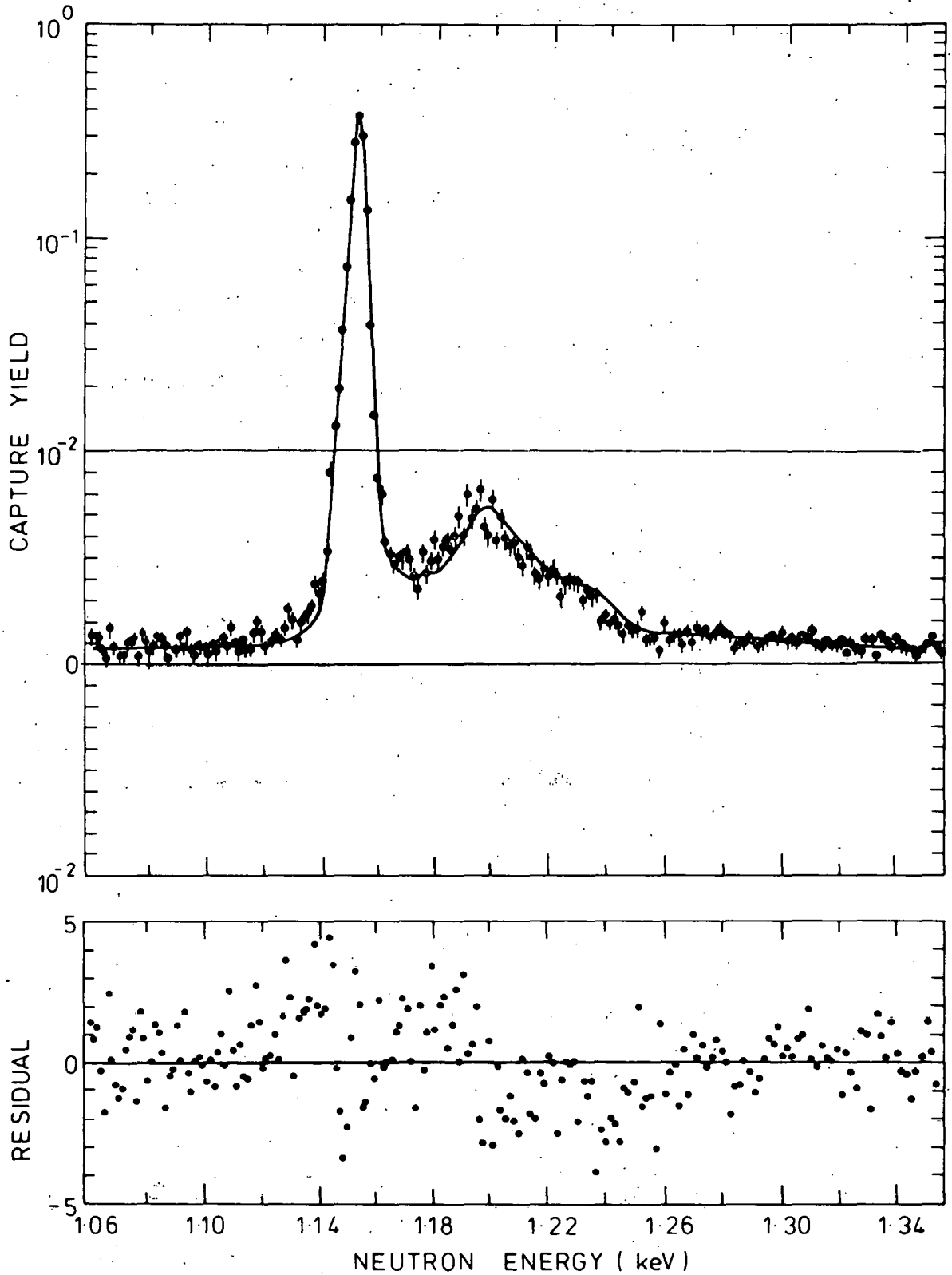

Fig. 32. Monte-Carlo Calculation and Fit of Experimental-Capture-Yield Data.

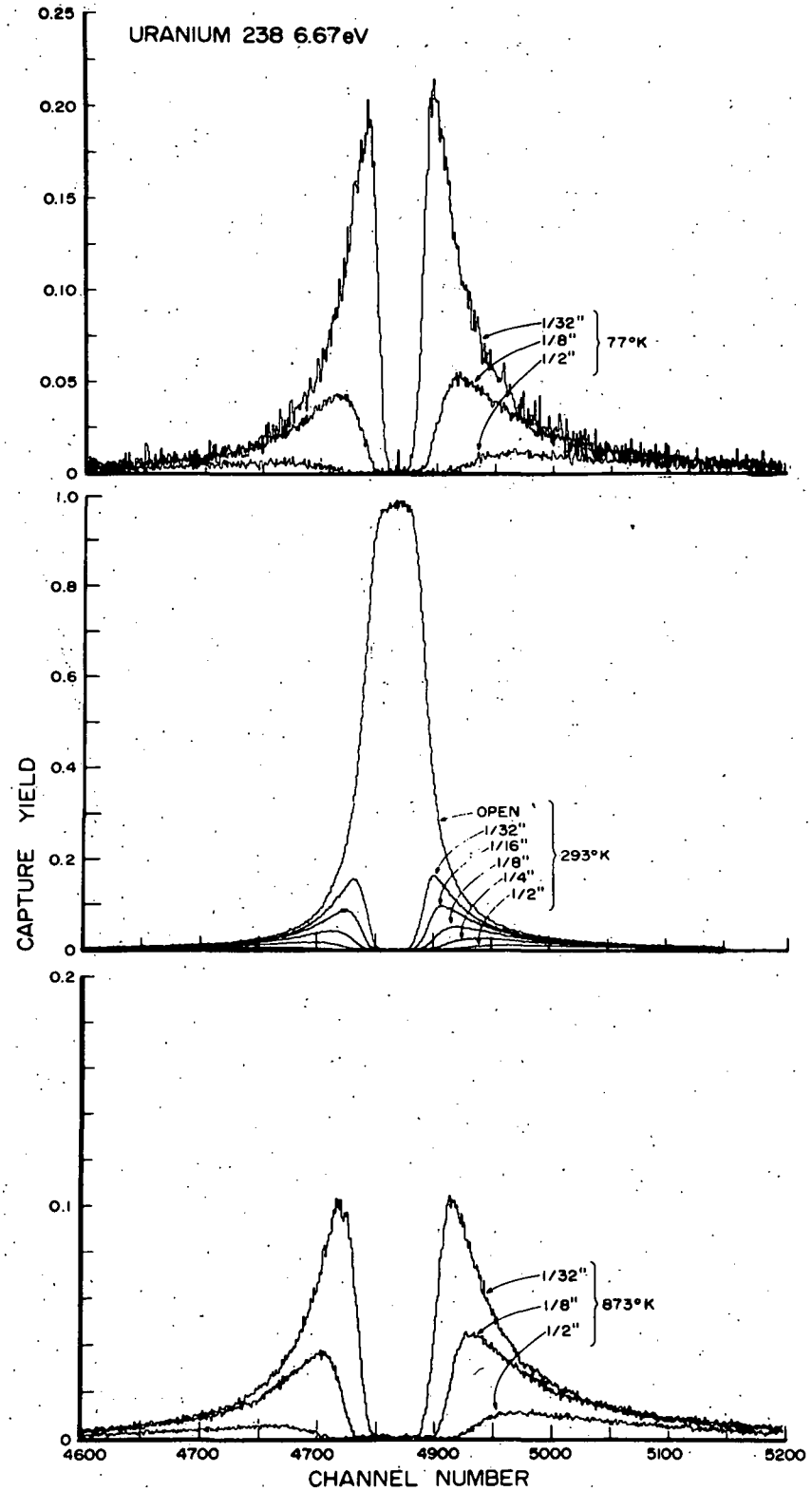

Fig. 33. Self-Indication Data Obtained at Different Temperatures for the Neutron Capture in the 6.67 eV Resonance of ^{238}U.

REFERENCES

1. J. M. Blatt and V. F. Weisskopf, "Theoretical Nuclear Physics", John Wiley and Sons, New York, 1952.

2. M. A. Lone, R. E. Chrien, O. A. Wasson, M. Beer, M. R. Bhat and H. R. Muether, BNL 12544

3. S. F. Mughabghab, R. E. Chrien, and O. A. Wasson, BNL 14982.

4. S. F. Mughabghab and R. E. Chrien, BNL 12548.

5. H. I. Lion, R. E. Chrien, J. Kapecky, and J. A. Konter, BNL 26537

6. M. Stefanon and F. Corvi, Nucl. Phys. A281, 240(1977).

7. C. W. Reich, "Resonance Averaged (n,γ) Spectra and Their Application to Nuclear Structure", Proc. Third Intern. Symp. on Neutron Capture γ-Ray Spectroscopy, Plenum Press, 105(1978).

8. The Oak Ridge National Laboratory Linear-Electron-Accelerator Facility. See Refs. 50 and 54.

9. R. L. Moessbauer, "The High-Flux Reactor at Grenoble and its Special Neutron Beam Installations", Proc. Intl. Conf. on the Interaction of Neutrons with Nuclei, Lowell 1976, (CONF-760715-P1, p. 65.

10. E. P. Schabalin, Proc. Fourth Conf. on Neutron Physics, Vol. 4, Kiev, 202(1977).

11. B. S. Diven, Proc. Int. Conf. on the Study of Nuclear Structure with Neutrons, Antwerp 1965, North Holland Publ. Comp. 1966, p. 441.

12. F. Mitzel and H. S. Plendl, Nucleonics 6, 371(1964).

13. D. J. Hughes, Neutron Cross Sections, Pergamon Press, (1957).

14. K. H. Beckurts and K. Wirtz, Neutron Physics, Springer Verlag, (1964).

15. H. Miessner and E. Arai, Nucleonik 8, 428(1966).

16. H. W. Schmitt and C. W. Cook, Nucl. Phys. 20, 202(1960).

17. R. L. Macklin, H. W. Schmitt and J. H. Gibbons, Oak Ridge National Laboratory Report, ORNL-2022(1956).

18. T. S. Belanova, JETP, 34, 574(1958).

19. T. S. Belanova et al., Nucl. Energy 20, 411(1966).

20. D. Bogart and T. T. Semler, Conf. on Neutron Cross Section Technology, Washington, CONF-66030, Vol. 1, p. 502(1966).

21. L. B. Miller and W. P. Poenitz, Nucl. Sci. Eng. 35, 296(1969).

22. F. Froehner, Int. Conf. Nucl. Data for Reactors, Helsink, Vol. I, 197(1970).

23. H. W. Schmitt, Oak Ridge National Laboratory, Private Communication (1966).

24. T. B. Ryves, J. C. Robertson, E. Y. Axton, I. Goodier, and A. Williams, J. Nucl. Energy A/B20, 249(1966).

25. H. Pauw, Energy Specta of Radioactive Neutron Sources, Thesis, Univ. Amsterdam, (1970).

26. K. Dietze, Proc. Conf. Neutron Physics, Kiev 1955, Vol. 3, p. 200, and ZFK-341 (1971).

27. A. Langsdorf, R. O. Lane, A. J. Elwyn, WASH-1046 (1964).

28. E. A. Pavlenko and N. L. Gridak, Conf. on Neutron Physics, Vol. 2, Kiev, 248(1977).

29. R. D. Evans, "The Atmic Nucleus", McGraw-Hill, 1955.

30. P. J. Campion, Int. J. Appl. Rad. and Isotop. 4, 232(1959).

31. C. LeRigoleur, J. C. Bluet, and J. L. Leroy, Proc. Intl. Conf. on Study of Nuclear Structure with Neutrons, Antwerp, (1966), North-Holland Publ. Comp., (1966).

32. R. L. Macklin, N. H. Lazar, and W. S. Lyon, Phys. Rev. 107, 504(1957).

33. R. E. Chrien, H. I. Liou, M. J. Kenny, and M. L. Stelt, Nucl. Sci. & Eng. 72, 202 (1979).

34. W. P. Poenitz, J. Nucl. Energy A/B20, 825(1966).

35. S. A. Cox, Phys. Rev. 133, B378(1964).

36. H. A. Grench and H. O. Menlove, Phys. Rev. 165, 1298(1968).

37. M. Lindner, R. J. Nagle, and J. H. Landrum, Nucl. Sci. & Eng. 59, 381(1975).

38. K. K. Harris, H. A. Grench, R. G. Johnson, F. V. Vaughn, J. H. Ferzinger, and R. Sher, Nucl. Phys. 69, 37(1965).

39. H. D. Warren, Proc. Second ASTM-EURATOM Symp. Reactor Dosimetry, Palo Alto, 775 (1977).

40. S. J. Bame and R. L. Cubitt, Phys. Rev. 113, 256 (1959).

41. A. E. Johnsrud, M. G. Silbert, and H. H. Barschall, Phys. Rev. 116, 927 (1959).

42. E. Meservey, Phys. Rev. 96, 1006(1954).

43. R. D. Albert and E. R. Gaerttner, Knolls Atomic Power Laboratory Report, KAPL-1083, 1954.

44. E. R. Rae and E. M. Bowey, J. Nucl. ENergy 4, 179(1957).

45. D. Kompe, Nucl. Phys. A133, 513(1969).

46. A. Ernst, F. H. Froehner, and D. Kompe, Proc. 2nd. Int. Conf. on Nuclear Data for Reactors, Helsinski, 1970, p. 693.

47. B. C. Diven, J. Terrell and A. Hemmendinger, Phys. Rev. 120, 556(1960).

48. E. Haddad, R. B. Walten, S. J. Friesenhahn, and W. M. Lopez, Nucl. Instr. Methods 31, 125(1964).

49. W. P. Poenitz, "Fast Neutron Capture and Activation Cross Sections of Niobium Isotopes", Argonne National Laboratory Report ANL/NDM-8, 1974.

50. E. G. Silver, J. Lewin, and J. Todd, Oak Ridge National Laboratory Reports, ORNL 4280, p. 135 and ORNL 4433, p. 11 (1969).

51. G. DeSaussure, E G. Silver, R. B. Perez, R. Ingle, and H. Weaver, Nucl. Sci. & Eng. 51, 385(1973).

52. S. K. Gupta, J. Frehaut, and R. Bois, Nucl. Instr. Methods 148, 77(1978).

53. D. B. Gayther, M. S. Coates, G. D. James, M. C. Moxon, D. B. Syme, B. W. Thomas and B. Thom, Atomic Energy Research Establishment Report, AERE-R-9058(1978).

54. R. L. Macklin, AERE-R-3744 (1961).

55. Yu. V. Adamdshuk, M. A. Voskanyan, G. V. Muradyan, G. U. Ustroev, and Yu. G. Tshepkin, Proc. Conf. Neutron Physics, Kiev, Vol. 2, 192 (1977).

56. H. Brandt, P. G. Gugelot, O. Huber, H. Medicus, P. Preiswerk, and P. Scherer, Helvetia Physika Acta 19, 77 (1946).

57. W. A. Fowler, C. C. Lauritsen, and T. Lauritsen, Rev. Mod. Phys. 20, 265 (1948).

58. N. T. Kashukeev, Yu. P. Popov, and F. L. Shapiro, J. Nucl. Energy A/B 14, 76 (1961).

59. A. I. Isakov, Yu. P. Popov, and F. L. Shapiro, Sov. Phys. JETP 38, 712 (1959).

60. V. A. Konks, Yu. P. Popov, and F. L. Shapiro, Sov. Phys. JETP 19, 59 (1964), also V. A. Konks and F. L. Shapiro, Sov. Phys. JETP 20, 531 (1965).

61. M. C. Moxon and E. R. Rae, Nucl. Inst. Methods 24, 445 (1963).

62. K. V. K. Iyengar, B. Lal, and M. L. Jhingan, Nucl. Instr. Methods 121, 33(1974).

63. R. L. Macklin, J. H. Gibbons, and T. Inada, Nucl. Phys. 43, 353(1963).

64. H. Weigmann, G. Carraro, and K. H. Boeckhoff, Nucl. Instr. Methods 50, 265(1967).

65. G. S. Hurst and R. H. Ritchie, health Physics 8, 117(1962).

66. H. Maier-Leibnitz, private communication to R. L. Macklin and J. H. Gibbons, 1967. (See Ref. 67).

67. R. L. Macklin and J. H. Gibbons, Phys. Rev. 159, 1007(1967).

68. G. B. Czirr, Nucl. Instr. Methods 72, 23(1969).

69. R. L. Macklin and B. J. Allen, Nucl. Instr. Methods 91, 565(1971).

70. L. V. Groshev, A. M. Demidov, V. N. Lutsenko,and V. L. Pelekhov, Atlas of Gamma Ray Spectra from Capture of Thermal Neutrons, Pergamon Press, London (1959).

71. W. Michaelis and F. Horch, Proc. Int. Conf. on Neutron Capture Gamma-Ray Spectroscopy, Int. Atom. Energy Agency, 35(1969).

72. W. Michaelis, D. Lange, and G. Wilhelmi, Proc. Conf. Neutron Capture Gammma-Ray Spectroscopy, Int. Atom. Energy Agency, 75(1969).

73. W. R. Kane, Proc. Conf. on Neutron Capture Gamma-Ray Spectroscopy, Plenum Press, 485(1979).

74. E. G. Kessler, Proc. Conf. Neutron-Capture Gamma-Ray Spectroscopy, Brookhaven 1978, p. 427.

75. H. Schmidt and D. Heck, Proc. Conf. Neutron Capture Gamma-Ray Spectroscopy, Int. Atom. Energy Agency, 371(1969).

76. K. Abrahams, Proc. Conf. on Neutron Capture Gamma-Ray Spectroscopy, Plenum Press, 385(1979).

77. CINDA, An Index to the Literature on Microscopic Neutron Data, Int. Atom. Energy Agency, Vienna (1979).

78. H. W. Schmitt, "Sample Scattering Corrections in Neutron Beam Experiments", Oak Ridge National Laboratory Report ORNL-2882, (1960).

79. L. Dresner, Nucl. Instr. and Methods 16, 176(1962).

80. R. L. Macklin, Nucl. Inst. Methods, 26, 213 (1964).

81. F. H. Froehner, "SESH", Gulf General Atomic Report, GA-8380 (1968).

82. J. J. Devaney, Nucl. Sci. & Eng. 51, 272(1973).

83. H. A. Bethe and G. Placzek, Phys. Rev., 51, 450(1937).

84. D. B. Gayther, M. C. Moxon, B. W. Thomas, R. B. Thom, and J. E. Jolly, U.K. Atomic Energy Authority Report UKNDC(79)P94, p.36(1979).

85. M. C. Moxon, REFIT, Proc. Conf. Neutr. Data of Structural Materials, Geel, 1977.

86. F. H. Froehner, FANAC, Nuclear Research Center, Karlsruhe Report KFK 2145, 1977.

87. R. C. Block, D. R. Harris and S. H. Kim, Electric Power Research Institute Report EPRI NP-996, (1979).